LA-13096-MS

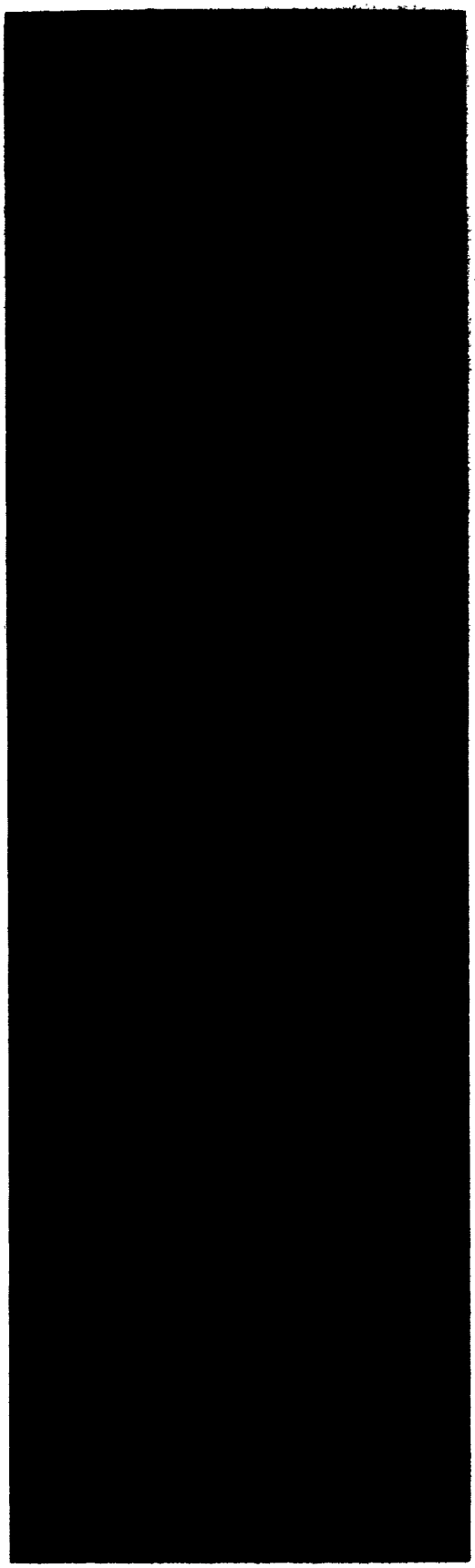

Petrography, Mineralogy, and Chemistry of Calcite-Silica Deposits at Exile Hill, Nevada, Compared with Local Spring Deposits

Los Alamos
NATIONAL LABORATORY

Los Alamos National Laboratory is operated by the University of California for the United States Department of Energy under contract W-7405-ENG-36.

This work was supported by the Yucca Mountain Site Characterization Office as part of the Civilian Radioactive Waste Management Program. This project is managed by the US Department of Energy, Yucca Mountain Site Characterization Project.

An Affirmative Action/Equal Opportunity Employer

LA-13096-MS
UC-802
Issued: December 1995

Petrography, Mineralogy, and Chemistry of Calcite-Silica Deposits at Exile Hill, Nevada, Compared with Local Spring Deposits

D. T. Vaniman, S. J. Chipera, and D. L. Bish

Los Alamos
NATIONAL LABORATORY
Los Alamos, New Mexico 87545

Table of Contents

PETROGRAPHY, MINERALOGY, AND CHEMISTRY OF CALCITE-SILICA DEPOSITS AT EXILE HILL, NEVADA, COMPARED WITH LOCAL SPRING DEPOSITS

by

D. T. Vaniman, S. J. Chipera, and D. L. Bish

ABSTRACT

Chemical, mineralogic, and petrographic analyses of siliceous calcretes from Exile Hill east of Yucca Mountain, Nevada, indicate that pedogenic processes alone account for the formation of the calcretes. These calcretes have been interpreted by some observers as evidence of seismically triggered eruptions of deep water. Such an origin could have important consequences if Yucca Mountain is developed as an unsaturated site for the disposal of high-level nuclear waste. At odds with this hypothesis are the absence of features that should be present at fault-fed springs (e.g., fissure-ridge mounds with microterraces) and the preservation within root casts of delicate pedogenic microfossils, such as calcified filaments and needle-fiber calcites. Mineral-chemical evidence of pedogenic origin is found in heavy-mineral concentrations, reflected in Fe and Sc enrichments. These concentrations, which occur in the most massive of the vein calcretes, require derivation of detritus from a mixture of weathered and eolian materials that occur in the overlying B soil horizons, as opposed to direct incorporation of adjacent unweathered bedrock. Carbonate and silica abundances and accumulation rates are well within the scope of pedogenic processes. Calcium is derived from rainwater or eolian sources, whereas silica is derived in part by dissolution of local volcanic glasses or from dissolution of unstable silica minerals that are abundant in the local tuffs. In contrast with local deposits that are of spring or seep origin, the siliceous calcretes at Yucca Mountain are pedogenic in origin as well as evolution and provide no evidence in support of conjectured spring activity.

INTRODUCTION

Laminated deposits of detritus cemented by calcite and opal, with minor sepiolite and amorphous Fe, Mn, and Ti oxides, are common at the surface of Yucca Mountain, Nevada. These calcite-silica deposits are siliceous calcretes. Calcrete is a nongenetic term that describes not only deposits that are pedogenic (i.e., formed in soil with the addition of only rainwater and dust) but also deposits with lacustrine, ground-water, or spring origins (Machette 1985). Closer study is necessary to determine the origins of a particular calcrete.

Most of the siliceous calcretes at Yucca Mountain have laminae parallel to the ground surface; however, they also occur within faults where the calcrete laminae are

complex, often cross-cutting, and in general are steeply dipping. Both orientations are exposed in Trenches 14 and 14A on the west side of Exile Hill, which were excavated across the Bow Ridge Fault along the east flank of Yucca Mountain (Fig. 1a,b). Taylor and Huckins (1986) mapped trench exposures of the siliceous calcretes and determined from geomorphology, fabric, and carbonate distributions that the deposits were pedogenic. Further work by Taylor and Huckins (1995) provides detailed maps of the walls of Trench 14, illustrating the relationship of the siliceous-calcrete K horizons to overlying clay-rich Bt horizons (~50-cm thick) and a thin sandy-to-loamy (~5-cm thick) vesicular A horizon with a large eolian component. This nomenclature for soil horizons follows standard usage; the occurrence of genetically related horizons (in this case, A over B over K) is one of the fundamental indications that this series is indeed a pedogenic soil association. In brief, the A horizon is a loose accumulation of organic and mineral matter, the Bt horizon is a zone of clay accumulation, and the K horizon is a zone of extensive laminar carbonate accumulation. Taylor and Huckins (1995) subdivide the Bt horizons into

(1) an upper Btk with scarce secondary carbonate on the undersides of pebbles (stage I; cf. Gile et al. 1966) and
2) a lower 2Btj (juvenile Bt), the top of which has a well-developed prismatic structure.

Simplified versions of their maps are shown in Fig. 2 (panels 2a and 2b) and in Fig. 3 (panel 3a). Figure 4 shows the relationships between vein and slope calcretes in Trench 14A, to the north of Trench 14, for that part of Trench 14A that intersected the Bow Ridge Fault. These figures emphasize the siliceous calcretes and subdivide them into those with horizonation parallel to the Bt horizons (slope calcretes) and those that include complex, steeply dipping laminae in the vicinity of faults (vein calcretes). Slope calcretes dip to the west at 6° to 7°. Details of laminae in the vein calcretes are shown in Figs. 2c, 2d, and 3b.

The formation of dense, platy calcrete laminae in the slope calcretes is characteristic of a mature stage-IV K horizon (Gile et al. 1966). Based on the more detailed soil descriptions provided by Taylor and Huckins (1995), the soils in the vicinity of Trench 14 can be classified as Typic Durargids (classification according to Soil Survey Staff 1975). In our cm-scale mapping, we have subdivided the calcrete laminae into five categories; these categories are described in section II.A "Petrography of Calcrete Laminae, B Soil Horizons, and Plant Roots" in this paper. Although a simple K-horizon stratigraphy is not preserved in the more complex cross-cutting laminae of the vein calcretes, the presence of similar lamina types is a sign of origin and maturity comparable to the slope calcretes.

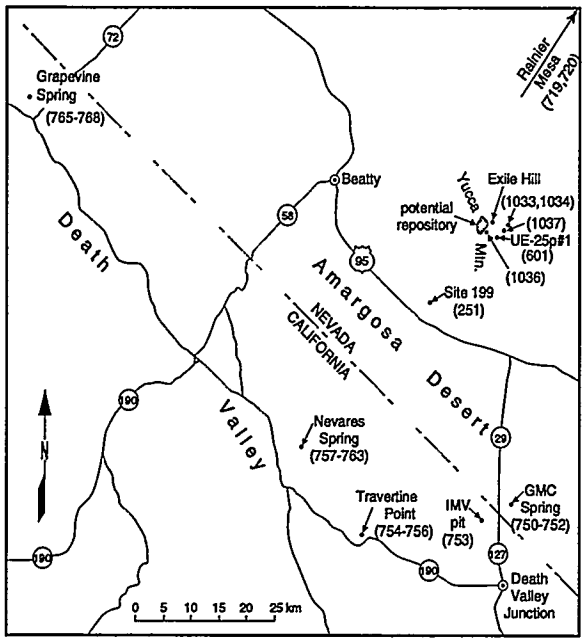

Fig. 1a: Regional map showing Exile Hill and the potential repository boundary relative to spring and seep localities sampled for comparison. Root samples from Rainier Mesa are off of this figure to the NE. Numbers in parentheses indicate LANL sample numbers used throughout the text (see Table 1).

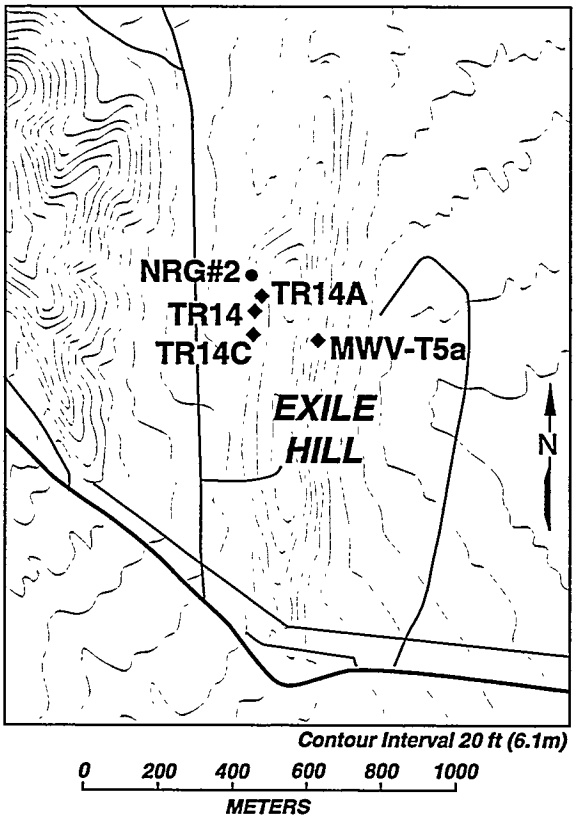

Fig. 1b: Map of Exile Hill showing the locations of trenches and of drill hole NRG#2. Root samples with LANL numbers 350, 351, and 352 are from the west slope of Exile Hill between trenches TR 14 and TR 14C.

In contradiction to the conclusions of Quaternary geologists mapping at Yucca Mountain, it was suggested by others that steeply dipping and disrupted calcrete laminae within faults and fractures of the area were formed from hydrothermal fluids that have risen as high as the crest of Yucca Mountain—over 700 m above the present water table—under seismic pressurization (Archambeau and Price 1991; Marshall 1991). This hypothesis was tested by stable-isotope analyses, which indicated that the carbonate component of the calcretes was not deposited from hydrothermal waters (Vaniman et al. 1985). A more detailed stable-isotope study reinforced the conclusion that the source waters for the calcite were cool and further indicated that the deposits are pedogenic, formed under the influence of piñon-juniper vegetation during cooler and wetter climates of the past (Quade and Cerling 1990). Radiogenic isotope data (Stuckless et al. 1991) supported the conclusion that these laminae originated by precipitation from rainwater within the soil zone and cannot be derived from the deep aquifers of the region. Roedder et al. (1994) found vapor-filled and methane-bearing inclusions in sparry calcite of the unsaturated zone, 130 to 314 m below the surface of Yucca Mountain, indicating that these crystals formed in unsaturated rocks at temperatures <100°C

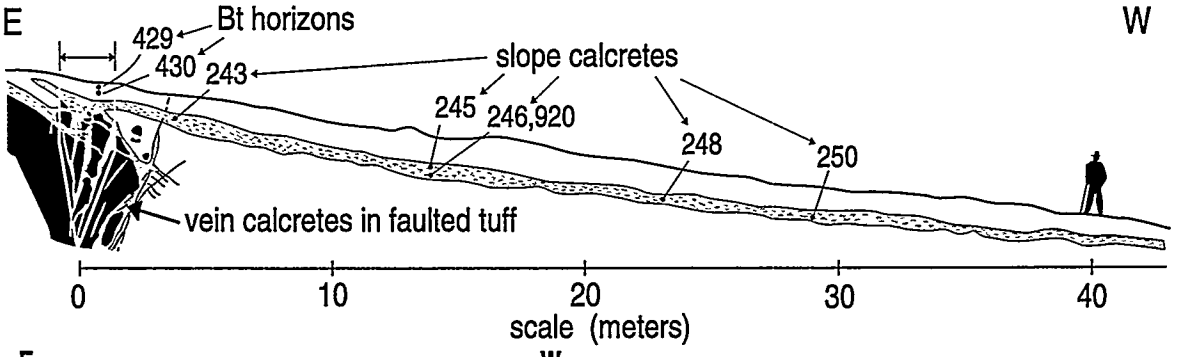

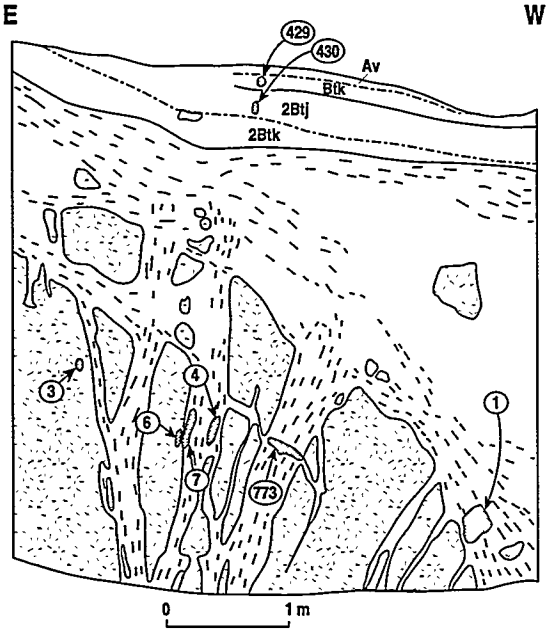

Fig. 2a (above): Map of the south wall of Trench 14 (modified from Taylor and Huckins in press), showing the locations of slope-calcrete samples (LANL numbers 243, 245, 246, 248, 250, and 920; see Table 1) cited in the text.

Fig. 2b (to the left): Close-up map of the wall-rock tuffs (stipple), vein calcretes and overlying slope calcretes (dashes), and A and B soil horizons from the south wall of Trench 14 (modified from Taylor and Huckins 1995). Circled numbers are LANL sample numbers used in the text.

and perhaps at ambient conditions. If these calcites are genetically related to calcretes that form at the surface (Whelan and Stuckless 1992; Vaniman 1993, 1994), these deeper calcites suggest dissolution, downflow, and reprecipitation of carbonate minerals via penetration of vadose-zone waters into fractures beneath the calcretes.

Suggestions of an unstable and episodically upwelling water table beneath Yucca Mountain are of general interest because of the implications of this hypothesis for interpreting similar deposits in many arid regions. The more direct impact of this hypothesis, however, is on the suitability of Yucca Mountain as a site for geologic disposal of high-level radioactive waste in deep but unsaturated rocks. Proponents of the hypothesis of an episodically upwelling water table regard this site as unsuitable principally because these deposits are seen as evidence of a recurring catastrophic process (Broad 1990).

Criteria for distinguishing pedogenic from nonpedogenic calcretes are thus important for making informed decisions about the Yucca Mountain site. Analysis of any suspect calcrete should begin in the field, where a variety of megascopic features could provide indications of spring activity. Such features include tufa dams, rimstone pools, cliff drapes, stream-mouth cones, and related deposits (Viles and Goudie 1990). Particularly relevant to Trench 14 is the absence of a fissure-ridge mound with internal

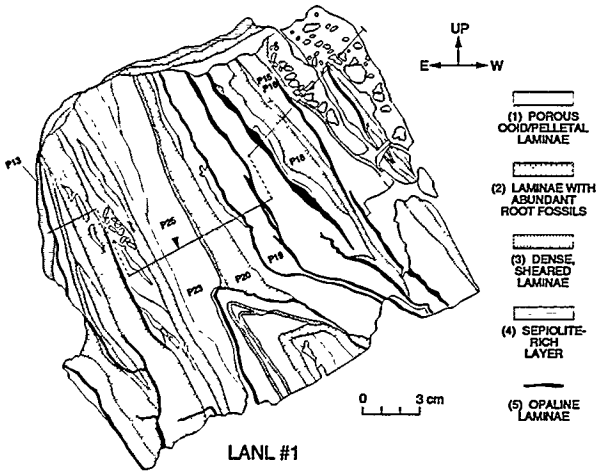

Fig. 2c: Detailed map of sample block LANL#1, showing distribution of calcrete lamina types (see text descriptions of laminae in section on *Petrography of Calcrete Laminae, B Soil Horizons, and Plant Roots*). Numbers beginning with P represent powders for which data are reported in Appendix 5; P25 (1,p25) is a channel sample representing the entire block.

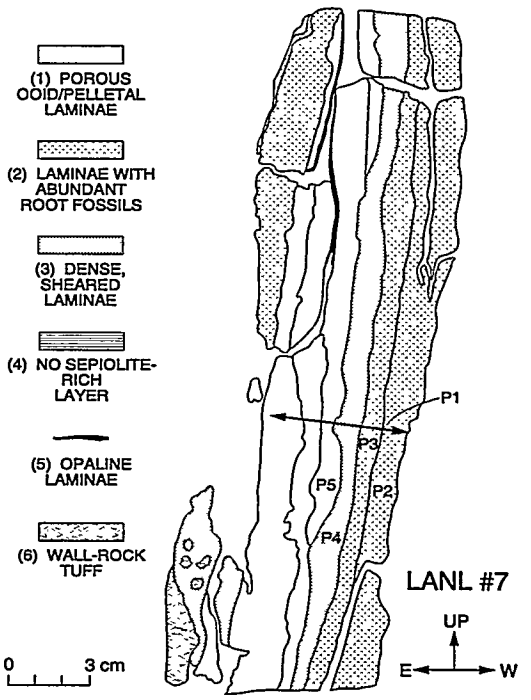

Fig. 2d: Detailed map of sample block LANL#7, showing distribution of calcrete lamina types. Numbers beginning with P represent powders for which data are reported in Appendix 5; P1 (7,p1) is a channel sample representing the entire block.

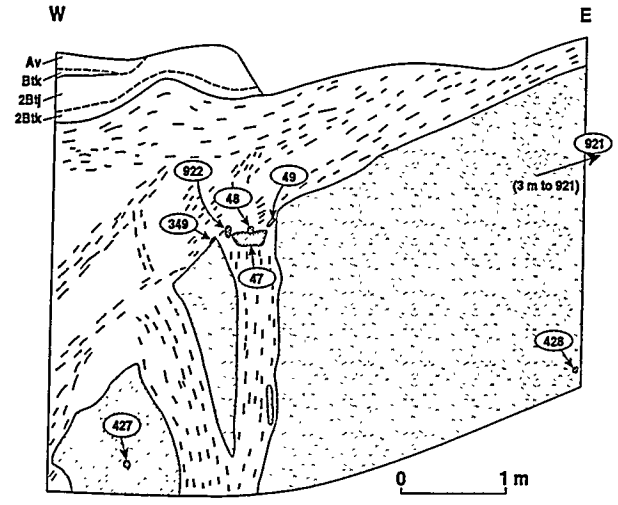

Fig. 3a: Close-up map of the north wall of Trench 14 (modified from Taylor and Huckins 1995), showing the wall-rock tuffs (stipples), vein calcretes and overlying slope calcretes (dashes), and A and B soil horizons. Circled numbers are LANL sample numbers cited in the text.

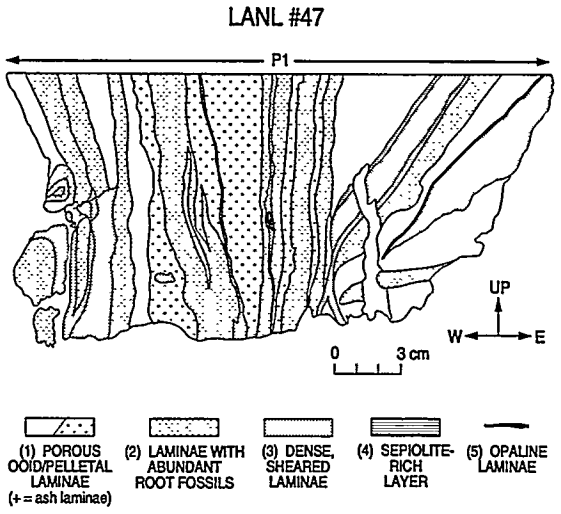

Fig. 3b: Detailed map of sample block LANL#47, showing distribution of calcrete lamina types (see text descriptions of laminae in section on *Petrography of Calcrete Laminae, B Soil Horizons, and Plant Roots*). Line P1 shows the location of a channel sample (47,p1) representing the entire block.

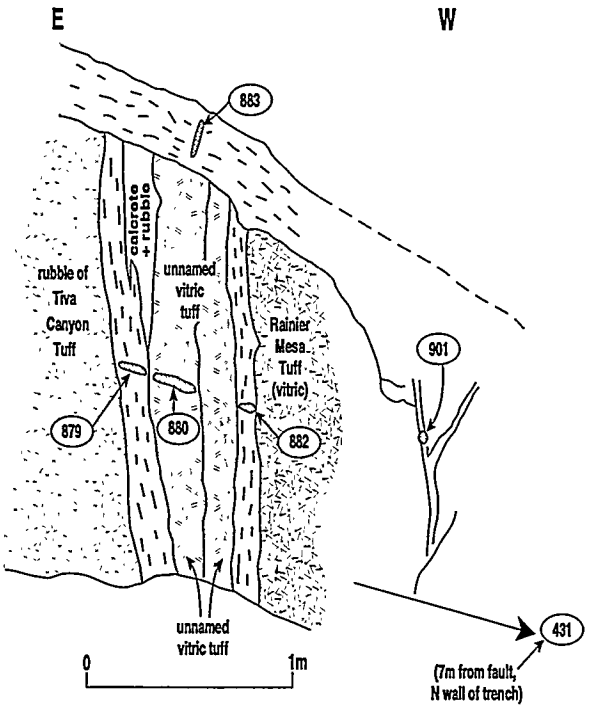

Fig. 4: Close-up map of the wall-rock tuffs, vein calcretes and tuffs, and overlying slope calcretes in Trench 14A. Circled numbers indicate the LANL sample numbers of channel samples cited in the text (879, 880, 882, and 883), of a thin calcrete vein sample (901), and of Rainier Mesa Tuff (431).

laminae parallel to the mound surface, corrugated by centimeter-scale microterraces. Such a mound would be definitive evidence of spring discharge along a fault. Such mounds are not found along the faults at Yucca Mountain. Nevertheless, the absence of evidence for spring deposition does not constitute proof of a pedogenic origin. Other lines of evidence must be developed, starting with field evidence for the presence or absence of soil horizonation related to the calcretes (Taylor and Huckins, 1995). Further examination of chemical systematics and microfossil development can be used to find indicators of pedogenic origin (Vaniman et al. 1994).

Vaniman et al. (1988) compared the bulk petrographic features, mineralogy, and mineral chemistry of the calcretes with that of several spring and seep deposits in the region. This preliminary comparison showed a number of distinctions between spring or seep deposits and the calcretes, but also noted that surficial spring or seep deposits that grade into soils could develop comparable mineralogic composition. For the present study, additional springs were studied, with more detailed chemical, petrographic, and mineralogic analysis. The goal of this study is to extend the work of Vaniman et al. (1988, 1994) to provide

(1) petrographic, mineralogic, and/or chemical criteria for determining the origin of a particular calcrete, and

(2) a summary of comparative petrography, mineralogy, and chemistry to illustrate those features that may be used to differentiate between calcite-silica deposits of either pedogenic or spring origin.

I. SAMPLES AND METHODS

A. Samples

Most of the samples used in this study were collected in joint field work with the U. S. Geological Survey. Under this collection program, samples were given an identi-

TABLE 1. Sample Number Cross-References and Descriptions

LANL #	HD #	SMF #	Location (Type)
1	HD-15-3	00003695	Trench 14, S wall, E16S (vein calcrete)
3	HD-41-3	00003650	Trench 14, S wall, D13S (Tiva tuff)
4	HD-42-1	00003651	Trench 14, S wall, D14S (altered Tiva tuff)
6	HD-42-5	00003651	Trench 14, S wall, D14S (altered Tiva tuff)
7	HD-42-6	00003651	Trench 14, S wall, D14S (vein calcrete)
47	HD-225	00003010	Trench 14, N wall, D13N (vein calcrete)
48	HD-225-01	00003010	within HD-225 (ash/detritus calcrete lamina)
49	HD-225-02	00003010	within HD-225 (dense calcrete lamina)
243	HD-1-1	00003618	Trench 14, S wall, C18S (top of platy-K)
245	HD-5-1	00003621	Trench 14, S wall, D28S (top of platy-K)
246	HD-6-1	00003622	Trench 14, S wall, E28S (bottom of platy-K)
248	HD-10-1	00003626	Trench 14, S wall, E37S (bottom of platy-K)
250	HD-12-1	00003628	Trench 14, S wall, F43S (bottom of platy-K)
251	HD-170	00002951	Site 199, seep (root fossil)
349	HD-465	00004657	Trench 14, N wall, D14N (vein calcrete)
350	HD-466	00004658	soil surface S of Trench 14 (boxthorn root)
351	HD-467	00004659	soil surface S of Trench 14 (creosote-bush root)
352	HD-468	00004660	soil surface S of Trench 14 (Mormon-tea root)
427	n/a	00005253	Trench 14, N wall (vitric nonwelded tuff, tb; Gibson et al., 1992)
428	n/a	00005254	Trench 14, N wall (Tiva tuff)
429	n/a	00005255	Trench 14, S wall (Btk soil horizon)
430	n/a	00005256	Trench 14, S wall (2Btj soil horizon)
431	n/a	00005257	Trench 14A, N wall (vitric Rainier tuff)
601	n/a	n/a	Roberts Mountain Formation dolomite (from core near Yucca Mtn.)
719	n/a	00005258	Rainier Mesa (piñon root)
720	n/a	00005259	Rainier Mesa (juniper root)
750	HD-472	00004663	GMC Spring (active; calcite, opal-CT, and quartz)
751	HD-476	00003712	GMC Spring (active; calcite, opal-A & -CT, quartz)
752	HD-477	00003713	GMC Spring (active; algal opal-A plus detritus)
753	HD-480	00003716	IMV Spring (inactive; opal-CT)
754	HD-485	00003721	Travertine Point vein (inactive; calcite)
755	HD-487	00003723	Travertine Point vein (inactive; calcite)
756	HD-491	00003727	Travertine Point vein (inactive; calcite)
757	HD-496	00003732	Nevares Spring (active; calcite mound)
758	HD-497	00003733	Nevares Spring (active; calcite mound)
759	HD-498	00003734	Nevares Spring (active; calcite mound)
760	HD-499	00003735	Nevares Spring (active; calcite mound)
761	HD-500	00003736	Nevares Spring (active; calcite mound)
762	HD-501	00003737	Nevares Spring (active; calcite mound)
763	HD-503	00003739	Nevares Spring (active; surface of calcite mound)
765	HD-508	00003744	Grapevine Spring (active; calcite vein)
766	HD-510	00003746	Grapevine Spring (active; calcite vein)
767	HD-511	00003747	Grapevine Spring (active; calcite plant casts)
768	HD-512	00004668	Grapevine Spring (active; surface efflorescence)
773	HD-97	00003684	Trench 14, S wall, D14S (vein calcrete)
879	n/a	00005295	Trench 14A, S wall (vein calcrete)
880	n/a	00005296	Trench 14A, S wall (vitric nonwelded tuff, tb; Gibson et al., 1992)
882	n/a	00005298	Trench 14A, S wall (vein calcrete)
883	n/a	00005299	Trench 14A, S wall (slope calcrete)
901	HD-31-2	00003643	Trench 14A, S wall, (vein calcrete)
920	HD-6	00003622	Trench 14, S wall, D28S (platy-K)
921	HD-49	00003654	Trench 14, N wall, C8N (Tiva tuff)
922	HD-52	00003657	Trench 14, N wall, D13N/D14N (vein calcrete)
1033	n/a	00005318	E of Exile Hill (eolian deposit under boulder; Guthrie et al., 1993)
1034	n/a	00005319	E of Exile Hill (eolian deposit in boulder fracture; Guthrie et al., 1993)
1036	n/a	00005321	SSW of Exile Hill (eolian deposit under boulders; Guthrie et al., 1993)
1037	n/a	00005322	ESE of Exile Hill (eolian deposit under boulders; Guthrie et al., 1993)

fication number in the field that began with the prefix HD (for "hydrogenic deposits"). Some samples were collected separately by the authors and do not have an HD identification. All samples used in preparing this report were assigned a Los Alamos National Laboratory (LANL) number as they were received at LANL. In addition, most samples received Yucca Mountain Project Sample Management Facility (SMF) tracking numbers. In this report, the LANL numbers are used throughout; however, to facilitate cross-reference, Table 1 lists the correlations between LANL, HD, and SMF numbers, as well as the location and type of each sample.

B. Methods

Petrographic analysis was performed on both polished thin sections and on broken or sawed pieces of calcrete. Petrographic analysis of polished thin sections was used to categorize the calcrete lamellae as mapped in the examples of Fig. 2c, 2d, and 3b. Optical observations were supplemented by imaging with an ISI DS-130 electron microscope in backscattered-electron mode (BSE-SEM).

X-ray fluorescence (XRF) analyses for Si, Ti, Al, Fe, Mn, Mg, and P and atomic absorption (AA) analyses for K were obtained at J. Husler's laboratory at the University of New Mexico. These analyses were only performed on several larger samples where sufficient material (>2 g) was available. As part of these analyses, volatile-component loss-on-ignition (LOI) was also determined. Ion chromatography analyses (Cl, N, S, P_2O_5, and C_2O_4) were obtained at LANL using a Dionex 4500i ion chromatograph with a conductivity detector. The species analyzed by ion chromatography, particularly the Cl, N, and oxalate, are abundant in the ashed root materials.

Trace-element, Ca, Fe, Na, and/or K data were obtained by instrumental neutron activation analysis (INAA) of coarse (<425 mm) and fine (<45 mm) fractions of the overlying Bt horizons; of bulk channel samples representing average calcretes; and of individual laminae separated from the calcretes. These data were collected in the trace-element geochemistry laboratory at Washington University, St. Louis, MO, using methods described in Korotev (1991). Results are listed in the appendices. Where a calcrete sample is listed as "bulk" or "channel," the sample was collected across several laminae in an attempt to obtain an "average" calcrete analysis for that particular part of the calcrete. The CaO values measured are attributable almost entirely to calcite; correlations between the INAA-measured CaO and the X-ray diffraction (XRD) determinations of calcite are good (R^2=0.95), providing a measure of confidence in the quantitative XRD method. One channel sample from the calcretes (1,p25) was collected with a small drill that had cutting diamonds mounted in Ni metal; this sample therefore has Ni contamination and its Ni is reported as not applicable (n/a) in Appendix 5. Several other samples were lightly crushed in a Fe-Cr percussion mortar; for these samples, the amount of Fe contamination is trivial because of their high Fe content, but the

amount of Cr contamination may be significant and their Cr values are reported as "n/a" in the appendices. The two clay separates (429,p3 and 430,p3; Appendices 3 and 8) required shatterbox treatment than can result in contamination by Co, Ta, and W; values for these elements are therefore also reported as "n/a" for these samples. Other samples were handled only with steel or W-carbide hand tools that left no apparent contamination. In general, the samples used for trace-element chemical analysis were handled as little as possible to avoid contamination. To avoid contamination, most samples were not finely powdered by severe crushing methods (e.g., shatterbox). This necessarily led to somewhat greater sample heterogeneity than would otherwise be obtained. The extent of this heterogeneity can be seen in Appendix 8, where replicate INAA analyses of subsplits are compared. We can obtain an idea of the reproducibility to be expected from very fine-grained samples by comparing the replicate analyses of clay separates (samples 429 and 430, Appendix 8). In general, the variability between other sample replicates is minimal to moderate (<1.5X) and reflects somewhat different concentrations of particular constituents within the coarse-crushed samples. Some exceptional variability (~5X) is seen, however, in the lanthanide series elements of the ashed inner portion of creosote-bush root (351,p2), where heavier constituents obviously separated from one portion of the very light ash.

Quantitative mineralogy was determined by powder XRD with a Siemens D-500 diffractometer using Cu-Kα radiation and a Kevex Psi Si(Li) solid-state detector. Splits of the same powders used for INAA were analyzed; results are listed in Appendices 1-5 and 7-8. Data were obtained on samples ground to <5 μm in an automatic agate Brinkman Micro-Rapid mill. A portion of each sample was mixed with a 1.0-μm corundum internal standard in a sample:corundum ratio of 8:2 by weight. The quantitative mineralogy was determined by the methods of Chung (1974). These methods have been coded into a computer program (QUANT) that accounts for analytical problems important in the analysis of tuffs, altered tuffs, and soils (for example, correction of cristobalite for overlap with albite and tridymite, correction of corundum for overlap with calcite, and correction of clinoptilolite and opal-CT for mutual overlap). Further details of these methods can be found in Bish and Chipera (1988, 1989).

Six root samples were heated for 502 hours under O_2 flow in a LFE Corporation LTA-504 low-temperature asher to determine proportions of ashable organic material. In addition, nine soil samples (four samples of clay-rich Bt horizons and five samples of calcrete) were heated for 266 hours in the same instrument under the same conditions. For the soil samples, both weight loss from LTA ashing and weight regained on cooling in the atmosphere were measured to determine both the amount of ashable organic matter and the weight changes attributable to dehydration/rehydration of inorganic constituents (clay and opal). Chemical analyses (ion chromatography, INAA)

and semi-quantitative XRD data for the ashed root materials are summarized in Appendix 6.

Bulk density determinations were made on rectangular blocks cut from the calcretes and from spring deposits. Densities were determined by dividing the block weights by the measured volumes of the right-rectangular blocks. Results are given in Tables 2 and 3 in section II.D.

Spot quantitative chemical analyses were obtained from thin sections using Cameca CAMEBAX and SX-50 electron microprobes, both operated at 15 kV and 15 na sample current; qualitative chemical data were collected by energy-dispersive scanning electron microscopy (EDS-SEM) at 19 kV.

II. PETROGRAPHIC, LOW-TEMPERATURE ASHING, AND BULK-DENSITY DATA

A. Petrography of Calcrete Laminae, B Soil Horizons, and Plant Roots

The petrographic data collected on calcretes from Exile Hill include thin-section and BSE-SEM analysis of grain size, texture, density, and fossil structures. Petrographic analysis permits mapping of five general types of laminae within the siliceous calcretes. These lamina types are shown in Fig. 2c, 2d, and 3b; more detailed descriptions are given below and in Figs. 5–9. The listing below is arranged in order from laminae with most detritus to laminae with essentially no detritus.

1. Porous and friable ooidal laminae. These contain abundant ooids and pellets (Fig. 5). The term *ooid* is used here to refer to single detrital grains or fragments of recycled calcrete enveloped by concentric layers of calcite and opal, often with some sepiolite (note that in these calcretes the structure of authigenic mineral rims around ooid cores is always concentric, never radial). The term *pellet* is used to describe composite grains of either single or multiple detrital or calcrete fragments encased in fine-grained calcite and opal without internal structure. Pellets are generally larger than ooids (70 μm to 1 mm, av. 520±610 μm for pellets, vs. 50 μm to 1 mm, av. 200±160 μm for ooids). The abundance of inherited rock and min-

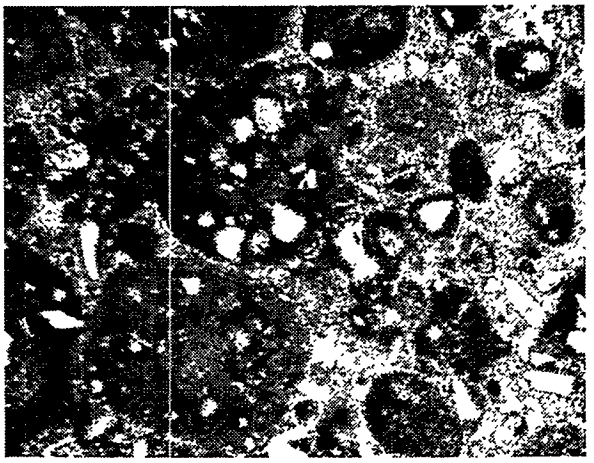

Fig. 5: Photomicrograph of porous, friable lamina with abundant detritus. Pellets composed of multiple detrital grains cemented in rounded, unstructured calcite-opal bodies are abundant in the left side of the image; ooids consisting of single (or few) detrital grains coated by concentric layers of calcite + opal are common in the right side of the image. Horizontal field of view is 2.36 mm.

eral fragments in both ooids and pellets gives these laminae a large component of detritus (for typical samples, 3 to 31%, average 14% detritus).

Within this classification is a relatively rare set of laminae in the vein calcretes that stand out in exposures because they are dark in color. These laminae are largely vertical and, although discontinuous, seldom have low-angle cross-cutting orientations. The dark color of these laminae is due in part to their relatively abundant basaltic ash. However, the bulk of the detritus in these laminae is derived from tuffaceous rocks. Modal analysis of one such lamina shows 48% tuffaceous detritus, 4% basaltic ash, and 48% authigenic calcite plus silica (volume percentages). This is in good agreement with the results of quantitative XRD of this lamina indicating 54% detritus (weight percent). Although detritus-rich, the ooid forms in these *ash-bearing laminae* have thin and poorly developed rinds of authigenic minerals, indicating either young or arrested authigenic mineralization.

2. Root-rich, friable laminae. These are weak and porous and contain abundant root fossils (Fig. 6a). The root fossils in these laminae are generally ~1 mm in diameter or less; coarser root features are not preserved. The characteristic root fossil in these laminae is an opalized root sheath, preserving the cell structure of the *rhizoderm.* The interior cells, constituting the *cortical parenchyma,* are not fossilized, leaving a void that is typically lined by *calcified filaments* (Fig. 6b). These calcified filaments are hollow tubules about 5 μm in diameter and tens of μm long, made up of small, equant, subhedral-to-euhedral calcite crystals <1 μm in size. Within this lining of calcified filaments, the void left by the cortical parenchyma contains extremely delicate splays of *needle-fiber calcites* (Fig. 6c). The needle-fiber calcites are highly elongate calcite crystals, 1–2 μm x 10–150 μm, with elongation ~45° to the crystallographic c-axis. Descriptive references for the terms in italics can be found in Jaillard et al. 1991 (root structure) and in Klappa 1979, Phillips and Self 1987, Wright 1986 and 1989, and Vaniman et al. 1994 (calcified filaments and needle-fiber calcites). Calcified filaments are common in pedogenic calcretes, where they may be formed by a number of microorganisms or by calcite precipitation around root hairs (Klappa 1979). The small diameters and hyphae-like morphology of the calcified filaments, and the demonstration of calcite precipitation by soil fungi in culture experiments (Monger et al. 1991), support a fungal origin for these features. Needle-fiber calcite has been described from a number of pedogenic environments and attributed to calcification of fungal hyphae within decaying roots (Phillips and Self 1987; Wright 1986 and 1989). Also found within some of the root casts are extremely delicate acicular microcrystals, tapering from ~0.5 μm at their bases to points (Vaniman et al. 1994). This fossil form can develop within fungal hyphae and consists of either calcite or Ca-oxalate crystals (Klappa 1979; Simkiss and Wilbur 1989). The root-rich, friable calcrete laminae have variable amounts of rock and

mineral fragments, giving them a range of detrital-mineral contents (0 to 13%, av 5% detritus).

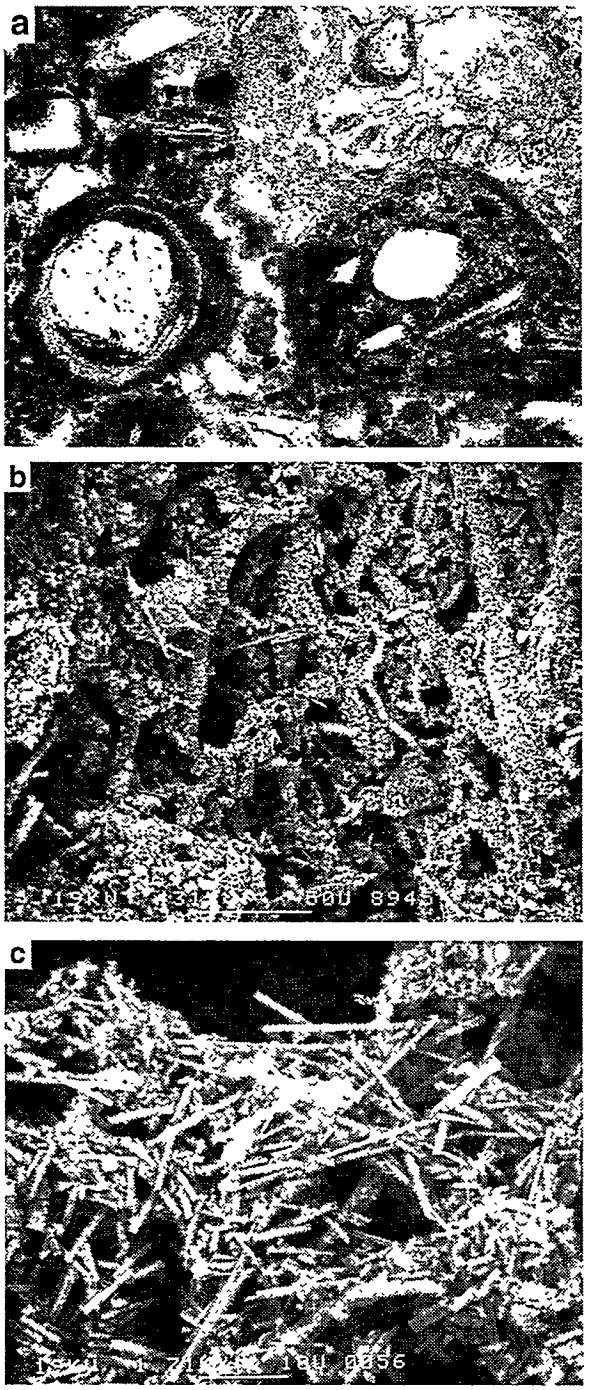

Fig. 6: (**a**) Photomicrograph of root-rich, friable lamina with ooid (lower left), pellet (lower right), and root fossil (upper right). Horizontal field of view is 1.18 mm. (**b**) Scanning electron micrograph of calcified filaments from within a root fossil. Scale bar is 50 μm. (**c**) Scanning electron micrograph of needle-fiber calcites from within a root fossil. Scale bar is 10 μm.

3. Dense and resistant laminae. These often show evidence of shearing within the vein calcretes (Fig. 7a). The laminae consist of densely intergrown fine-grained (<5 μm) calcite plus opal; they constitute the hardest component in the calcretes, appearing dense in hand sample with vitreous luster and brown to white color. Evidence of shearing is best seen in thin section as a sigmoidal fabric within some of the dense laminae. Interestingly, these dense laminae also commonly contain root fossils, like the root-rich, friable laminae that are much softer (see above). However, the root fossils within the dense laminae include both the delicately opalized roots described above, with calcified filaments and needle-fiber calcites, in dense laminae that are unsheared (Fig. 7b), as well as root fossils in which the cells of the cortical parenchyma are sometimes outlined by opal (and/or sepiolite) and often filled by calcite crystals (Fig. 7c). Other root fossil forms include relicts of calcareous fossilization in which the root fossil and its surroundings have been opalized. As in the root-rich, friable laminae described above, root fossils larger than ~1 mm are not preserved. The dense and resistant laminae generally have few detrital rock or mineral grains (0 to 9%, av 2% detritus).

4. Rare sepiolite-plus-calcite laminae. Sepiolite, a chain-structure clay mineral [$Mg_4(Si_2O_5)_3(OH)_2{\cdot}6H_2O$], is common in all of the laminae described above, but

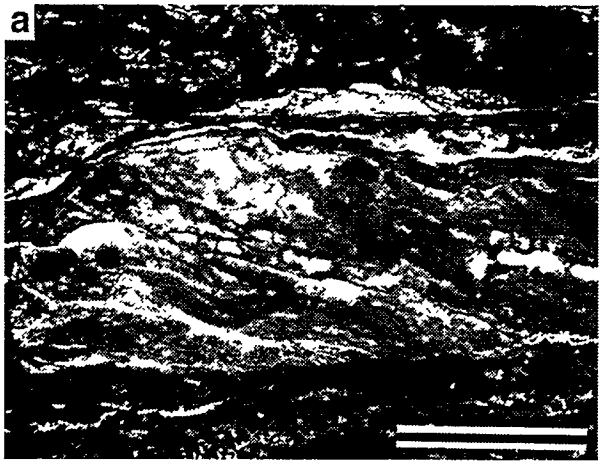

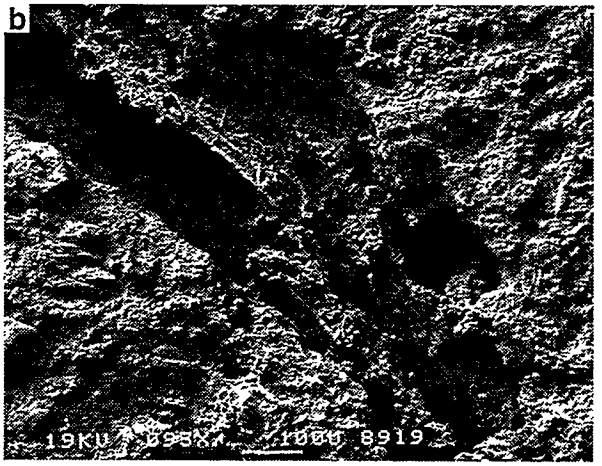

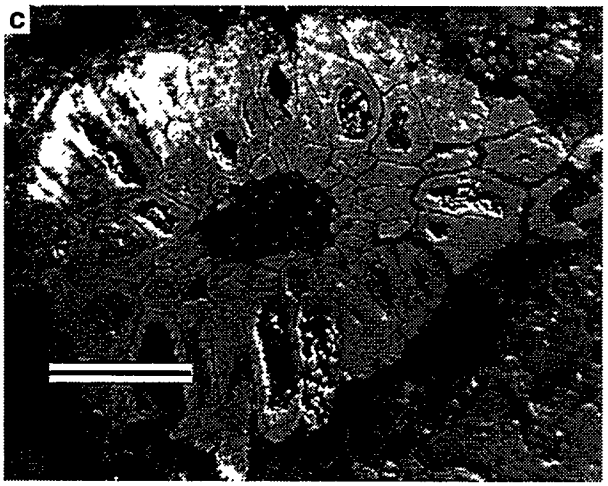

Fig. 7: (a) Photomicrograph of dense, resistant lamina. Scale bar is 1 mm long. (b) Scanning electron micrograph of an open root fossil in a dense lamina, showing calcified filaments that drape the walls of the open structure. Scale bar is 100 μm. (c) Scanning electron micrograph of a root fossil cross-section showing cell walls replaced by calcite, with some cell interiors replaced by opal and with septae of sepiolite between the cells. Scale bar is 200 μm.

only in abundances less than ~5%. There are a few small discontinuous laminae with higher sepiolite concentrations and there is one sample block from the south wall of Trench 14 in which a late-formed lamina of intergrown calcite-plus-sepiolite (Fig. 8) drapes earlier laminae in a small-scale unconformity (Fig. 2c). Parts of this lamina contain 39% sepiolite, 61% calcite, and essentially no detritus (sample 1,p13 in Appendix 5).

5. Laminae of pure opal. These are discontinuous and thin, and occur within fractures, particularly in the vein calcretes (Fig. 9). These opaline laminae provide the only authigenic minerals that can readily be separated from other authigenic minerals in the calcretes; the other common authigenic minerals (calcite and sepiolite) are too fine-grained and too intimately

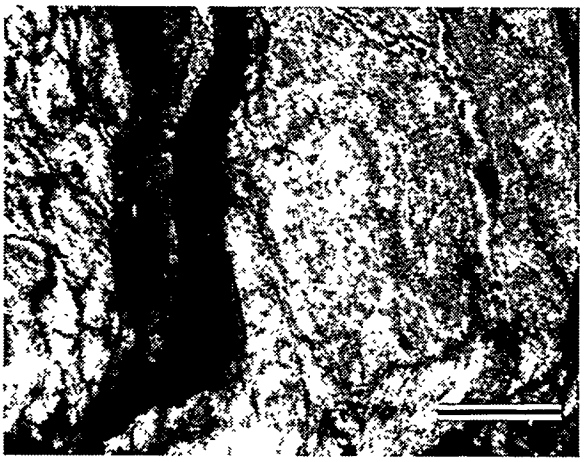

Fig. 8: Photomicrograph of sepiolite-plus-calcite lamina (right) that drapes calcrete block LANL#1 (see Fig. 2c). Scale bar is 250 μm.

intergrown to be separated. In all other laminae, the opal is also too intimately intergrown with fine-grained calcite to be separated. In contrast, the pure opaline laminae may be a few millimeters wide and several centimeters long. Most of these laminae occur in open fractures and have a botryoidal surface morphology indicating precipitation against one wall of the fracture and outward growth into the fracture void. Both opal-A (amorphous silica) and opal-CT (largely amorphous but with both cristobalite-like and tridymite-like stacking) can occur as pure laminae. These laminae contain no detectable detritus (sample 245,p2 in Appendix 4 and sample 349,p1 in Appendix 5).

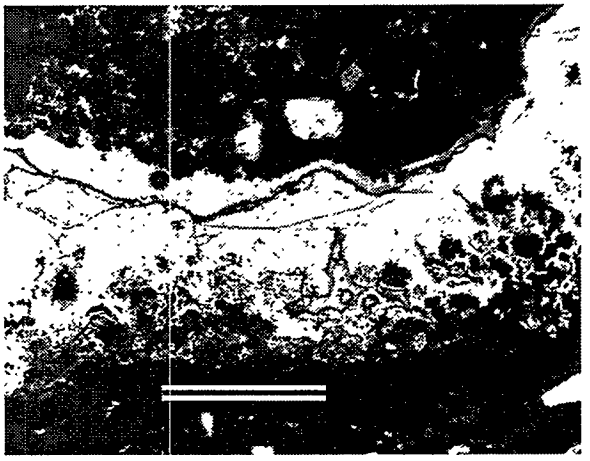

Fig. 9: Photomicrograph of pure opal lamina (opal-A) from within calcrete block LANL#1 (see Fig. 2c). Scale bar is 0.5 mm.

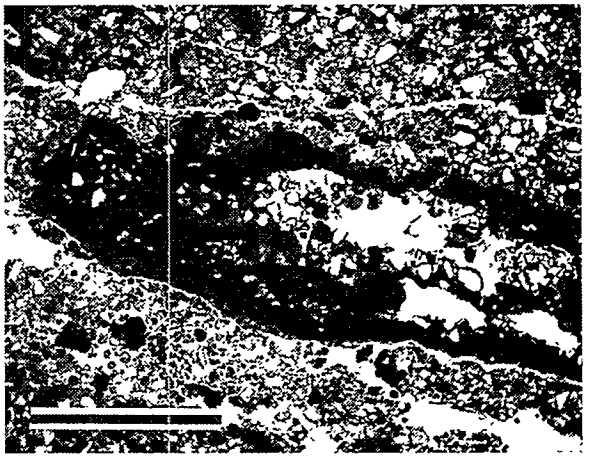

Fig. 10: Photomicrograph of opalized root fossil from 2Btj soil horizon in LANL#430. Scale bar is 2 mm.

In addition to the petrographic analysis of calcrete laminae, thin-section and/or SEM studies were made of the overlying B soil horizons and of plant roots from some of the species currently growing at Exile Hill (creosote bush— *Larrea divaricata*; Mormon tea or Nevada joint fur—*Ephedra nevadensis*; and desert thorn or twin fruit—*Menodora spinescens*) and some that have been inferred to have grown in the vicinity under past pluvial climates (piñon—*Pinus monophylla*; juniper—*Juniperus osteosperma*). Further discussion of these and other plants, with their relevance to the calcretes at Exile Hill, can be found in Quade and Cerling (1990).

In the B-horizon soils (Fig. 2b), weathered detrital grains are abundant and include both vitric and devitrified tuff fragments as well as mineral fragments of quartz, tridymite, cristobalite, alkali feldspars, biotite, pyroxenes, amphiboles, Fe,Ti-oxide minerals, sphene, and zircon. The principal authigenic mineral is a dispersed clay; opal is seldom visible, but can be seen associated with calcite in deposits that drape the undersides of pebbles. In the lower (2Btj) horizon, above the calcrete, opalized root fossils occur with a form (Fig. 10) similar to those that occur in the underlying root-rich, friable laminae of the calcretes (see above).

The petrographic observations on roots from living plants are limited; most of the plant solids are amorphous and although whewellite [$CaC_2O_4 \cdot 2H_2O$] occurs as a mineral in all of the roots studied, it is seldom visible as discrete crystals. The sole exception is in the roots of the creosote bush, where whewellite can be seen as equant crystals (Fig. 11).

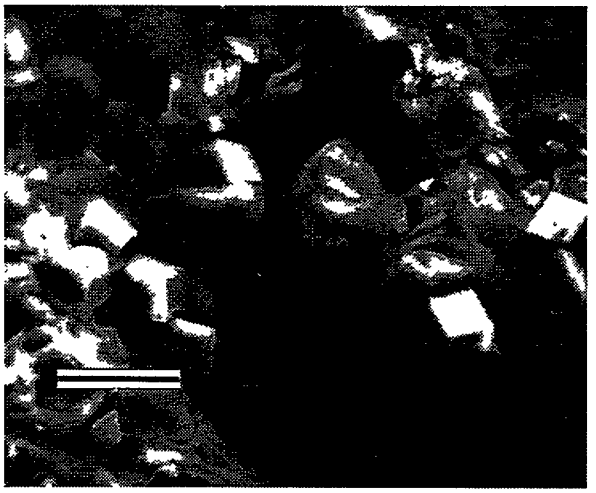

Fig. 11: Scanning electron micrograph of equant whewellite crystals in root sample LANL#351 (inner part of creosote bush root). Scale bar is 200 μm.

B. Comparative Petrography: Spring Deposits

Spring deposits of the Amargosa Valley and Death Valley, as well as calcified plant material from a seep at Crater Flat, were studied for comparison with the calcite-silica deposits at Exile Hill. The localities sampled represent both active springs (GMC, Grapevine, and Nevares springs) and fossil springs (site 199 in south Crater Flat, IMV spring, and Travertine Point). Both veins and surface deposits were studied. These localities are shown in Fig. 1a.

The vein deposits and tufa mounds associated with spring activity are laminated, but the laminae are markedly different from those observed in the calcretes. Laminated vein deposits at spring localities typically include mm-scale or finer bands that represent growth bands within splays of calcite crystals that radiate from the fracture walls toward the vein center. Alternations in texture, crystal size, and morphology typically parallel the fracture walls (Fig. 12a). Massed growths of fibrous calcites are common, although in some veins individual crystal sizes range up to 1 cm or more (Fig. 12b). The laminae in tufa mounds are developed without the fine growth banding seen in the veins but contain instead a variety of fine-grained calcite textures (Fig. 13). Most spring deposits contain fossil remnants of a wide range of organisms, ranging from bacteria and algae to encrusted remains of vascular plants (Pentecost 1992). Common in the surface deposits of springs in the vicinity of Yucca Mountain are bacterial clumps (Fig. 13a) and ostracod shells (Fig. 13b). Chafetz and Folk (1984) identified bacterial clumps— brownish spots included within single crystals or aggregates of sparry calcite, 10 to 60 μm in diameter—as the elementary building blocks of travertines. Such features are typical of spring mounds in the vicinity of Yucca Mountain (Fig. 13a), but not of the calcretes at Exile Hill.

The fossilized remains of vascular plants in spring deposits of the vicinity are particularly important because they contrast markedly with those found in the calcretes

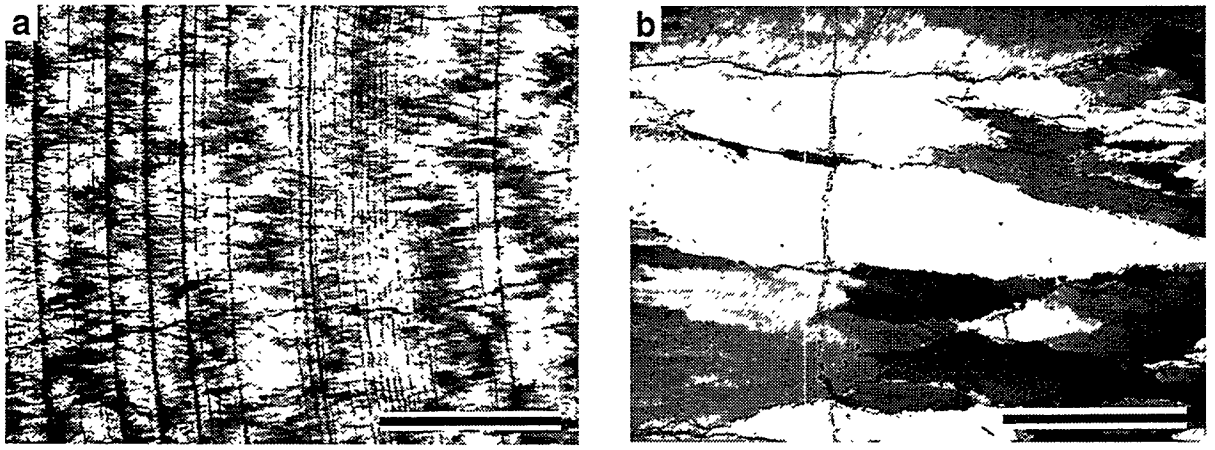

Fig. 12: Photomicrographs of (**a**) fibrous-structure vein calcite and (**b**) massive vein calcite from Travertine Point. Both photomicrographs are from the same thin-section of a single sample (LANL#755). Scale bars are 2 mm.

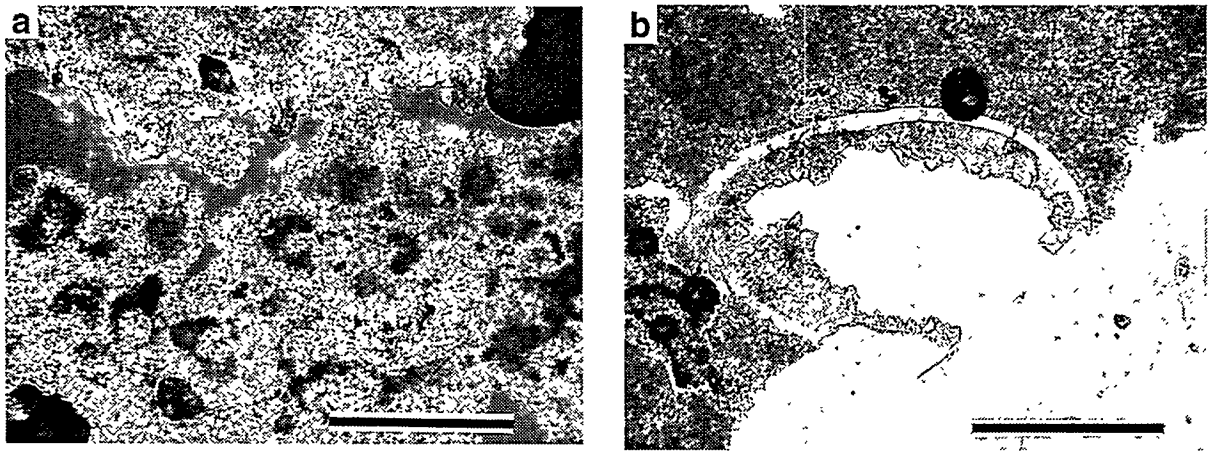

Fig. 13: Photomicrographs of (**a**) bacterial clumps (ref. Chafetz and Folk 1984) and (**b**) ostracod fossil from the Nevares spring mound (LANL#760). Calcite forming the ostracod shell is exceptionally Sr-rich; microspar lining the interior of the ostracod shell is Mg-rich (Table 4). Scale bar in each photomicrograph is 200 μm.

at Exile Hill. Root fossils are typical of the calcretes at Exile Hill, with common preservation of calcified filaments and needle-fiber calcites (Fig. 6). In contrast, plant remains associated with spring discharge in the region are dominated by calcite casts that have formed around the stems of plants, preserving none of the cell structure and lacking the delicate filaments and needle-fibers that are characteristic of the calcretes. Meniscal septae, formed by small calcite crystals that formed by precipitation at the water/air interface are indicative of standing water between and within the fossilized plant remains (Fig. 14a). The root fossil from the seep at Site 199 has complete calcite replacement of the root form with poor preservation of cellular structure but with abundant bacterial clumps (Fig. 14b). Features like this are not found in any of the calcretes at Exile Hill.

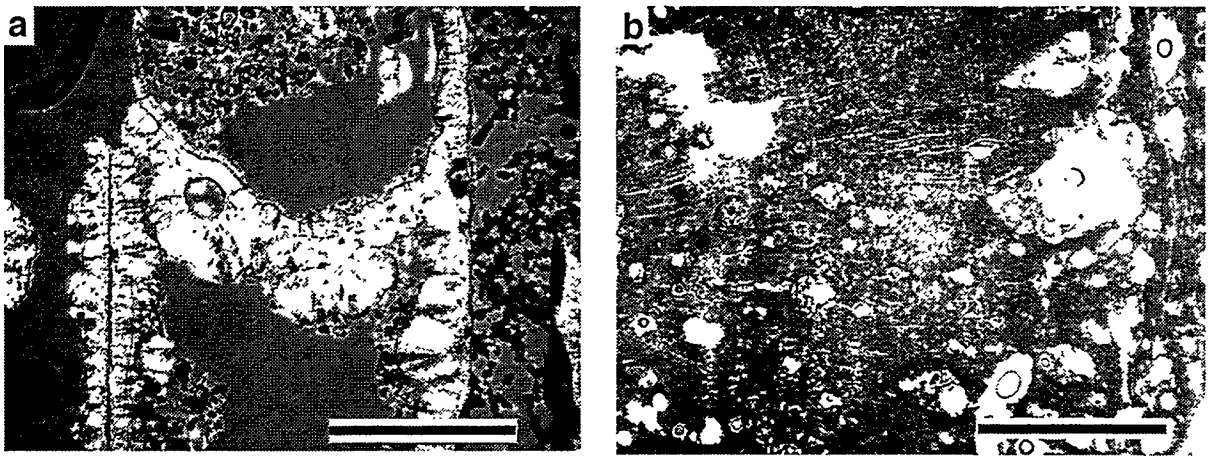

Fig. 14: (a) Photomicrograph of fossilized plan stem from the Nevares spring mound (LANL#762). Stem walls (vertical) provided nucleation sites for radial-fabric calcite; concave-upward meniscal forms can occur both within and between stems. Note abundance of loosely cemented bacterial clumps (see Fig. 13a). (b) Photomicrograph of fossilized root from the seep at Site 199 (LANL# 251; see Fig. 1a). Radial fabric extends from root center at left to concentric fabric at root rim on right. Note that fine-scale cell structure is very poorly preserved, because fossilization is principally by bacterial clumps of about 30 μm diameter. Fossilization is by Mg-rich calcite with minor amounts of dolomite (Table 4). Scale bar in each photomicrograph is 2 mm.

C. Low-Temperature Ashing of Roots and Calcretes

The results of low-temperature ashing (LTA) of root samples are illustrated in Fig. 15. The LTA process removes organic C, H, and N from plant material by oxidation under gentle microwave heating; the remaining material consists of amorphous and crystalline ash constituents of the roots. The weight fractions of mineral material in desiccated root samples (roots that had been removed from the ground for several months) range from 4% (piñon) to 14% (outer sheath of creosote root). These results, derived from the data illustrated in Fig. 15, are listed as the ash/root weight fraction in Appendix 6.

Several calcrete and B-horizon soil samples were also heated by LTA to determine the content of oxidizable organic matter in these samples. Results are shown in Fig. 16. These samples were found to regain weight after LTA treatment; this behavior is attributable to the high clay content in these samples. Clay content correlates with the percentage of weight regained after LTA (Fig. 17). The net final weight loss for most calcrete

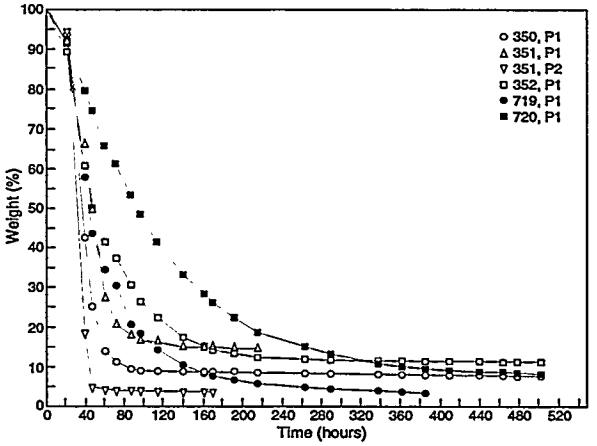

Fig. 15: Percentage weight loss versus time in LTA of root samples.

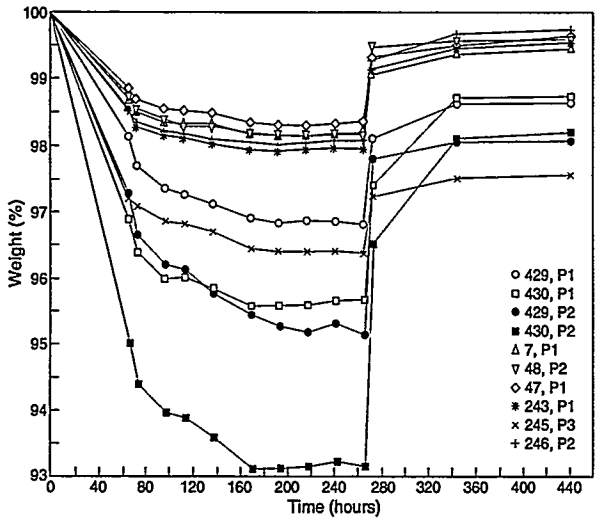

Fig. 16: Weight variation in LTA for calcretes (LANL samples 7, 47, 48, 243, 245, and 246) and B soil horizon samples (LANL samples 429 and 430; p1=<425 μm and p2=<45 μm). Samples were removed from LTA and allowed to rehydrate at 266 hours.

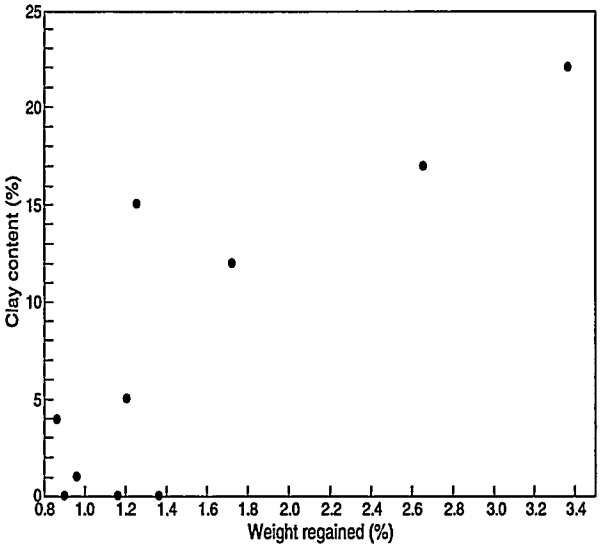

Fig. 17: Weight regained by calcrete and B soil horizon samples after LTA treatment, versus clay content (cf. Fig. 16).

samples, attributable to organic components, is ~0.5%. An exception is one of the dense laminae from the slope calcretes (sample 245,p3) of Trench 14, with a net final weight loss of ~2.5%. The results from this sample suggest that a few laminae may be higher than others in oxidizable organic matter, although the bulk or channel samples, averaged across several laminae, are not (samples 7,p1; 47,p1; 243,p1). The B-horizon soil samples have net oxidizable organic-matter contents of ~1.3–2.0%.

D. Bulk-Density Data

The bulk densities of calcrete samples were determined from measured blocks. Right-rectangular blocks of calcrete samples from Trench 14 were sawed, dried at 50°C, measured, and weighed. The volume, weight, and bulk-density data are listed in Table 2.

Comparable measurements were made of the bulk densities of spring deposits; these data are shown in Table 3. All vein samples from the spring deposits analyzed have bulk densities ≥2.5; the coarsely banded vein from Travertine Point (LANL #756) has a density close to that of ideal calcite (2.7). Porous surface deposits at active springs, such as Nevares (LANL #760), can have lower densities that are close to those found in the dense calcrete lamellae (LANL #49, Table 2).

E. Mineralogic Data

1. Mineralogy of calcite-silica deposits at Exile Hill. The quantitative mineralogic data collected by XRD for samples from Exile Hill are summarized in Appendices 1 to

TABLE 2. Bulk Densities of Calcrete Samples from Trench 14

sample	type	weight (g)	volume (cm^3)	bulk density (g/cm^3)
LANL #7	bulk vein calcrete	33.1745	21.0	1.6
LANL #49	dense calcite-opal lamina in vein calcrete	1.2950	0.7	1.9
LANL #244	ooidal-porous lamina in slope calcrete	3.7955	2.7	1.4
LANL #245	bulk slope calcrete	12.4890	7.8	1.6
LANL #246	root-rich lamina in slope calcrete	4.8616	3.1	1.6
				av. 1.6 ± 0.2

TABLE 3. Bulk Densities of Spring Deposits

sample	location/type	weight (g)	volume (cm^3)	bulk density (g/cm^3)
LANL #753	IMV Spring/ opal-CT	66.6490	26.2	2.5
LANL #754	Travertine Point/ finely-banded calcite vein	8.6485	3.4	2.5
LANL #756	Travertine Point/ coarse-banded calcite vein	90.8592	34.2	2.7
LANL #760	Nevares Spring/ calcite mound	19.2067	9.4	2.0
LANL #766	Grapevine Spring/ black calcite vein	17.1716	6.8	2.5

5, with semi-quantitative root mineralogy in Appendix 6. The only pure mineral separates obtained from the calcretes have been of opal, from the opaline laminae mapped in Figs. 2c, 2d, and 3b. Large opaline root fossils have also been collected from sand ramps east of Exile Hill (Vaniman et al. 1988). In all other calcrete laminae, calcite and opal, or calcite and sepiolite, are closely intergrown. Calcite crystals are small—most (>95%) are <5 μm. Attempts to obtain pure calcite separates by crushing and density separation have failed because of intimate intergrowth with other minerals. Sepiolite is locally abundant (~40%) in only a few laminae (Fig. 2c); the overall abundance of sepiolite and amorphous Fe, Mn, and Ti oxides is <1%. Rare evaporite minerals (gypsum and halite) have been found in the B soil horizon in Trench 14C (Fig. 1b).

Quantitative XRD provides a direct measurement of calcite, clay, and igneous mineral abundances in rocks and soils at Exile Hill. Although both opal-A and opal-CT are recognized in the XRD data, opal-A abundance must be determined by difference from 100%, using internal-standard methods. The errors introduced in this manner are primarily those of ignoring volcanic glass and organic material that have amorphous

diffraction properties similar to opal-A; the opal-A values for soil samples in the Appendix tables are therefore maximum contents. Nevertheless, petrographic analysis indicates a low abundance of volcanic glass (<2%) and low-temperature ashing indicates <3% ashable organic material in the calcretes and in the size fractions of Bt horizons described here (see above, section II.C on Low-Temperature Ashing of Roots and Calcretes). The opal-A values cited are therefore believed to be accurate within the errors listed in the Appendix tables. The authigenic calcrete constituents are described below by mineral or amorphous-material type; smectite is included in this list, even though it may be both an authigenic and allogenic mineral in the B soil horizons and calcretes. The mineralogy of the detritus is complex; complete descriptions of the detrital minerals are not dealt with in this paper because they do not affect the conclusions, although the relevant heavy-mineral constituents (especially hematite and amphibole) are described in section IV, Discussion.

a. Calcite. Calcite is the most abundant authigenic mineral in the calcretes. Calcite contents of the calcretes, determined by quantitative XRD, range from 26% to 70% for individual laminae (with the exception of ash-bearing laminae, containing only 17% calcite, and pure opaline laminae containing no calcite). Averages representing multiple laminae (bulk or channel samples) contain 47% to 59% calcite. There are no pure-calcite laminae, and (as noted above) the fine grain size and intimate intergrowth of calcite with other minerals made separation and concentration of calcite impractical. Contrasted with its abundance in the calcretes, calcite is only a rare constituent of the overlying B horizons (Appendix 3). Calcite can be seen in hand sample and in thin section in the Btk horizon as fine-grained coatings on the undersides of pebbles, where the calcite is commonly associated with opal. The very low calcite contents reported for B-horizon soil samples in Appendix 3 (<1%) are in part a result of sample selection, because the >425 μm size fraction, containing the partially calcite-coated pebbles, was not crushed to be included in the XRD analysis.

Although chemical compositions of pure calcite in the calcretes could not be determined on mineral separates, some of the calcites in thin section are large enough (>10 μm) to permit electron-microprobe analysis. Calcite analyses from the calcrete are listed in Table 4, along with calcite and dolomite analyses from the seep at Site 199 and calcite analyses from several springs. Calcite is the only significant reservoir for Ca and for Sr in the calcretes; even though calcite could not be separated for analysis, the chemical and quantitative-XRD data for the calcretes (Appendices 1, 4, and 5) can be used to plot Sr, against either percent CaO (with 56% CaO representing ideal calcite) or against the XRD-determined percent calcite, to estimate the range of Sr contents in calcites of the calcretes. The results are shown in Fig. 18a and 18b. The range of Sr contents in calcite of the calcretes is ~800 to 2100 μg/g, excluding samples with Sr-

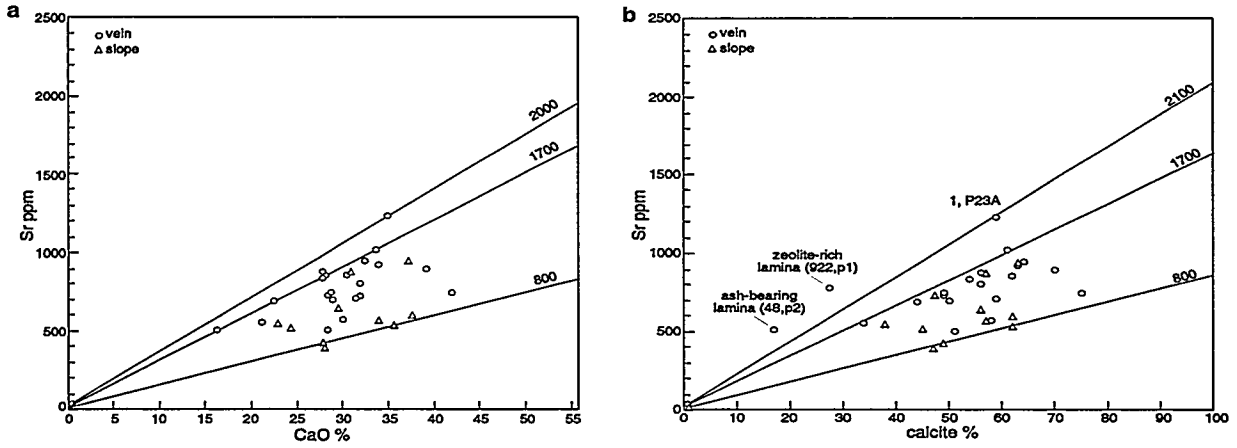

Fig. 18: (**a**) Content of Sr versus weight-percent CaO (by INAA) and (**b**) content of Sr versus weight-percent calcite (by XRD). These two plots, using independent measures of the content of authigenic calcite, indicate a consistent range of 800 to 2000–2100 μg/g Sr in authigenic calcites of both slope and vein calcretes, although the vein calcretes have a somewhat higher average Sr content.

rich basaltic ash or zeolites. Comparable Sr contents are found in calcites of the Site 199 seep and in the spring deposits (Appendix 7). The coarsest calcite observed in the calcretes of Trench 14 (anhedral crystals of up to ~60 μm intergrown in open voids of sample 49) have no detectable Sr in electron microprobe analysis (Table 4), although Fig. 18 indicates that the more typical, fine-grained calcites of the calcrete should have SrO contents ranging from ~0.09 to 0.25%. Earlier electron microprobe analyses of relatively coarse calcite from Trench 14 do report detectable SrO at the lower end of this range (Vaniman et al. 1988), but the highest SrO contents apparently occur in the more abundant, fine-grained calcites that are too small (<5 μm) for electron microprobe analysis. It is worth noting that the highest SrO contents observed in any sample are in ostracod fossils from the spring mound at Nevares (sample 760,t1a; Table 4).

b. Opal. The calcretes at Exile Hill are siliceous, containing variable amounts of opaline silica. The forms of opal in these deposits include both opal-A and opal-CT. Opal contents of individual calcrete laminae range from 0% to 57% (with the exception of ~100% pure opaline laminae). Averages representing multiple laminae (bulk or channel samples) contain 31% to 42% opal. Pure opaline laminae in the calcretes occur as both opal-A and opal-CT; INAA chemical analyses of both kinds of opal from the calcretes are reported in Appendix 4 (opal-CT from a slope calcrete) and in Appendix 5 (opal-A from a vein calcrete). Electron microprobe data from opals in the calcretes indicate only minor amounts of Al_2O_3 (<0.2%).

c. Sepiolite. Sepiolite is ubiquitous in the calcretes, but only reaches significant abundances (up to 39%) in rare laminae, where sepiolite is intergrown with calcite in pods several millimeters in length (Fig. 8). Elsewhere in the calcretes sepiolite can occur within ooid rims, as a component of fossilized roots, as small fibrous deposits, or

TABLE 4. Electron Microprobe Analysis of Corase (≥50 μm) Calcites

sample:	49,t1a	49,t1a	251,t1a1	251,t1a2	750,t1a	750,t2a	753,t1a	753,t1a
locality:	Trench 14 calcrete	Trench 14 calcrete	Site 199 seep	Site 199 seep	GMC spring mound	GMC spring mound	IMV spring	IMV spring
				weight percent oxides				
CaO	54.3	56.4	29.8	50.0	56.0	55.7	55.4	54.0
MgO	0.88	0.20	22.5	5.59	0.42	0.33	0.91	1.06
FeO	0.0	0.0	0.0	0.0	0.0	0.0	0.0	0.0
MnO	0.0	0.0	0.0	0.04	0.0	0.0	0.0	0.0
SrO	0.0	0.0	0.0	0.22	0.0	0.0	0.0	0.0
BaO	0.0	0.0	0.0	0.0	0.0	0.0	0.0	0.0
*CO_2	44.8	43.4	47.7	44.1	43.5	43.9	43.7	44.9
				cation formulae normalized to 3 oxygens				
Ca	0.960	1.011	0.489	0.881	1.002	0.995	0.989	0.954
Mg	0.022	0.005	0.515	0.137	0.010	0.008	0.023	0.026
Fe	0.000	0.000	0.000	0.000	0.000	0.000	0.000	0.000
Mn	0.000	0.000	0.000	0.001	0.000	0.000	0.000	0.000
Sr	0.000	0.000	0.000	0.002	0.000	0.000	0.000	0.000
Ba	0.000	0.000	0.000	0.000	0.000	0.000	0.000	0.000
*C	1.009	0.992	0.998	0.990	0.993	0.998	0.994	1.010
Σ	1.991	2.008	2.002	2.011	2.005	2.001	2.006	1.990

sample:	754,t1	754,t1	755,t1a	755,t1a	755,t1a	766,t1a	760,t1a	760,t1a
locality:	Travertine-Point Vein	Travertine-Point Vein	Travertine-Point Vein	Travertine-Point Vein	Travertine-Point Vein	Grapevine-Spring Vein	Nevares Spring Mound	Nevares Ostracod Fossil
				weight percent oxides				
CaO	54.1	54.8	52.5	52.3	53.4	53.3	54.2	54.3
MgO	1.64	0.26	2.47	2.63	1.53	1.90	2.06	0.33
FeO	0.0	0.0	0.0	0.0	0.0	0.0	0.0	0.0
MnO	0.0	0.0	0.0	0.0	0.0	0.0	0.0	0.0
SrO	0.0	0.0	0.14	0.26	0.0	0.11	0.0	0.46
BaO	0.0	0.0	0.0	0.0	0.0	0.0	0.0	0.0
*CO_2	44.2	44.9	44.9	44.7	45.0	44.7	43.7	44.9
				cation formulae normalized to 3 oxygens				
Ca	0.960	0.970	0.924	0.922	0.941	0.940	0.964	0.961
Mg	0.040	0.006	0.060	0.064	0.037	0.047	0.051	0.008
Fe	0.000	0.000	0.000	0.000	0.000	0.000	0.000	0.000
Mn	0.000	0.000	0.000	0.000	0.000	0.000	0.000	0.000
Sr	0.000	0.000	0.001	0.002	0.000	0.001	0.000	0.004
Ba	0.000	0.000	0.000	0.000	0.000	0.000	0.000	0.000
*C	0.999	1.012	1.007	1.005	1.011	1.006	0.992	1.013
Σ	1.999	1.988	1.992	1.993	1.989	1.994	2.007	1.986

*CO_2 and C by difference

as clasts reworked into later-formed calcretes. The abundances of sepiolite in individual laminae containing these other occurrences do not exceed 5%. Sepiolite can also occur in the hematite-altered tuffs within and adjacent to the calcretes (Appendix 2). Sepiolite has not been found in the B-horizon soil samples. Representative electron microprobe analyses of sepiolite are listed in Table 5. As with other hydrous minerals, water is estimated by difference and may be lost by volatilization during analysis. These analyses are therefore constrained by summing the measurable cations (Si, Al, Fe, Ca, Mg, Na, and K) to equal 10 in the ideal sepiolite formula: $Mg_4(Si_2O_5)_3{\cdot}(OH)_2{\cdot}6(H_2O)$, or $4MgO+6SiO_2+7H_2O$. The quality of analysis is best evaluated by examination of how close the Si content is to 6 and how close the Mg content is

to 4, although some substitution of Al for Si is suggested in several of the sepiolite analyses and most samples have significant substitution of Al, Fe, Ca, Na, and/or K for Mg. The sepiolite clast in thin section 1,t11 is notably Fe-rich and the clast in thin section 4,t1 is Al-rich. In contrast, the sepiolite of the mappable sepiolite lamina (Fig. 2c) is closer to the ideal Si-Mg composition. From these data it is apparent that there is a range of sepiolite compositions in the calcretes.

TABLE 5. Electron Microprobe Analyses of Sepiolites from Trench 14 Calcretes

sample:	1,t11	1,t11	4,t1	4,t1	4,t1	1,t13	1,t13	1,t13
type:	sepiolite clast	sepiolite clast	sepiolite clast	sepiolite clast	sepiolite clast	large sepiolite lamina	large sepiolite lamina	small sepiolite lamina
				weight percent oxides				
SiO_2	55.7	55.0	56.3	52.3	53.7	57.0	56.1	56.6
Al_2O_3	1.15	1.21	2.72	2.51	2.26	0.28	0.44	0.37
TiO_2	0.0	0.0	0.0	0.0	0.0	0.0	0.0	0.0
Fe_2O_3	5.41	4.60	0.0	0.0	0.0	0.0	0.0	0.0
MnO	0.00	0.0	0.0	0.0	0.0	0.0	0.0	0.0
CaO	0.31	0.29	0.0	0.0	0.0	0.14	0.31	0.22
MgO	20.0	19.4	23.7	22.0	22.4	25.2	24.9	24.0
Na_2O	0.41	0.47	0.0	0.0	0.0	0.15	0.14	0.21
K_2O	0.29	0.30	0.0	0.0	0.0	0.08	0.11	0.09
*H_2O	16.7	18.8	17.3	23.2	21.6	17.1	18.0	18.5
				cation formulae normalized to 10 cations (excluding H)				
Si	6.026	6.085	5.933	5.938	5.979	5.974	5.941	6.049
Al	0.147	0.158	0.338	0.336	0.297	0.035	0.055	0.047
Ti	0.000	0.000	0.000	0.000	0.000	0.000	0.000	0.000
Fe	0.440	0.383	0.000	0.000	0.000	0.000	0.000	0.000
Mn	0.000	0.000	0.000	0.000	0.000	0.000	0.000	0.000
Ca	0.036	0.035	0.000	0.000	0.000	0.016	0.035	0.025
Mg	3.225	3.196	3.727	3.720	3.714	3.934	3.924	3.820
Na	0.086	0.101	0.000	0.000	0.000	0.030	0.029	0.044
K	0.040	0.042	0.000	0.000	0.000	0.011	0.015	0.012
*H_2O	6.016	6.924	6.064	8.768	8.026	5.974	6.360	6.609

*H_2O by difference

d. Amorphous Fe, Mn, and Ti oxides. Voids in the vein calcretes of Trench 14 may contain fillings or linings of amorphous Fe, Mn, or Ti oxides. These deposits are a minor constituent of the vein calcretes (generally <1%), but they can be a significant reservoir for Fe and associated elements (esp. Sc) because of their often high Fe contents. The possibility of some crystallinity within these features can not be ruled out, but the compositions of these metal-rich deposits are highly variable, suggesting largely amorphous composition or a fine-grained mixture of poorly crystalline phases (Table 6). The electron microprobe data in Table 6 also suggest some intergrowth of calcite

and opal with these oxide deposits, as well as intermixtures of lesser amounts of Mg and Al, particularly within the more Mn-rich deposits. In some instances, these deposits appear to fill root-fossil voids (Fig. 19a); in other instances they replace ooid rims or line cavities and fractures in the calcretes (Figs. 19b-c). The chemical data in Table 6 separate these opaque deposits into three types (Fig. 19d): Fe-rich deposits with minor amounts of Mg; Ti-rich deposits with minor amounts of Al; and complex Mn-rich deposits with appreciable amounts of Si, Al, and Mg. Amorphous metal oxides also occur in the slope calcretes and in the B-horizon soil samples, but they appear to be even less common there than they are in the vein calcretes.

TABLE 6. Electron Microprobe Analyses of Amorphous Fe, Mn, and Ti oxides from Trench 14 Calcretes

sample:	1,t10	1,t10	1,t3	7,t2	7,t2	7,t2	7,t3	7,t3
type:	Fe-rich	Fe-rich	Fe-rich	Mn-rich	Mn-rich	Ti-rich	Ti-rich	Ti-rich
SiO_2	6.62	10.4	9.64	29.3	49.9	5.00	6.08	4.82
Al_2O_3	1.09	1.41	1.26	2.12	2.04	5.20	5.16	4.14
TiO_2	0.0	0.0	0.0	0.17	0.08	81.0	72.9	78.3
Fe_2O_3	75.4	48.0	57.7	0.74	0.66	0.0	0.0	0.43
MgO	0.79	1.24	1.09	2.28	3.49	0.0	0.0	0.0
MnO	0.13	0.23	0.25	35.5	11.1	0.0	0.0	0.0
CaO	2.88	4.80	4.15	3.7	1.56	0.70	0.70	0.30
K_2O	0.0	0.0	0.0	0.16	0.19	0.0	0.0	0.0
Na_2O	0.55	0.56	0.17	0.49	0.23	0.31	0.33	0.30
diff.	12.5	33.3	25.7	25.6	30.7	7.74	14.8	11.7

In addition to the elements listed in Table 6, energy-dispersive spectra of some Fe-rich amorphous deposits indicate minor amounts of S, Cu, Zn, and perhaps Ni. These are many of the same elements that are highly elevated in the root ash samples from Exile Hill (Appendix 6).

e. Smectite. Smectite clays are more abundant in the calcretes of Trench 14A than they are in Trench 14. The calcretes of Trench 14A contain up to 34% smectite, whereas the calcretes of Trench 14 contain no more than 10% smectite and generally <5%. At Trench 14, smectite contents of 9–12% are found in the <425 μm size fractions of B-horizon soil samples from above the calcretes. The Btk horizon also contains 6% illite. Clays were separated from the B-horizon soil samples at Trench 14 for further characterization (samples 429,p3 and 430,p3; Appendix 3).

XRD analyses of the separated clays indicate poor crystallinity. What appears as a well-crystallized illitic component in the 1–3 μm fraction is much degraded in the <0.35 μm fraction (Fig. 20). This poorer crystallinity with finer grain size, plus the exceptionally Fe-rich composition of the finest (<0.35 mm) clay fraction (>5% FeO; see the analyses of Btk and 2Btj clay separates in Appendix 3), indicate that the "illitic" component is in fact largely due to degradation of detrital biotite. Much of the clay may be eolian.

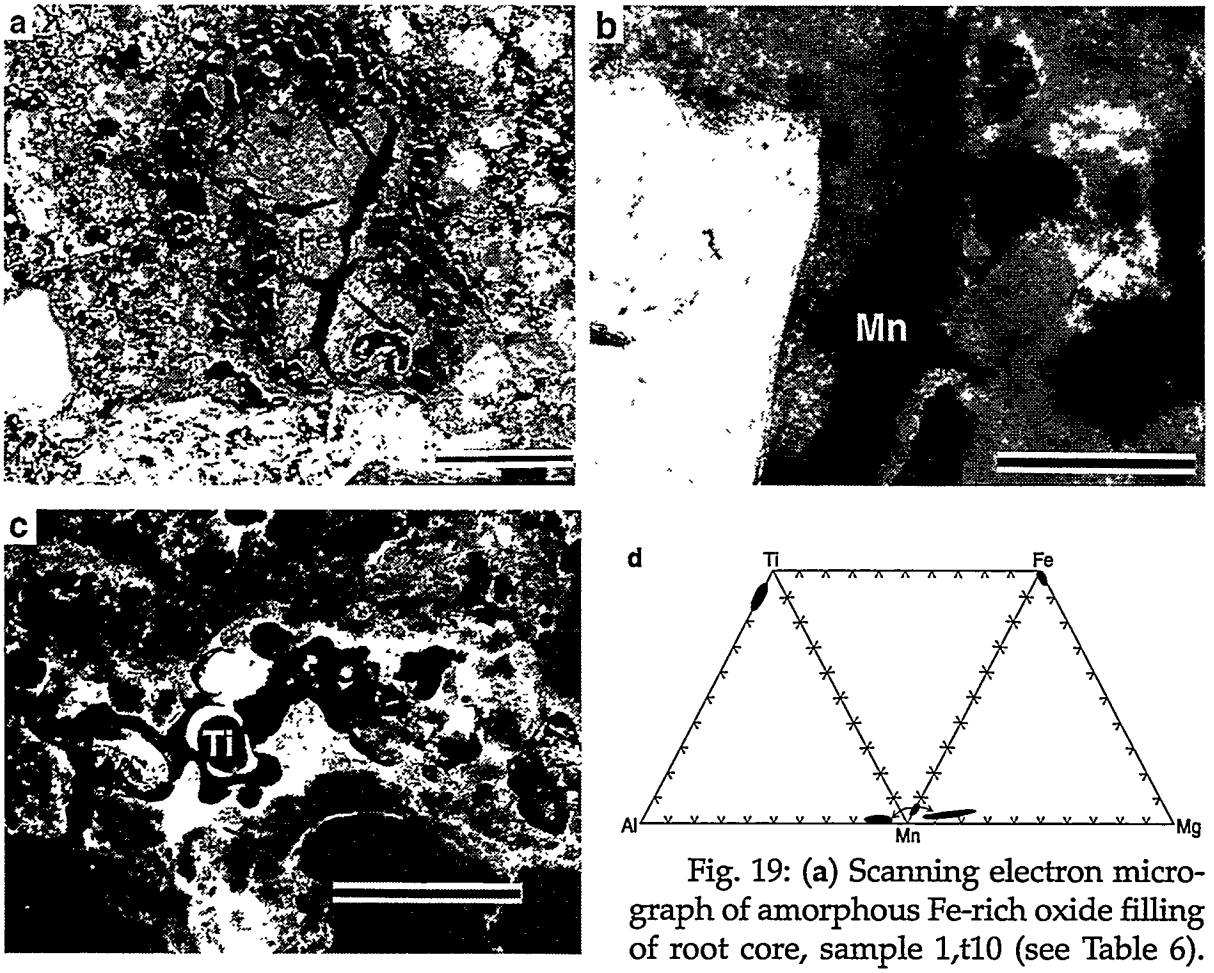

Fig. 19: (**a**) Scanning electron micrograph of amorphous Fe-rich oxide filling of root core, sample 1,t10 (see Table 6). Upper part of image shows opalized cell structure of outer root. Scale bar is 70 μm. (**b**) Photomicrograph of Mn-rich replacement of outer part of ooid rim in sample 7,t2 (see Table 6); scale bar is 100 μm. (**c**) Photomicrograph of Ti-rich bodies filling voids in sample 7,t3 (see Table 6); scale bar is 400 μm. (**d**) Combined ternary plots illustrating relatively simple composition of metals in Fe-rich deposits, aluminous nature of Ti-rich deposits, and complex variation of Mn-rich deposits.

Long-range eolian transport is especially effective at size ranges of ~2 to 40 μm (Junge 1979).

f. Other minerals. The only other authigenic minerals yet found associated with B-horizon soils or calcretes at Exile Hill are whewellite, gypsum, and halite. Gypsum and halite are rare; they are found in trace amounts in the B-horizon soils at Trench 14C, either associated with decaying roots (Fig. 21) or with deposits in open soil voids. Gypsum occurs within some voids as small, curved crystals resembling the gypsum cave flower forms found in some underground deposits. Whewellite appears to be strictly restricted to occurrences within living roots (see Fig. 11). Gypsum and halite occur only in rare and localized portions of the Exile Hill soils. Whewellite, although restricted to living roots, may be a significant contributor of Ca to the near-surface calcite deposits by virtue of many repetitions of root growth and death cycles in the upper 15 m of soil and rock into which roots penetrate (Vaniman and Whelan 1994).

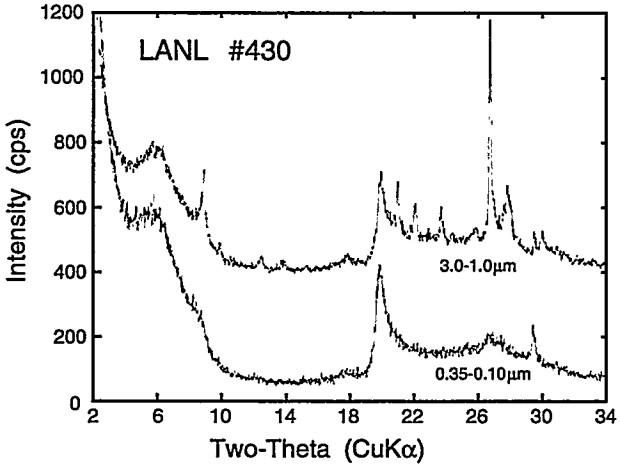

Fig. 20: X-ray diffraction patterns of clay separates from the 2Btj soil horizon, showing the loss of sharp illitic peaks in the finest fraction. This particle-size dependence indicates that the illitic component is in fact an inheritance of altered biotite.

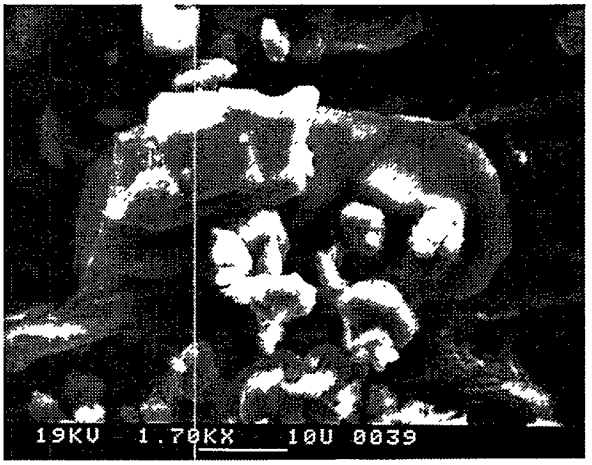

Fig. 21: Scanning electron micrograph of gypsum crystals (bright angular grains) on top of larger, rounded, halite grains. Specimen is from the inner wall of a partially decayed root within the B soil horizon in Trench 14C. Scale bar is 10 μm.

2. Comparative mineralogy: Spring deposits and Paleozoic dolomite. For comparative purposes, XRD data from spring and seep deposits of the region around Yucca Mountain are listed in Appendix 7. Table 7 summarizes the common mineralogy observed in spring deposits that were sampled for this study. A variety of veins, mounds, and discharge features in the vicinity were sampled. Calcite predominates in these deposits; the mineral chemistry of calcites from spring deposits can be compared with calcites from the Trench 14 vein calcrete in Table 4. Although poorer stoichiometry is obtained in analysis of the fine-grained calcites from the calcretes, electron microprobe analyses of 20 calcrete calcites from Trench 14 indicate a lack of any calcites with MgO > 1%. This contrasts with the calcites from seeps and springs that may have calcites with such low MgO contents but generally include calcites with higher MgO (Table 4; Fig. 22). Exceptionally high MgO contents were found in the calcites of the seep at Site 199, in a root fossil formed of Mg-rich calcite and minor amounts of dolomite (Table 4; Fig. 22). The generally higher MgO content of most of the spring calcites sampled is in accord with the minor occurrence of dolomite along with calcite in several of the samples from the Travertine Point veins and from the active spring mound at Nevares.

As in the calcretes, both opal-A and opal-CT are found in the spring deposits. However, the opal-A that was sampled occurs as algal mats near the active discharge at GMC spring; small veins of opal-CT occur in older, inactive portions of the GMC Spring. Opal-CT also occurs as massive white nodules of vitreous luster, often several centimeters in diameter, at the inactive IMV spring mound. The chemical data for the

two opal samples analyzed from calcretes (Appendices 4 and 5) and for the two opals analyzed from spring deposits (Appendix 7) vary widely, indicating no systematic chemical distinctions. However, a notable distinction from the calcrete deposits is the

TABLE 7. Quantitative-XRD Determinations (Weight %) of Spring-Deposit Mineralogy* (*"smectite" component may include smectite, sepiolite, or both)

locality:	Site 199	GMC Spring	GMC Spring	GMC Spring	GMC Spring	GMC Spring
sample:	251,p1	750,p1	750,p2	750,p3	751,p1	752,p1
type:	root fossil	bulk calcareous deposit	green siliceous deposit	bulk calcareous deposit	algal mat	bulk siliceous deposit
quartz	tr	24(2)	85(4)	1(1)	-	3(1)
feldspar	tr	-	-	-	-	11(1)
amphibole	-	-	-	-	-	tr
smectite*	-	-	-	-	-	6(2)
illite	-	-	17(5)	-	-	6(2)
zeolite	-	-	-	3(1)	-	-
gypsum	-	-	-	-	-	-
opal-A	-	-	-	-	100	74(3)
opal-CT	-	17(3)	-	16(3)	-	-
calcite	100(2)	57(3)	2(1)	78(4)	-	-
dolomite	tr	-	-	-	-	-
other	-	-	kaolinite (tr)	-	-	-

locality:	IMV Spring	IMV Spring	Travertine Point	Travertine Point	Travertine Point
sample:	753,p1	753,p2	754,p1	754,p2	755,p1
type:	siliceous deposit, waxy luster	siliceous deposit, porcelaneous	white vein	black vein	white vein
quartz	tr	-	-	-	-
feldspar	-	-	-	-	-
amphibole	-	-	-	-	-
smectite*	-	-	-	-	-
illite	-	-	-	-	-
zeolite	-	-	-	-	-
gypsum	-	-	-	-	-
opal-A	-	-	-	-	-
opal-CT	100(2)	62(12)	-	-	-
calcite	-	42(2)	100(2)	82	100(2)
dolomite	-	-	tr	-	-
other	-	-	-	hematite: 14 göethite: 4	

TABLE 7 (cont.). Quantitative-XRD Determinations (Weight %) of Spring-Deposit Mineralogy* (*"smectite" component may include smectite, sepiolite, or both) (cont.)

locality:	Nevares	Nevares	Nevares	Nevares	Nevares	Nevares	Nevares
sample:	757,p1	758,p1	759,p1	760,p1	761,p1	762,p1	763,p1
type:	spring mound	spring mound	spring mound	spring mound	spring mound	spring mound	active surface
quartz	1(1)	2(1)	1(1)	tr	tr	1(1)	-
feldspar	-	3(1)	-	-	3(1)	1(1)	-
amphibole	-	tr	tr	-	-	tr	-
smectite*	-	-	-	-	-	tr	-
illite	1(1)	2(1)	1(1)	-	-	1(1)	-
zeolite	-	-	-	-	-	-	-
gypsum	-	-	tr	-	-	-	tr
opal-A	-	-	-	-	-	-	-
opal-CT	-	-	-	-	-	-	-
calcite	94(5)	93(5)	95(5)	100(1)	93(5)	94(5)	104(5)
dolomite	1(1)	tr	tr	-	-	-	-
other	kaolinite (tr)	-	-	-	-	-	-

locality:	Grapevine	Grapevine	Grapevine	Grapevine	Grapevine
sample:	765,p1	766,p1	766,p2	767,p1	768,p1
type:	white vein	black vein	black vein	plant casts at surface	efflorescence at surface
quartz	-	-	-	tr	-
feldspar	-	-	-	-	-
amphibole	-	-	-	-	-
smectite*	-	-	6(2)	-	-
illite	-	-	-	-	-
zeolite	2(1)	-	-	-	-
gypsum	-	-	-	-	-
opal-A	-	-	-	-	-
opal-CT	-	-	-	-	-
calcite	98(10)	100(2)	94(10)	96(5)	-
dolomite	-	-	-	-	-
other	-	-	-	-	halite trona thenardite aphthitalite burkeite(?)

occurrence of authigenic masses or bands of quartz at GMC Spring (samples 750,p1 and 750,p2). Minor occurrences of quartz at the other spring localities represent detrital material (feldspar and amphibole are also detrital wherever they are found in the spring deposits).

The clay minerals in the spring deposits often include a well-crystallized illite component, unlike the B-horizon soils and calcretes at Exile Hill. There the clays consist of smectite, sepiolite, and an illitic component that appears to be predominantly a degradation product of detrital biotite. Sepiolite may be a constituent of what is listed here

as smectite; further study would be needed to identify and quantify the smectite and/or sepiolite in the spring deposits. Sepiolite is not unexpected in surface seeps and springs (Vaniman et al. 1992).

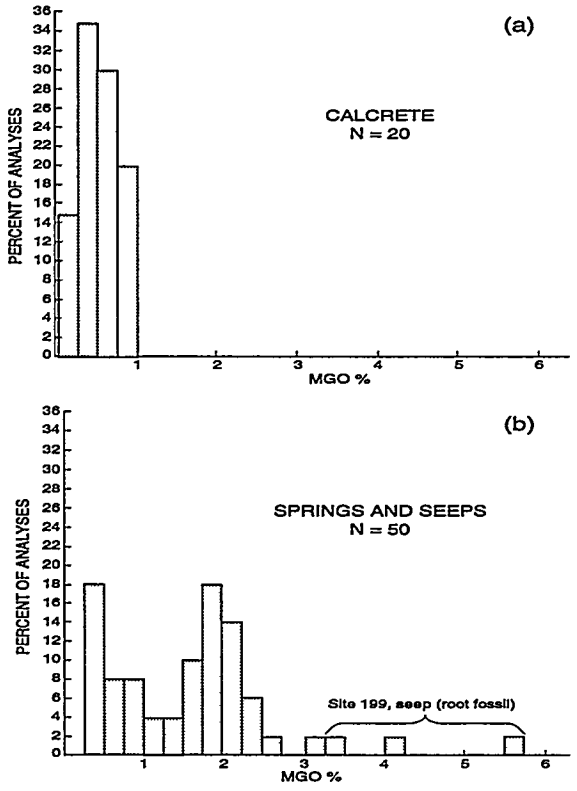

Fig. 22: Comparison of wt % MgO contents of calcites from (a) calcretes at Exile Hill and (b) springs and seeps of the region.

The active deposits at Grapevine Spring include surface efflorescence features (sample 768,p1 in Table 7) that are white, fragile, and have a slightly bitter taste. XRD analysis of this efflorescence reveals major amounts of the minerals halite, trona [$Na_3H(CO_3)_2 \cdot 2H_2O$], and thenardite [$Na_2SO_4$] with minor amounts of aphthitalite [$K_3Na(SO_4)_2$] and possible burkeite [$Na_6CO_3(SO_4)_2$]. Halite, trona, and burkeite have also been reported from efflorescence deposits in Oasis Valley (Vaniman et al. 1988). With the exception of halite, none of these minerals have yet been identified at Yucca Mountain, and certainly no significant deposits comparable to sample 768,p1 have been found.

The Paleozoic dolomite of the Roberts Mountain Formation was collected from drill core UE-25 P#1. This sample consists almost entirely of dolomite, with minor calcite and quartz (Appendix 7). Deep carbonates with abundant dolomite could be contributors of Mg to the relatively Mg-rich carbonates found in spring deposits of the region (Fig. 22).

III. CHEMICAL DATA

A. Chemistry of Calcite-Silica Deposits at Exile Hill

The chemical data collected by XRF, AA, LOI, ion chromatography, and principally by INAA for samples from Exile Hill are summarized in Appendices 1 to 6. In addition, electron-microprobe chemical analyses of several calcrete minerals and amorphous bodies from Trench 14 at Exile Hill are summarized in Tables 4–6 (discussed above). The appendix tables provide most of the chemical information in this report; several details of the chemical data in these tables are described below for various groups of elements.

1. Lanthanide elements (rare-earth elements). The lanthanide elements or rare-earth elements (REE) serve as important markers of many petrogenetic processes. Although used mostly in systems where their fluid-solid or solid-solid partitioning can be used to model chemical evolution, they can also provide useful fingerprints of particular rocks or minerals. Figure 23 compares the Trench 14 chondrite-normalized REE patterns, including the wall-rock tuffs exposed in the trench (Fig. 23a); the B soil horizons, including various size fractions (Fig. 23b); the slope calcretes (Fig. 23c); and the vein calcretes (Fig. 23d). Notable in these figures are

- the diminution of the negative Eu anomaly and the increase in light REE (La, Ce, Nd) and decrease in heavy REE (Yb, Lu) in the hematite-altered Tiva Canyon Tuff ("hem.Tiva" in Fig. 23a), compared to unaltered and vapor-phase ("v.p.") Tiva;
- the similarity of diminished Eu anomaly in the B soil horizons to the hematite-altered Tiva Canyon Tuff (Figs. 23a and 23b); and
- the maintenance of this same hematite-altered Tiva Canyon Tuff pattern in the parallel curves with comparable Eu anomalies for most of the calcrete samples (Figs. 23c and 23d). The calcrete samples with deviatory patterns are principally those with very low REE contents in the slope calcretes (~1X chondritic; Fig. 23c), where detection limits and analytical errors may lead to irregularities, although among the vein calcretes (Fig. 23d) the opal-A and opal-CT laminae have low-REE patterns that suggest La enrichment and a possible negative Ce anomaly.

Figure 24 shows comparable REE data for the root ashes from the B soil horizons at Trench 14 on the same chondrite-normalized y-axis scale as used in Fig. 23. The Mormon tea, boxthorn, and outer creosote samples have REE patterns comparable to but lower in concentration than the B soil horizons; the inner creosote root ash has strongly diminished heavy-REE abundances. The plants that have existed at this site during past pluvial episodes (piñon and juniper) have higher REE contents and the juniper sample has a negative Ce anomaly; it is important to note, however, that the piñon and juniper samples analyzed for this study were collected from a surrogate locality (Rainier Mesa) because these plants no longer occur at Exile Hill. These plants grew in a tuff substrate different from that at Trench 14 and at a higher elevation.

Figure 25, showing the REE patterns from Trench 14A, illustrates the short-range variability in REE patterns along the Bow Ridge Fault at Exile Hill. At Trench 14A, the calcrete samples that are closest to the Tiva Canyon Tuff (879,p1) and forming the overlying slope calcrete (883,p1) have chondrite-normalized REE patterns similar to the calcretes of Trench 14 (cf. Fig. 4). However, the vein calcretes adjacent to or within the Rainier Mesa Tuff (882,p1 and 901,p1) have a flatter chondrite-normalized REE slope and a more pronounced negative Eu anomaly than the calcretes at Trench 14. This different pattern at Trench 14A has similarities to two of the different tuffs found at

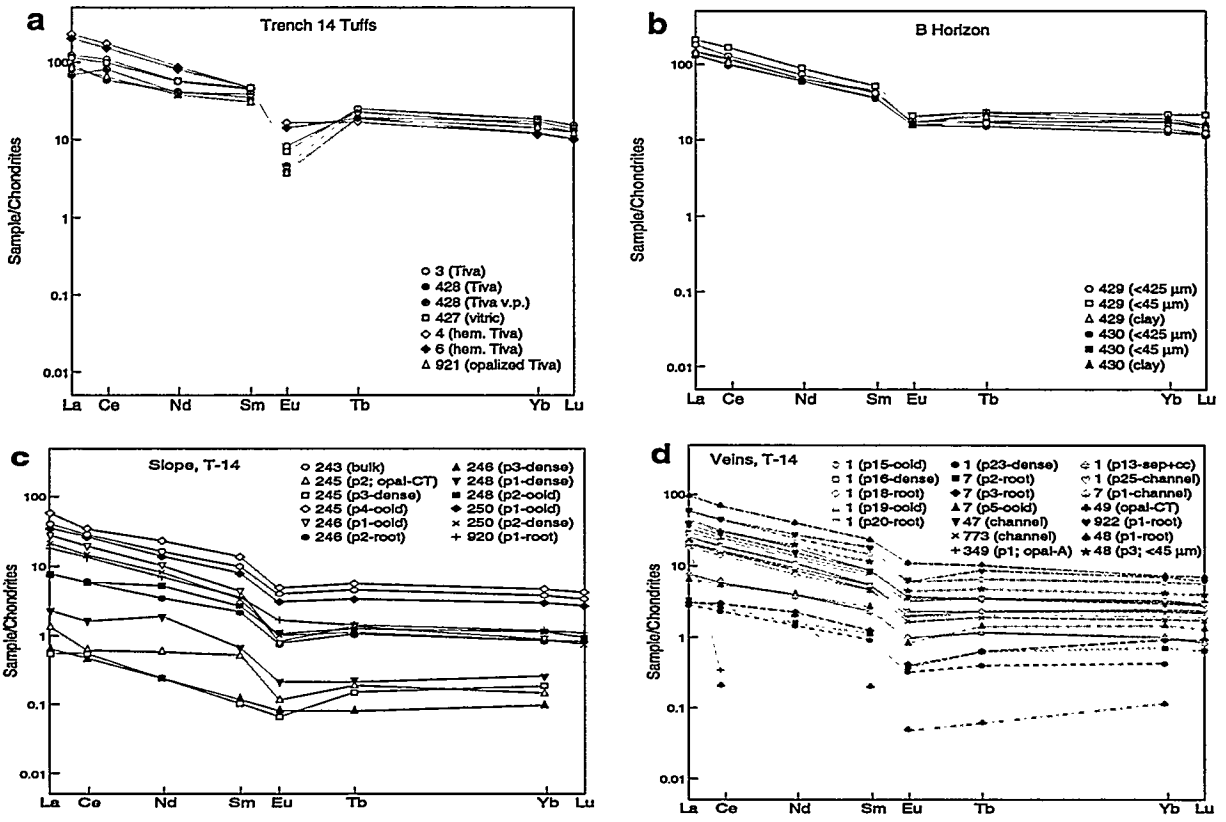

Fig. 23: (a) Chondrite-normalized REE patterns for wall-rock tuffs near the vein calcretes of Trench 14. Note the subdued Eu anomaly in the hematite-altered samples of the Tiva Canyon Tuff (LANL sample numbers 4 and 6). (b) Chondrite-normalized REE patterns for B soil horizon samples, including clay-mineral separates, from Trench 14. (c) Chondrite-normalized REE patterns for slope-calcrete samples from Trench 14. (d) Chondrite-normalized REE patterns for vein-calcrete samples from Trench 14.

Trench 14A (the Rainier Mesa Tuff, sample 431,p1, that forms the hanging wall of the fault, and an unnamed vitric nonwelded tuff within the fault, sample 880,p1, that is part of the unit designated *tb* by Gibson et al. 1992).

2. Zirconium. Zirconium has been used as an immobile element against which soil dilation or collapse can be quantified (Brimhall et al. 1991). Concentrated in detrital zircons that are relatively immune to chemical weathering, Zr is physically cycled through the open channels left by root decay and mixed into soils by root-growth stirring. Zirconium concentration profiles, when measured on relatively large samples (hand samples approximately 5 cm in diameter), can provide useful stratified profiles that clarify processes of soil evolution (Brimhall et al. 1991). Figure 26 shows the relationships between the percentage of detritus (as determined by quantitative XRD) and Zr content of the Trench 14 and Trench 14A tuff, B soil horizon, and calcrete samples. Note that smectite clays in the B-horizon samples contain a significant component of weathered biotite and are therefore treated as detritus. In this type of diagram, the percentage of detritus provides a measure of the amount of local lithic plus eolian material contributed to the B soil horizons and to the calcretes. Direct admixture of a

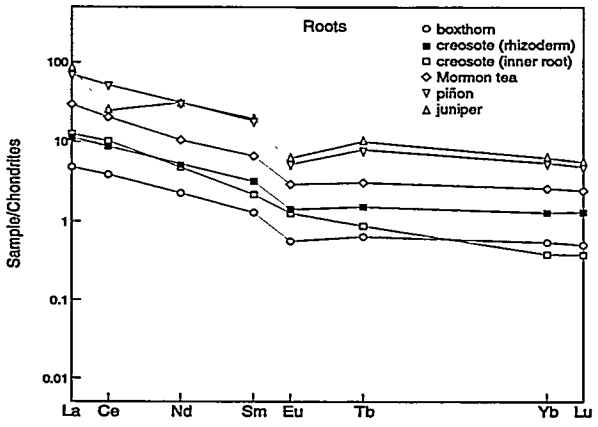

Fig. 24: Chondrite-normalized REE patterns for ashed root samples. Note negative Ce anomaly in the juniper sample.

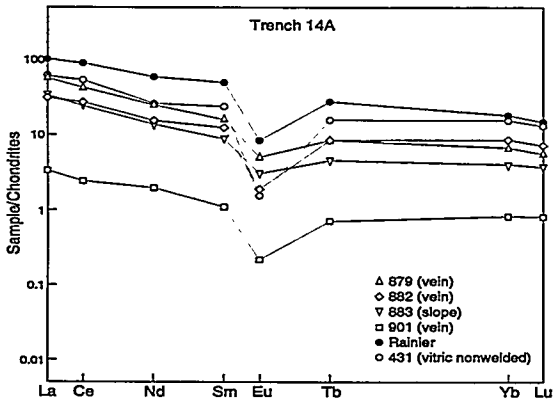

Fig. 25: Chondrite-normalized REE patterns for samples from Trench 14A. Contrast the commonly deeper Eu anomaly with the shallow Eu anomalies in altered tuff, B soil horizon, and calcrete samples from Trench 14 (Fig. 23).

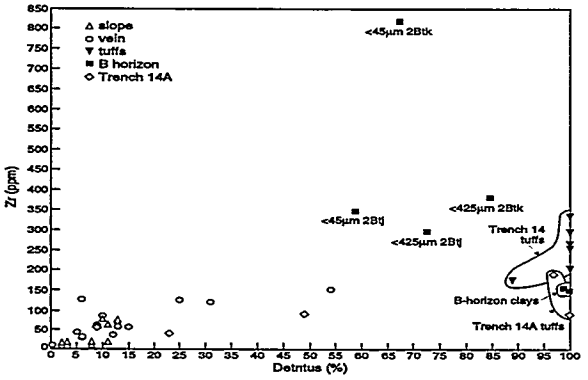

Fig. 26: Zirconium (by INAA) versus detritus (by XRD) for samples from Trenches 14 and 14A. Note highly variable Zr content of the fine fractions from the B soil horizon of Trench 14.

uniform ratio of these two components, derived from a uniform population of local detritus and a uniform population of eolian materials, should follow a simple mixing line. Instead, the calcrete data scatter widely and the B-horizon samples are slightly to highly enriched in Zr, most notably in the <45 µm Btk sample that represents fine material at the top of the B horizon. Zirconium, which is principally controlled by the abundance of detrital zircon (Brimhall et al. 1991), is concentrated in the finer-grained soils. It is this finer size range that should include eolian materials from the most distant sources (Junge 1979). The strong variability of Zr content in the <45 µm fractions of the B-horizon soils suggests that either the mixture of distant eolian materials with local sources does not provide a constant and uniform source of detritus, or the processes of weathering and soil formation at Exile Hill fractionate the trace heavy minerals derived from these sources. Further study of size fractions from 100% eolian deposits would be needed to clarify the detailed role of distant eolian sources in contributing material to the B soil horizons and calcretes at Exile Hill.

3. Iron-scandium. Many interelement regressions have been tested in the calcrete samples, with the result that one element pair in particular has been found to be strongly correlated in the Trench 14 calcretes. Iron and scandium are correlated with regression coefficients >0.99 in both the slope and vein calcretes at Trench 14; the regressions for these two calcrete

types are essentially identical (Fig. 27a). When the samples from Trench 14A are plotted along with those from Trench 14 (Fig. 27b), it can be seen that the slope calcrete sample and two of the vein calcrete samples from this trench fit the regression relationship developed for samples from Trench 14, but the calcrete sample that is adjacent to the Rainier Mesa Tuff at the hanging wall of the fault (sample 882,p1; see Fig. 4) has a significantly higher Sc/FeO ratio, approaching that of the adjacent tuff. The Fe and Sc contents are controlled principally by the detritus and are not significant constituents of the major authigenic minerals. Only minimal amounts of Fe and Sc (0.136% FeO, 0.319 μg/g Sc) are present in a calcite-plus-sepiolite sample of the vein calcrete (sample 1,p13, Appendix 5); even less Fe and Sc occur in the most pure opal or calcite-plus-opal samples (≤0.02% FeO, ≤0.03 μg/g Sc) of both the slope and vein calcretes (samples 245,p2, 245,p3, and 246,p3 in Appendix 4; samples 49,p1 and 349,p1 in Appendix 5). Some sepiolite samples may contain appreciable Fe and Sc; indeed, Fe in several sepiolite samples is readily detectable by electron microprobe (Table 5). Clearly the amorphous Fe-oxides are rich in Fe (Table 6) and probably also contain significant amounts of Sc, but no direct measurements of Sc content have been made on these minor (<1%) constituents.

Because the principal authigenic constituents of the calcretes have so little Fe or Sc, these elements correlate well with the amount of detritus in the samples. The ratio of Sc/FeO in the calcretes is quite constant and, from purely chemical arguments, could be interpreted as indicating that the detritus in Trench 14A is derived principally from the closest wall-rock tuffs (Fig. 27c). Figure 27c compares the Trench 14 calcretes with their wall-rock tuffs and shows a scatter in Sc/FeO ratios considerably wider than the restricted Sc/FeO ratio of the calcretes that occur in this trench. Of the wall-rock tuffs, the hematite-altered Tiva Canyon Tuff samples (4,p1 and 6,p1) that are immediately adjacent to the vein calcretes and immediately up-slope from the slope calcretes are sufficiently close to the calcretes in Sc/FeO to be the principal sources of FeO and Sc in the calcretes. The vitric nonwelded tuff is also similar in Sc/FeO ratio but, unlike the hematite-altered tuffs, has a chondrite-normalized REE pattern with a deeper Eu anomaly than found in the calcretes (Figs. 23a, 23c, and 23d). The unaltered Tiva Canyon Tuff and the opalized Tiva Canyon Tuff that are farther from the fault have lower Sc/FeO ratios, as well as having REE patterns that do not match the calcretes (Figs. 23a, 23c, and 23d).

Although the hematite-altered wall-rock tuffs have Sc/FeO ratios and chondrite-normalized REE patterns that are appropriate if they are to be the primary source of Fe and Sc in the calcretes, they do not have the abundances of these elements that would be appropriate if they were to be direct sources. Figure 27c shows that the hematite-altered wall-rock tuffs have FeO and Sc concentrations no greater than some of the

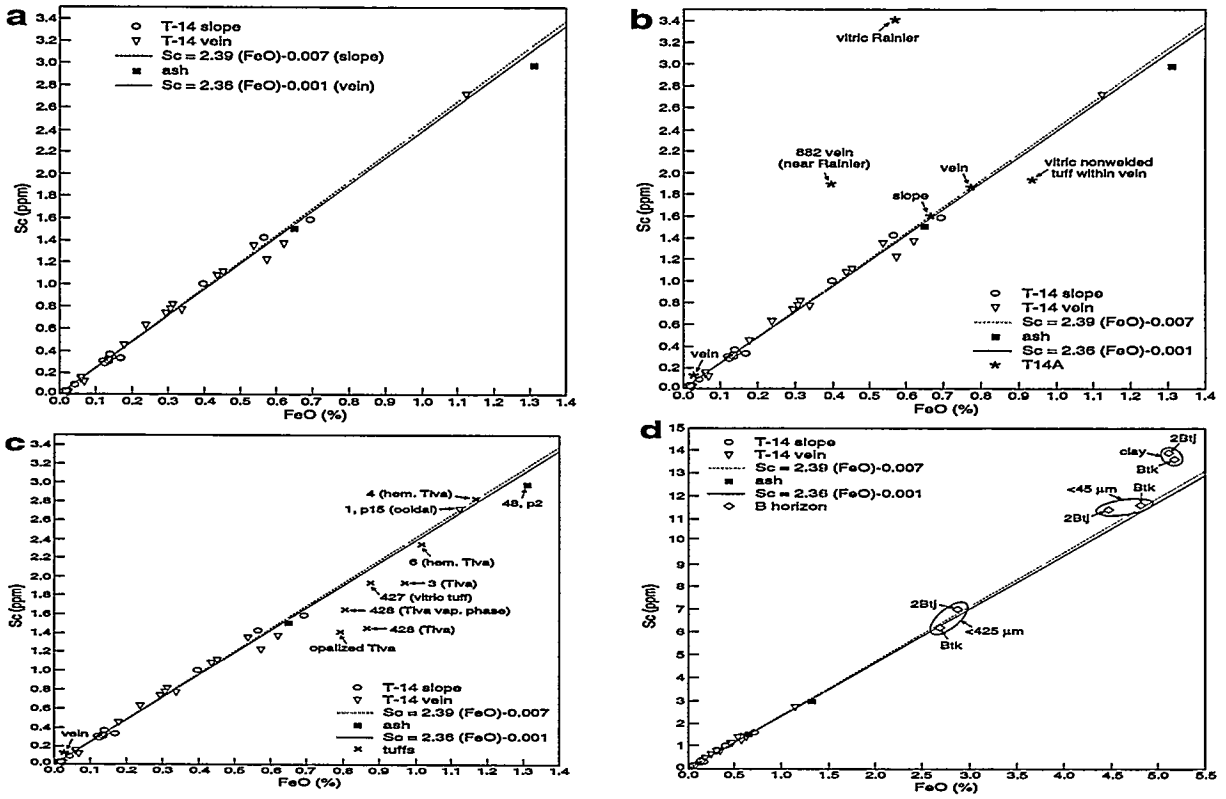

Fig. 27: (a) Scandium versus FeO for calcrete samples from Trench 14. The ash sample represents coarse and fine fractions of LANL sample 48, which contains some basaltic ash. Regression lines are fit separately to the vein and slope calcretes; both regressions have regression coefficients >0.99 and essentially overlap, with intercepts near zero. (b) Samples from Trench 14A superimposed on the previous figure. Note that the slope and most vein calcrete samples fall close to the same regressions lines as defined by the calcretes in Trench 14, with the exception of LANL sample 882, which deviates to higher Sc/FeO and toward its closest wall-rock tuff (vitric Rainier Mesa Tuff; see Fig. 4). (c) Wall-rock tuffs of Trench 14 superimposed on the calcrete data of (a). Note that the closest fits to the calcrete Sc/FeO ratio are for the hematite-altered Tiva Canyon Tuff. (d) Expansion of the scale of (a) to include samples from the B soil horizon in Trench 14. Note the B-horizon size fraction corresponding to most of the detrital material in the ooids and pellets of the calcretes (<425 µm) falls very close to the Sc/FeO regression lines for the calcretes; one of the finer-sized fractions and particularly the clay fractions of the B soil horizons have higher Sc/FeO ratios.

calcrete laminae that contain only 25% to 50% of detritus that could be derived from these tuffs. If these wall-rock tuffs provide the bulk of the Fe and Sc to the calcretes, then some process must have concentrated the mafic constituents of the wall-rock tuffs prior to incorporation into the calcretes. Moreover, the effects of eolian contributions to FeO and Sc are not included in this analysis. Further consideration of possible eolian constituents can be found in the Discussion (section IV) of this paper.

Figure 27d adds data from the B soil horizons at Trench 14 to the plot of Sc and FeO for Trench 14 calcretes. The coarser B-horizon soil fractions (<425 µm) have FeO and Sc contents about 2X those of the most Fe-, Sc-enriched calcrete laminae, and the

finer B-horizon soil fractions (<45 μm) have FeO and Sc contents about 4X the highest calcrete concentrations. As noted above in the section on smectite, it is this finer fraction that should contain the largest proportion of eolian material. The lower B subhorizon (2Btj) is not as close to the calcretes in Sc/FeO ratio as is the upper B subhorizon (Btk), and the clay separates from both subhorizons have significantly higher Sc/FeO ratios. Thus, although some constituents of the B soil horizons are appropriate in both Sc+FeO and in Sc/FeO to be sources of Sc and Fe for the calcretes, there is either variation in Sc/FeO of detrital sources or fractionation of Sc/FeO within the B soil zone that leads to divergence of some of the <45 μm material and all of the clay fraction away from this characteristic composition.

4. Calcium-strontium. Strontium contents of calcites in the calcretes could not be measured directly because pure calcite separates could not be obtained for INAA analysis. However, as noted above in section II.E.1.a. on calcite and in Fig. 18, Sr contents of the calcites can be estimated at ~800 to 2100 μg/g based on comparisons of Sr with Ca data and with quantitative-XRD data for calcite abundances in the calcrete samples. All other constituents within the calcretes have relatively low Ca contents, with the exception of the ashed root samples (Fig. 28). The ashed root samples, with the exception of piñon, have a narrow range of Ca compositions. There is exceptionally high Sr in two of the common plants presently found at Exile Hill (boxthorn and creosote bush); both of the plants that are now absent at Exile Hill but were more common in the past (piñon and juniper) have lower Sr contents in their root ashes and have Ca/Sr ratios more similar to the calcretes.

5. Uranium. Uranium is associated with opal in the calcretes and in the B-horizon soil samples (Fig. 29). The pure opal-A lamina from vein calcrete in Trench 14 (349,p1; Appendix 5) contains 23 μg/g U and the pure opal-CT lamina from the slope calcrete (245,p2; Appendix 4) contains 18 μg/g U. These contents of U in opal compare with the lower to middle portions of the 15 to 58 μg/g U range for opals in unsaturated fractures at Yucca Mountain (Szabo and Kyser 1990). Aside from the separates of pure opaline laminae, the laminae with highest opal or U contents in the calcretes are typically those that are dense and commonly sheared (Appendix Tables 4 and 5).

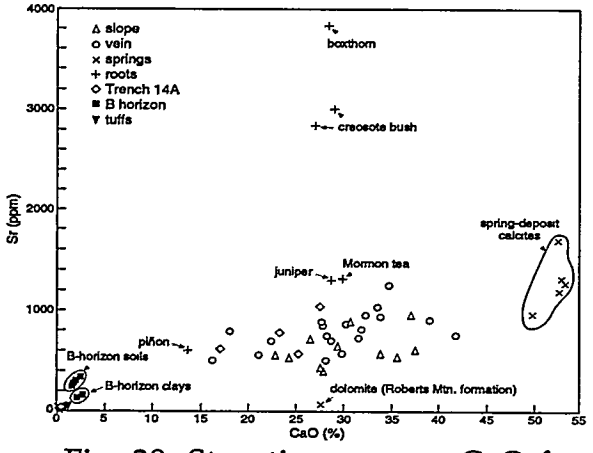

Fig. 28: Strontium versus CaO for calcrete, root ash, and spring-deposit samples. Note the very high Sr/CaO for some ashed root samples (boxthorn and creosote bush) from Exile Hill.

6. Gold-arsenic. The Au and As data in this report were collected by INAA.

Weiss et al. (1991) report Au contents determined by graphite furnace–atomic absorption spectrometry and As determined by inductively coupled plasma emission spectrometry for large (2–10 kg) samples. Their detection limits for Au (0.20 ng/g) are lower than those obtained by INAA (generally >0.8 ng/g); the detection limits for As by INAA, however, are generally comparable (~0.2 µg/g). They are capable therefore of reporting measurable Au contents for volcanic rocks with <1 ng/g Au that are below detection limits in our data set (Appendix 2). In our data set only one tuff sample, the opalized Tiva Canyon Tuff from Trench 14 (921,p1 in Appendix 2) has measurable Au (12.6 ng/g). However, Au was measurable by INAA in most of the calcrete samples and can be compared directly with the data of Weiss et al. (1991). They report a range of 0.5 to 7.3 ng/g Au and 4 to 12 µg/g As from Trench 14. Our As and Au values for calcrete samples cover essentially the same range, although the opaline laminae contain essentially no As and our Au values for most calcrete samples are somewhat higher (2 to 12 ng/g). In Au content, two particular laminae from the vein calcretes are outliers: the sepiolite-plus-calcite lamina (1,p13 in Appendix 5: 15 ng/g Au) and the clay-rich, zeolite-rich lamina (922,p1 in Appendix 5: 29 ng/g Au). The absence of such high Au values in the analyses by Weiss et al. (1991) may be due to the fact that they analyzed large bulk samples rather than individual calcrete laminae. Even the high-Au calcrete laminae, however, are overshadowed by the high Au contents of most of the root ash materials with the exception of the juniper sample and the outer part of the creosote-bush root (Fig. 30). The ash component of plants is typically enriched in Au relative to the soils in which the plant grows, with higher Au contents in the ultrastructure than in the roots (Boyle 1979). In this regard, most of the plants that now exist at Trench 14 and one (piñon) that once existed there appear to concentrate Au in their root ash components by moderate amounts (an average of ~8X).

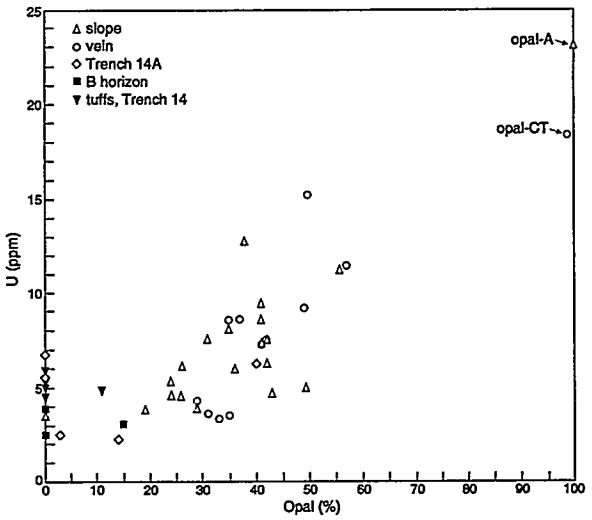

Fig. 29: Uranium versus opal content of calcrete, B soil horizon, and wall-rock tuff samples from Trench 14 and of calcrete and wall-rock tuff samples from Trench 14A, showing general correlation between U and opalization.

Arsenic is sometimes useful as a pathfinder element in Au exploration. Figure 30 shows considerable As variation and an apparent lack of strong correlation with Au. The ashed root materials that are strongly Au-enriched have little As. Any correlation of Au with As is weak in the calcretes and nonexistent in the root ash materials.

B. Comparative Chemistry: Spring Deposits

Although a smaller chemical database was collected from known spring and seep deposits than from Exile Hill, the data that were obtained illustrate both similarities and differences between these deposits and those at Exile Hill. The data in Appendix 7 provide the basis for this comparison.

1. Lanthanide elements (rare-earth elements). In contrast to the analyses from Exile Hill, few of the spring deposits have REE contents that were measurable by INAA. Those deposits that did provide sufficient measurable REE data to generate chondrite-normalized plots are surficial: the opal-A algal mat from GMC Spring (751,p1; compare Fig. 31 with the opal REE patterns in Fig. 23d); the Mg-calcite/dolomite root sample from the seep in at Site 199 Crater Flat (251,p1); and the surface of the spring mound at Nevares (760,p1). Plots of the REE patterns for these samples are shown in Fig. 31, using the same vertical scale as in Figs. 23–25. None of the vein-forming calcites from known spring localities had sufficient REE content to plot, and their measurable La contents indicate that these samples probably have general REE contents that are <0.1 x chondrites. Included in Fig. 31 are data for the dolomite paleozoic sediment from drill core UE-25 p#1 (Fig. 1a).

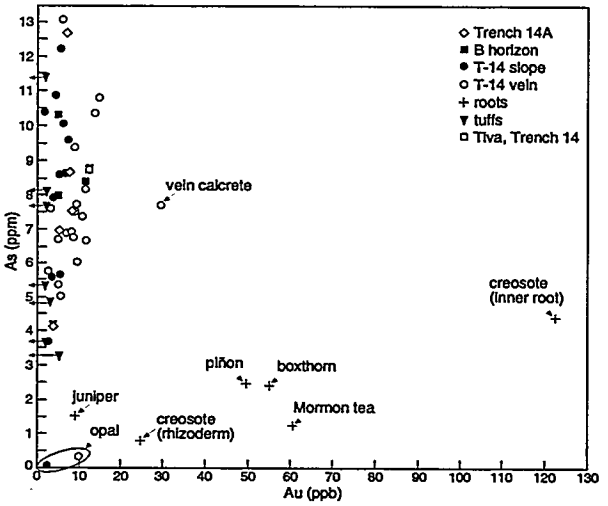

Fig. 30: Arsenic versus gold in tuffs, calcretes, B soil horizons, and ashed root samples (samples from Trenches 14 and 14A). Note the especially high Au/As for some of the ashed root samples.

2. Zirconium. Only very small amounts of Zr (~3 µg/g) were detected in the calcite veins from Travertine Point. Somewhat more Zr was detected in the sedimentary dolomite sample from the Roberts Mountain Formation beneath Yucca Mountain (19 µg/g). All other spring and seep samples, whether opaline or carbonate, had no detectable Zr. These low concentrations appear to be related to the general absence of detritus in these samples.

3. Iron-scandium. Because Sc and FeO are so strongly correlated at Exile Hill

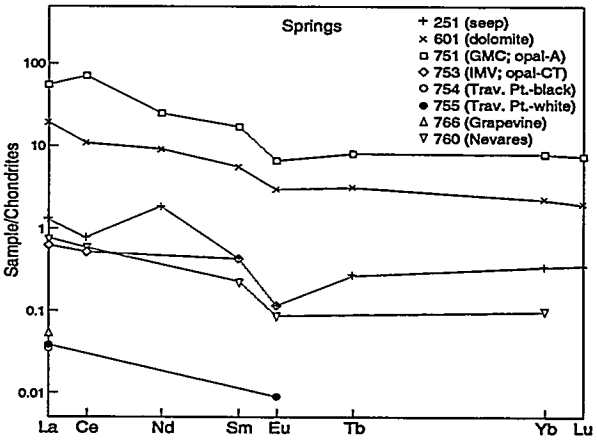

Fig. 31: Chondrite-normalized REE patterns for spring-deposit samples and Paleozoic dolomite.

and are apparently controlled by local detritus, only similar multisample suites from other localities can provide adequate comparison of the controls on this ratio. Although such a comparison cannot be made for the spring samples in this report, the data are sufficient to show the very low Sc (<0.2 μg/g) and FeO (<0.1%) in these samples. As with Zr, this low content of metals appears to be related to the lack of detritus.

4. Calcium-strontium. As noted above, the Sr contents of the calcites in calcretes are estimated at ~800 to 2100 μg/g (Fig. 18). This calculated range of Sr contents is broader than (but comparable to) the measured range of Sr contents in calcites of the seeps, veins, and tufa mounds analyzed for this study (960 to 1694 μg/g; Appendix 7 and Fig. 28). However, the lower ends of both of these ranges are significantly higher than the Sr contents of coarse-crystalline calcites found in fractures of the unsaturated zone at Yucca Mountain (11 to 338 μg/g; Vaniman 1994). Thus the Ca/Sr ratios in calcites of the calcretes at Exile Hill are more similar to those of distant spring materials, 17 to 90 km away, than to those of calcites that line many unsaturated fractures that are just tens to hundreds of meters beneath the surface at Yucca Mountain.

5. Uranium. As at Exile Hill, uranium is higher in opaline constituents than in the calcareous materials in spring and seep deposits. The abundances of U in algal opal-A of the active GMC Spring deposit and in the massive opal-CT of the inactive IMV deposit are comparable to those of opaline laminae in Trench 14 at Exile Hill. In contrast to the Exile Hill samples, however, calcite was coarse enough to separate and analyze in the spring and seep deposits. The U contents of these calcites are <0.8 μg/g in the spring deposits and 2.85 μg/g in the root fossil from the Crater Flat seep.

6. Gold-arsenic. Figure 32 illustrates the same data from Exile Hill that are plotted in Fig. 30 but adds the data from spring and seep deposits. This combination of both data sets requires an expanded vertical axis to accommodate the high As contents of the calcite veins from Travertine Point. None of the spring or seep samples have >1 ng/g Au except for the black calcite vein from Travertine Point; measurable gold was also found in the dolomitic sediment of the Roberts Mountain Formation (6.7 ng/g).

IV. DISCUSSION

A. Provenance and Evolution of Detritus at Exile Hill

If a calcrete is pedogenic, the detritus within it may have been modified by surface exposure and weathering. Nonpedogenic calcretes can also incorporate soil detritus, but if they occur as veins formed from upwelling waters, then the veins should show more evidence of interaction with their wall rock than with the overlying soil. This is particularly the case for the vein calcretes in Trench 14, where proposals of deep origin are based on a hypothesis of explosive injection and wall-rock brecciation by the vein-forming fluids (Broad 1990; Archambeau and Price 1991). Chemical and mineralogic

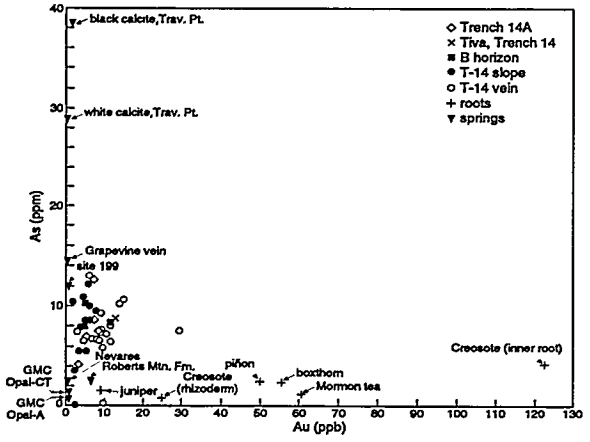

Fig. 32: Arsenic versus gold for spring deposits, superimposed on the data from Exile Hill shown in Fig. 30. Note low Au and high As content of several calcite samples from spring deposits.

data for both vein and slope calcretes at Trench 14 provide clear evidence for surface origin of their detrital component. This evidence is recorded in heavy-mineral enrichments (resulting in high Fe and Sc contents) with significant contributions of eolian material.

1. Heavy-mineral enrichment. Figure 23 shows the similarities between tuff detritus and the lanthanide-series signature of B soil horizons and the calcretes at Trench 14. There is a slight enrichment of the heavy lanthanide elements (Yb, Lu) in the B horizons relative to the wall-rock tuffs (Figs. 23a and 23b). Petrographic and XRD data indicate that this difference is accounted for by an enrichment in the Bt horizons of heavy minerals (principally biotite, amphibole, oxide minerals, and some clinopyroxene) that have relatively high heavy-lanthanide abundances. This effect is most notable in the <45 μm and clay fractions; indeed, the clays are notably Fe-rich (5% FeO, compared to <1% FeO in the bulk tuffs) and may be derived principally from the weathering of heavy mafic minerals. Total concentrations of the heavy minerals are 4 to 6% in the <45 μm B soil horizons, but these minerals are detectable only in trace amounts in the wall-rock tuffs. Disaggregation of the wall-rock tuffs in surface weathering, with subsequent deflation or slopewash, may remove lighter minerals and leave the heavier minerals behind. However, a contributing factor in this process may be the addition of mafic eolian minerals.

2. Local versus eolian sources for heavy minerals. Both the Bt horizons and the calcretes contain small amounts (≤1%) of amphibole fragments with characteristic pleochroism (α = light yellow-brown, β = brown, γ = green). These amphiboles occur as small grains, mostly <45 μm in diameter (note that the concentration rises to 3% in the <45 μm fraction of the upper B horizon, Btk; Appendix 3). Figure 33 compares the FeO and MgO contents of these small amphibole grains with the published range of amphibole compositions that occur in the Tiva Canyon Tuff that is a local source of detritus (Warren et al., 1989). There is some overlap, but the amphiboles in the Bt horizons and calcretes include compositions more Fe-rich and Mg-poor. Many of these amphibole fragments may be derived from distant sources and brought to Exile Hill by eolian processes.

If detrital grains, particularly those of silt to clay size, are in part brought to the site by eolian processes, then the mineralogic makeup of those sources may provide con-

straints on the relative proportions of local and distant contributions. Guthrie et al. (1993) have analyzed eolian dusts from four natural dust traps (under boulders above soil horizons, or from fractures within boulders above the soil) near Exile Hill. They used the same XRD methods as used in this report to determine the quantitative mineralogy of the <425 μm fractions of these eolian samples, and of several size fractions from one of them (Table 8).

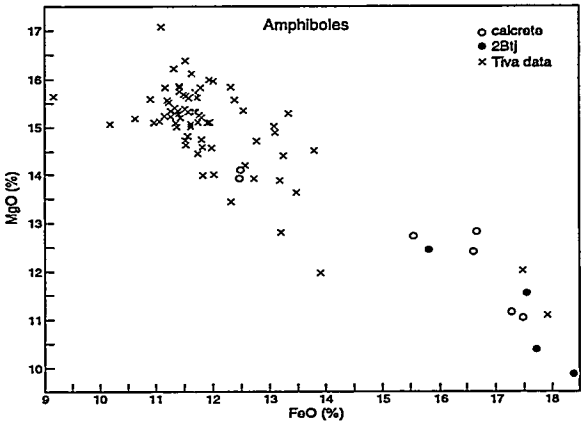

Fig. 33: MgO versus FeO in fine-grained (<45 μm) amphibole fragments of the B soil horizon and calcretes at Trench 14, compared with literature data for amphiboles from the Tiva Canyon Tuff (Warren et al. 1989).

In general, the mineral constituents of these eolian deposits are similar to the corresponding <425 μm and <45 μm fractions of the Btk and 2Btj horizons of Trench 14 (Appendix 3). Notable differences, however, are the rarity of tridymite and absence of cristobalite, higher feldspar content, and lower clay content (particularly smectite) in the eolian deposits. These differences may reflect the modifications that occur when

TABLE 8. Quantitative-XRD Determinations of Mineral Abundances in Eolian Deposits near Exile Hill

	<425 μm				
sample (LANL#):	**1036**	**1037**	**1034**	**1033***	**1033 (<45 μm)****
quartz	18(1)	22(2)	22(2)	22	24(2)
tridymite	1(1)	1(1)	1(1)	tr	tr
cristobalite	-	-	-	-	-
feldspar	47(7)	45(6)	48(7)	46	38(5)
amphibole	2(1)	2(1)	1(1)	tr	3(1)
biotite†	3(1)	2(1)	2(1)	1	3(1)
chlorite	1(1)	1(1)	1(1)	1	2(1)
hematite	1(1)	1(1)	1(1)	1	1(1)
amorphous (glass)‡	16(8)	15(7)	13(8)	16	16(7)
illite	-	-	-	-	-
smectite	8(2)	7(2)	8(2)	7	10(3)
kaolinite	1(1)	1(1)	1(1)	1	2(1)
calcite	tr	tr	-	-	-
zeolites	3(1)	4(1)	3(1)	4	4(1)
gypsum	tr	-	-	-	-

*composite of size-fraction data (425-180, 180-90, 90-45, 45-38, and <38 μm)
**composite of size-fraction data (45-38, and <38 μm)
†reported as "mica"
‡including some opal-A (silica phytoliths)

local detritus is mixed with the eolian materials. Most important to this discussion, however, is the high content of Fe-rich heavy minerals in the eolian samples (amphibole, biotite, chlorite, and hematite total 3–7% in the <425 μm material and 9% in the <45 μm material).

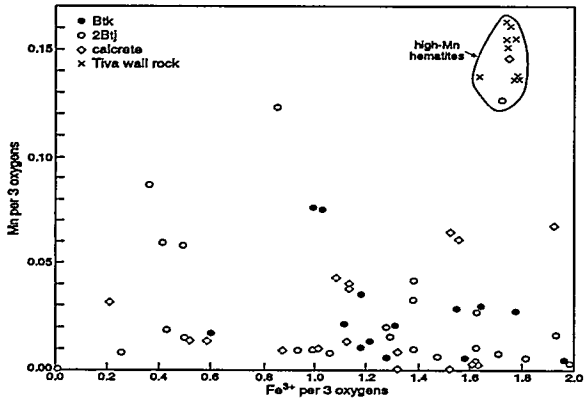

Fig. 34: FeO versus MnO in fine-grained (<45 μm) hematite fragments of the B soil horizon, calcretes, and hematite-altered Tiva Canyon Tuff at Trench 14. Hematites of the B horizon and calcrete are more Al-rich and Mn-poor than those of the tuff.

Of the Fe-rich minerals common to the hematite-altered wall-rock Tiva Canyon Tuff, Bt soil horizons, and vein calcretes, hematite is the most ubiquitous. Electron microprobe data for Fe-Mn contents of fine-grained (<45 μm) hematites from these three rock and soil types are summarized in Fig. 34. The data available show strong similarities between hematites of the Bt soil horizons and the calcretes, but generally higher MnO in the hematites of the hematite-altered Tiva Canyon Tuff. These differences indicate that hematites of the altered wall-rock tuff and the vein calcretes did not form together from a uniform alteration event, and also indicate that there is a common source for hematite detritus in both the Bt soil horizons and the calcretes. Although the data do not prove that the Bt horizon and calcrete hematites are brought in by eolian processes, the foreign compositions of many amphiboles (Fig. 33) and hematites (Fig. 34) in the Bt horizons and calcretes suggest a large component of eolian input. Further studies of eolian deposits would be required to test this hypothesis.

3. Sc/FeO ratios: Sizes and sources of detritus. Another effect of heavy-mineral enrichment is seen in the Fe and Sc data (Fig. 27). The Sc/FeO ratio of both the calcretes and the overlying bulk (<425 μm) Bt horizons is the same as that of the hematite-altered wall rock tuffs (Figs. 27c and 27d). Slightly higher Sc/FeO ratios are seen in the <45 μm fraction of the 2Btj horizon, and the clay fractions of the B soil horizons have significantly higher Sc/FeO (Fig. 27d). Because the principal nondetrital constituents of the calcretes (calcite and opal) contain essentially no Fe or Sc, the strong Sc/FeO fingerprint of the calcretes can be used to help discern the various sources of detritus. The B-horizon clay fraction, much of which may be illite/smectite derived from distant eolian sources, cannot be a major contributor to the calcretes, because the clay Sc/FeO ratio is too high. This conclusion is supported by the low clay abundances (other than sepiolite) of the calcretes in Trench 14 (<10%). The silt-sized fraction of the B horizons can have slightly higher Sc/FeO than found in the calcretes, but this deviation is

slight. Even though the fine-grained amphiboles and hematites in the B horizons are from distant sources, their Sc/FeO ratios are apparently close enough to those of the local tuffs that there is little or no deviation in the net Sc/FeO ratio.

The most abundant detrital component of the calcretes, however, is the <425 μm fraction that provides almost all of the detrital nuclei for the very common calcrete ooids (detrital nuclei for the ooids average 163±154 μm; only 5% are <45 μm). For this size fraction, in the B horizons, Sc/FeO ratios align very well with those of the calcretes and with the hematite-altered wall-rock tuffs (Figs. 27c and 27d). In this size range, detritus can be moved as drifting sand but is unlikely to be carried as an aerosol suspension from distant sources (Junge 1979). The Sc/FeO ratios of detritus in Trench 14 thus link the local wall-rock tuff, the sand-sized fraction of the B soil horizons, and the ooidal nuclei in the calcretes. Silt- and clay-sized material in the B soil horizons, however, may be partly to largely eolian in origin.

4. Scandium and iron abundances. Scandium and iron abundances are linked to B-horizon soils rather than to wall-rock tuff breccias in Trench 14. Figure 35 uses the combined INAA data for Sc abundance and the quantitative-XRD measure of total detritus to assess the extent to which wall-rock detritus may be directly mixed with the calcretes. Because of the heavy-mineral enrichments in the B soil horizons, whether from weathering or eolian additions, the Sc/detritus ratios are distinctly higher in these sources than in the wall-rock tuffs. Because of this variation in Sc/detritus, there is a family of mixing curves between the purely authigenic calcrete constituents (calcite-opal, ± sepiolite) without detritus and with very low Sc contents (<0.4 μg/g) and the various sources of detritus. The sources of detritus range from the high-Sc clays and silts (<45 μm fraction) of the B soil horizons, to the moderately Sc-rich sands (<425 μm fraction) of the B soil horizons, to the low-Sc wall-rock tuffs. The predominant pattern of Sc/detritus mixing in the calcretes is linked to the constituents of the B soil horizons. A small group of three slope-calcrete samples appears to have a larger component of intermixed wall-rock tuff materials, as does vein-calcrete sample 922,p1. However, all of these samples have higher clay contents (5–10%) than any of the other Trench-14 calcretes (≤3%). This additional clay may be a smectite different from that of the B soil horizons with lower FeO and Sc contents. The data from Trench 14A indicate that another form of smectite is locally abundant in the vein calcretes.

5. Differences between trenches 14 and 14A. The vein calcretes of Trench 14A occupy a much narrower fault zone than those of Trench 14 (compare Figs. 2b and 3a with Fig. 4). The fabric of laminae in the vein calcretes of Trench 14A is also simpler, with predominantly vertical orientation and very few cross-cutting laminae. Moreover, the vein calcretes at Trench 14A do not grade into the slope calcretes but rather

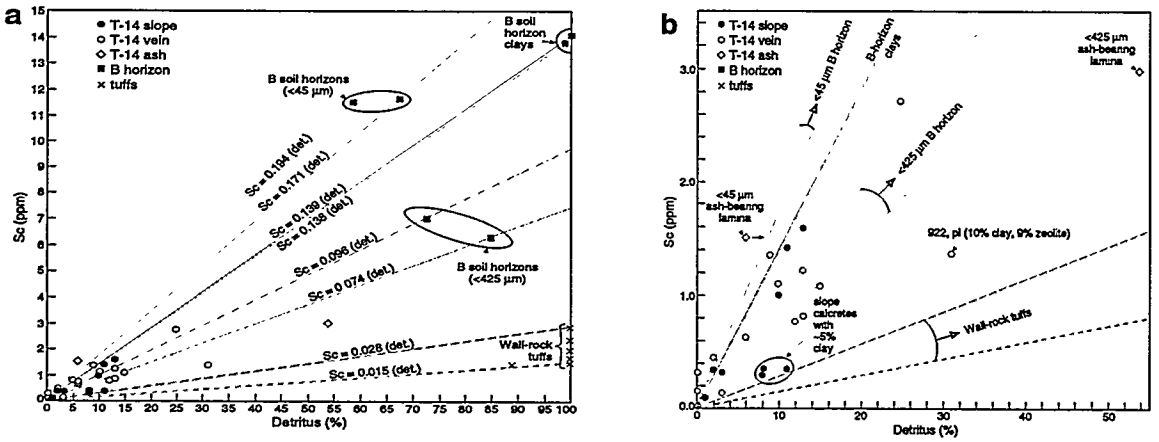

Fig. 35: (a) Scandium (by INAA) versus detritus (by XRD) for Trench 14 calcretes, B soil horizon samples, and wall-rock tuffs. Expanded scale (b) concentrates on the calcrete samples.

are capped unconformably by the slope calcrete. These structural features suggest a more restricted history of vein-calcrete formation at Trench 14A.

In addition to the structural differences, the vein calcretes at Trench 14A have gained much of their detritus from local tuffs rather than from weathered or eolian detritus. This is evident in part from the Sc/FeO ratios of the vein calcretes, which match the vitric Rainier Mesa Tuff at the west end of the fault but are more similar to the calcretes of Trench 14 at the eastern end of the fault, near the Tiva Canyon Tuff (Fig. 27b). Figure 36 uses the same axes as Fig. 35 to examine Sc/detritus ratios at Trench 14A. Here there is apparently strong support for derivation of much of the detritus in the vein calcretes from the wall-rock tuffs; only the slope calcrete that lies unconformably above the vein is similar to the Trench 14 calcretes. However, this interpretation is complicated by the very clay-rich compositions of the vein calcretes at Trench 14A (9 to 34% smectite). Because the clay-rich calcretes at Trench 14A are Sc- and Fe-poor, this smectite must be very different from the Fe-rich smectite of the B soil horizons at Trench 14. Clearly the chemistry of smectites at Exile Hill is variable and may reflect a number of alteration processes plus, in at least the B soil horizons, some component of eolian input. Nevertheless, much of the detritus in the simple vein calcretes at Trench 14A appears to come directly from the adjacent wall-rock tuffs, whereas the structurally complex vein calcretes at Trench 14 show little evidence of such direct wall-rock interaction. The multiple episodes of fracturing and refracturing in the complex vein calcretes at Trench 14 provide a gradation into the slope calcretes and ultimately link the vein calcretes to the B soil horizons. It is these fractures that have provided the predominant pathways for introducing detritus into the calcretes at Trench 14. Without this extensive fracturing, the introduction of authigenic calcite, opal, and sepiolite is also curtailed and only minimal vein calcretes are developed in Trench 14A.

B. Sources and Rates of Authigenic Mineralization

1. Sources of authigenic constituents. There is a considerable body of evidence that the calcite in many desert soils is derived from Ca dissolved in rainwater, or carried as eolian dust, and atmospheric or root-respired CO_2 (Machette 1985; Quade et al. 1989; Reheis et al. 1992). Opal may be attributed to the dissolution of unstable volcanic glass, where both local and eolian sources are available (Chadwick et al. 1989). At Trench 14 there is a source of nonwelded vitric tuff in the western wall of the fault, but another silica source may be found in the welded crystalline tuffs that are widely distributed at Yucca Mountain. The quantitative-XRD mineralogic data in Appendices 3 (B-horizon soil samples), and 4–5 (calcretes) indicate that although weathering of vitric tuff along the western side of the fault may provide some of the silica deposited as opal in these particular calcretes, some silica may also be acquired by dissolution of tridymite and cristobalite. The B soil horizons have weight ratios of (tridymite+cristobalite)/quartz of ~0.3 in the <425 μm fractions and <0.1 in the <45 μm fractions (Appendix 3). In the siliceous calcretes, this ratio is essentially zero (Appendices 4 and 5). This loss of the least-stable silica polymorphs occurs along with the dilution of all detrital silica and the increase of authigenic opal-A. Dissolution of unstable crystalline silica polymorphs may thus be a contributing source for the silica that is deposited as opal in the calcretes.

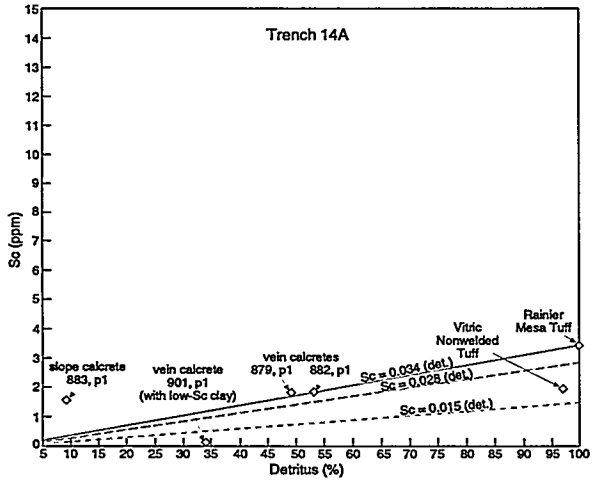

Fig. 36: Scandium (by INAA) versus detritus (by XRD) for Trench 14A calcretes and wall-rock tuffs. The axes in this figure span the same range as the axes in Fig. 35a. The two lower regression lines (Sc=0.0145*detritus and Sc=0.0283*detritus) are the same as the two lowest lines in Figs. 35a and 35b; the highest regression line (Sc=0.034*detritus) extends toward the Rainier Mesa Tuff. Only the slope calcrete at Trench 14A has the higher Sc/detritus ratio similar to the Trench 14 calcretes (Fig. 35a). The vein calcretes, unlike those at Trench 14, have Sc/detritus ratios which, when considered with their Sc/FeO ratios (Fig. 27b), indicate direct incorporation of detritus from the closest wall-rock tuffs. The differences between Trench 14 and Trench 14A show that fault development and structure on a very local scale can have profound effects on the type of detritus incorporated by vein calcretes. Where the vein calcretes are most extensively developed, as at Trench 14 (Figs. 2b and 3a), surface rupturing and fracture connections with upper soil horizons provide the dominant pathway for both detritus and fluid penetration to deposit calcite, opal, and sepiolite. Where an unconformity separates the vein and slope calcretes, as at Trench 14A (Fig. 4), the vein calcretes are minimally developed and lack direct connections to the active soil surface.

2. Rates of authigenic accumulation. It has been suggested that there is too much calcite and opal in the calcretes at Trench 14 to be accounted for by gradual pedogenic accumulation (Archambeau and Price 1991). This is not the case. The greatest accumulations of calcite and opal occur within the vein calcretes. The vein calcrete at Trench 14 forms a wedge, 2.25 m wide near the surface, that pinches down to a few centimeters' width at 4.75 m depth (Fig. 2a). Six-tenths of the material in this wedge is laminated calcrete; the remainder consists of blocks of altered Tiva wall-rock tuff. The average bulk density of the calcretes is 1.6 g/cm^3 (Table 2). The average calcite weight fraction of the calcretes is 53%, leading to an estimated calcite abundance of 1.2×10^6 g per m^2 of overlying surface above this wedge of vein calcrete. Estimates of eolian carbonate accumulation rates for soils on noncalcareous parent materials in the southwestern United States range from 0.3 to 5 g/m^2/yr (Machette 1985; Reheis et al. 1992). At these rates, the amount of calcite within the excavated veins at Trench 14 could accumulate over a time span between 4,000,000 and 240,000 years (1/3 to 1/50 of the age of the wall-rock tuffs). Carbon and oxygen isotopic data indicate that most of the calcite in Trench 14 was deposited during colder and wetter Pleistocene climates (Quade and Cerling 1990). The timespans estimated here could allow pedogenic accumulation of all Trench 14 calcite within the 1.6 million years of the Pleistocene Epoch.

Because the calcretes of Trench 14 are siliceous, it is possible to compare the rates of silica and calcite accumulation. Within the same calcrete wedge described above, the average opal weight fraction is 36%, leading to an estimated opal abundance of 0.8×10^6 g/m^2. The solubility of SiO_2 in arid soils containing abundant siliceous glass may exceed 0.07 g/L (Chadwick et al. 1989). However, waters in local higher-elevation soils at Rainier Mesa, Nevada, have SiO_2 contents of 0.02–0.04 g/L (Kerrisk 1987). For the SiO_2 concentration range of 0.07–0.02 g/L, 1.1 to 4.0×10^6 cm/cm^2 of rain water can form enough soil water to deposit the opal within the calcrete wedge. Current rainfall at the elevation of Trench 14 is ~15 cm/yr (Spaulding 1983). At this precipitation rate, sufficient rainwater to form the opal in the vein calcrete could infiltrate, dissolve local silicates, and evaporate within 70,000 to 270,000 years. The longer time estimate may be more appropriate, since the wetter and cooler climates that prevailed during calcrete formation (Quade and Cerling 1990) may have resulted in deposition from relatively silica-poor soil waters like those of Rainier Mesa. A 30–100% increase in rainfall during the Pleistocene (Spaulding et al. 1984) could shorten the longer estimate to as little as 135,000 years. These estimated time spans for opal accumulation could be low if quantities of silica in solution have been lost through runoff and by flow into deeper fractures. Nevertheless, the independent estimates for rates of eolian accumulation (of Ca for calcite) and of *in situ* dissolution (of SiO_2 for opal) fall within time spans that are

typical of pedogenic processes. Nonpedogenic sources are not required to account for the observed volume of calcrete.

C. Comparisons with Known Spring Features

Portions of this study provide some comparative data from known active or inactive spring and seep localities. Inferences of origin from analogy or degree of similarity provide only a secondary method for testing assumptions based on more direct evidence of chemical or physical processes operating within a particular deposit. Nevertheless, there are some features that do provide a guide in the identification of calcite-silica deposits of various origins.

The intimate intergrowth of calcite and opal in the calcretes of Exile Hill is atypical of spring deposits. Cool and warm springs, from deep or perched sources, have higher water flow and can maintain stable pH regimes that precipitate either calcite or silica but rarely both (White et al. 1956; Chafetz and Folk 1984; Viles and Goudie 1990). In contrast, evaporative processes within arid soils formed of siliceous detritus can cause a rise in pH from only slightly alkaline to >9 (Chadwick et al. 1989; Boettinger and Southard 1990), passing from regimes of calcite dissolution and silica precipitation into those of calcite precipitation and silica dissolution (Watts 1980). Numerous wetting and drying cycles can thus lead to repeated pH-driven dissolution-precipitation cycles that can account for the complex calcite and opal intergrowths seen in the calcretes of Trench 14. The closest analogous spring deposits are surface discharges that may deposit both calcite and silica, as at GMC and IMV springs. In these deposits, however, the opal and calcite are largely segregated or easily separable and not as intimately intergrown as in the calcretes of Exile Hill. The spring deposits analyzed for this study have a greater bulk density than the calcretes at Exile Hill (Tables 2 and 3). This is particularly true for the vein deposits at known spring localities. However, the more porous tufa mounds, as at Nevares, can develop low-density deposits that have densities low enough to approach those of the most dense of the vein deposits at Exile Hill. Other physical and chemical features provide more definitive distinctions between the calcite-silica deposits of spring or soil-process origins.

Many of the same authigenic minerals (calcite, opal, and sepiolite) that occur in the calcretes can also be found in known spring or seep deposits. However, there are certain key differences in the deposits that form in these two different environments. Veins of pure calcite are common at spring localities but do not occur in the calcretes. Individual calcite crystals of >1 cm are common in travertine veins at springs but are not found in any of the calcretes, including the vein calcretes. Where comparable fine-grained calcite does occur in travertine mounds at springs, it is still very common to obtain deposits of relatively pure calcite with characteristic bacterial clumps and ostracod fossils. Fossil casts from the stems of phreatophyte plants, connected by meniscal

septae, provide readily visible field evidence of spring activity. None of these features are found in the calcretes at Trench 14.

Although mineral-chemical data provide further evidence of some distinctions between spring deposits and calcretes (Table 4, Fig. 22), it is important not to rely solely on such comparisons. For example, the commonly higher MgO content of many spring- and seep-deposited calcites is useful in comparing the particular calcretes at Exile Hill with spring deposits of the region, but calcretes of pedogenic origin with other eolian sources could have carbonate components of more Mg-rich composition. On the other hand, apparent similarities such as the comparable calculated or measured Sr contents of calcite in the calcretes and spring deposits (Fig. 28) cannot be used to imply a common origin unless considered separately from all of the other data, both petrographic and chemical, that differentiate between these two types of calcite deposits. This would be a narrow assessment and a misuse of the available data. Taken together, the comparative data for local spring deposits illustrate many dissimilarities between the regional spring or seep deposits and the calcretes at Exile Hill.

D. Constraints on Origin Based on Pedogenic Fossils

Springs and evaporative seeps retain biogenic evidence of their past higher water content, including ostracod fossils, casts of phreatophyte plants, and algal or diatomaceous deposits of opal-A. Pedogenic calcretes have a different set of fossils. Calcified filaments (Fig. 6b) are typically pedogenic. Superficially similar calcareous filaments occur as algal products in active springs, but these delicate filaments are not preserved in accumulated inactive spring deposits, whereas bacterial "shrub" structures commonly are (Chafetz and Folk 1984; Viles and Goudie 1990). In contrast, the calcified filaments in the Trench 14 calcretes are found in the oldest as well as the youngest laminae. Moreover, algal filaments in springs are not restricted to associations with fossil roots, as are the calcified filaments of the Trench 14 calcretes. Needle-fiber calcites (Fig. 6c) are unlikely to form and less likely to be preserved in areas of spring discharge.

These delicate fossils within root casts provide two important constraints on the origins of the siliceous calcretes. First, the fragile fossil forms are preserved even within the earliest-formed calcrete laminae (Fig. 2c); such preservation would be unlikely if the calcretes were emplaced by successive forceful fluid injections with catastrophic brecciation. Indeed, the pervasive distribution of root fossils suggests that root penetration plays a distinctly noncatastrophic but nevertheless forceful role (Klappa 1980) in the brecciation of these calcretes. The dense, sheared laminae (Figs. 2c, 2d, and 3b) are pervaded by root-fossil remnants and may represent collapsed zones where coarser roots were once concentrated. Second, similar needle-fiber calcites and calcified filaments within fossil roots are characteristic of pedogenic calcretes (Klappa 1979; Phillips

and Self 1987; Wright 1986 and 1989). In evaporative seeps and in calcareous tufa mounds around springs, the fossilization of vascular plants typically leaves casts of the plant form without preserving such fine features of root decay (Fig. 14). The high water flux in seeps and springs flushes out the products of decay, leaving only the plant casts behind. Calcified filaments, needle-fiber calcites, and other delicate fungal fossils within root forms thus provide an important guide to pedogenic calcretes, particularly where they occur beneath a genetically related B horizon. Intermittently saturated desert soils without pedogenic horizonation might retain delicate fungal fossils (Mack and James 1992), but the retention of such features is unlikely in zones of forceful spring discharge.

V. CONCLUSIONS

The accumulated petrographic, mineralogic, and chemical data from siliceous calcretes at Exile Hill indicate that pedogenic processes alone account for the formation of these soil features. Surface tufa mounds at spring discharge areas can have some similarities to calcite-silica deposits that are pedogenic in origin and evolution, but they contain particular features (bacterial clumps, ostracod fossils, fossilized casts of phreatophyte plants, and readily separable calcite) that are distinctive. In determining the origin of a particular calcrete, it is best to consider the broader field evidence first. Features such as tufa dams and rimstone pools would be definitive evidence of deposition from surface discharge and flow. The absence of such features should lead to a closer search for indications of pedogenic origin. Detection of calcified filaments, needle-fiber calcites, and related fungal microfossils throughout a calcrete—and specifically in calcrete that formed beneath a related B soil horizon—can confirm a pedogenic origin. Site-specific studies of mineralogy and chemical evolution requiring the derivation of detritus from overlying soil horizons (Figs. 27, 34–35), with isotopic evidence for calcite precipitation from soil waters (Quade and Cerling 1990; Stuckless et al. 1991), should remove any lingering uncertainty.

ACKNOWLEDGMENTS

This work was supported by the Yucca Mountain Site Characterization Project Office as part of the Civilian Radioactive Waste Management Program. This Project is managed by the U.S. Department of Energy, Yucca Mountain Site Characterization Project. Review comments by S. Levy, A. Simmons, and V. Stewart helped to improve the manuscript. Typesetting and illustrations were done by L. Piotrowski and A. Garcia. The Yucca Mountain Project Technical Catalog Data Tracking Number for this work is LA-000000000094.001. The record package containing traceability information is LA-EES-1-05-94-003.

REFERENCES

Archambeau, C. B. and Price, N. J., "An assessment of J. S. Szymanski's conceptual hydro-tectonic model and its relevance to hydrologic and geologic processes at the proposed Yucca Mountain nuclear waste repository, (minority report of the special DOE review panel)," Yucca Mountain Site Characterization Project Office, Las Vegas, Nevada, (1991), NNA.911210.0057.

Bish, D. L. and Chipera, S. J., "Problems and solutions in quantitative analysis of complex mixtures by X-ray powder diffraction," *Advances in X-Ray Analysis*, **31**:295–308, (1988), NNA.890405.0178.

Bish, D. L. and Chipera, S. J., "Revised mineralogic summary of Yucca Mountain, Nevada," Los Alamos National Laboratory report LA-11497-MS, (1989), NNA.891019.0029.

Boettinger, J. L. and Southard, R. J., "Micromorphology and mineralogy of a calcareous duripan formed in granitic residuum, Mojave Desert, California, USA," in *Soil Micromorphology: A Basic and Applied Science*, (Elsevier, Amsterdam, 409–415, 1990), NNA.940523.0005.

Boyle, R. W., "Biogeochemistry of gold," in *The Geochemistry of Gold and Its Deposits*, Geol. Survey of Canada, Bull. 280, 79–88, (1979), NNA.940523.0011.

Brimhall, G. H., Chadwick, O. A., Lewis, C. J., Compston, W., Williams, I. S., Danti, K. J., Dietrich, W. E., Power, M. E., Hendricks, D., and Bratt, J., "Deformational mass transport and invasive processes in soil evolution," *Science*, **255**:695–702, (1991), NNA.940531.0001.

Broad, W. J., "A mountain of trouble," *New York Times Magazine*, (Nov. 18, 1990), NNA.921019.0177.

Chadwick, O. A., Hendricks, D. M., and Nettleton, W. D., "Silicification of Holocene soils in northern Monitor Valley, Nevada," *Soil Science Society of America Journal*, **53**:158–164, (1989), NNA.921019.0165.

Chafetz, H. S. and Folk, R. L., "Travertines: Depositional morphology and the bacterially constructed constituents," *Journal of Sedimentary Petrology*, **54**:289–316, (1984), NNA.921019.0167.

Chung, F. H.. "Quantitative determination of X-ray diffraction patterns of mixtures. I. Matrix-flushing method for quantitative multicomponent analysis." *Journal of Applied Crystallography*, **7**:519–525, (1974), NNA.890405.0179.

Gibson, J. D., Swan, F. H., Wesling, J. R., Bullard, T. F., Perman, R. C., Angell, M. M., and DiSilvestro, L. A., "Summary and evaluation of existing geological and geophysical data near prospective surface facilities in Midway Valley, Yucca Mountain Project, Nye County, Nevada," Sandia National Laboratories report SAND90-2491, (1992).

Gile, L. H., Peterson, F. F., and Grossman, R. B., "Morphological and genetic sequences of carbonate accumulation in desert soils," *Soil Science*, **101**:347–360, (1966), HQS.880517.2684.

Guthrie, G. D., Jr., Raymond, R., Jr., Chipera, S. J., and Bish, D. L., "The distribution of airborne minerals around UZ-16," Los Alamos National Laboratory Letter report TWS-EES-1-09-93-009, (1993).

Jaillard, B., Guyon, A., and Maurin, A. F., "Structure and composition of calcified roots, and their identification in calcareous soils," *Geoderma*, **50**:197–210,. (1991), NNA.940523.0002.

Junge, C., "The importance of mineral dust as an atmospheric constituent," in Morales, C., ed., *Saharan Dust: Mobilization, Transport, Deposition*, John Wiley & Sons, New York, 49–60, (1979), MOL.19940927.0001.

Kerrisk, J. F., "Groundwater chemistry at Yucca Mountain, Nevada, and vicinity," Los Alamos National Laboratory report LA-10929-MS, (1987), NNA.870507.0017.

Klappa, C. F., "Calcified filaments in Quaternary calcretes: Organo-mineral interactions in the subaerial vadose environment," *Journal of Sedimentary Petrology*, **49**:955–968, (1979), NNA.921019.0170.

Klappa, C. F., "Brecciation textures and tepee structures in Quaternary calcrete (caliche) profiles from eastern Spain: The plant factor in their formation," *Geological Journal*, **15**:81–89, (1980), NNA.921019.0171.

Korotev, R. L., "Chemical stratigraphy of two regolith cores from the Central Highlands of the Moon," In: V. L. Sharpton and G. Ryder (Editors), Proceedings of the 21st Lunar and Planetary Science Conference, Lunar and Planetary Institute, Houston, 229–289, (1991), NNA.921019.0612.

Machette, M. N., "Calcic soils of the southwestern United States," Geological Society of America Special Paper 203, (1985), NNA.900712.0001.

Mack, G. H. and James, W. C., "Calcic paleosols of the Plio-Pleistocene Camp Rice and Palomas Formations, southern Rio Grande Rift, USA," *Sedimentary Geology*, **77**:89–109, (1992), NNA.940523.0007.

Marshall, E., "The geopolitics of nuclear waste," *Science*, **251**:864–867, (1991), NNA.921019.0164.

Monger, H. C., Daugherty, L. A., Lindemann, W. C., and Liddell, C. M., "Microbial precipitation of pedogenic calcite," *Geology*, **19**:997–1000, (1991), NNA.940523.0010.

Pentecost, A., "Travertine: Life inside the rock," *Biologist*, **39**:161–164, (1992), NNA.940523.0009.

Phillips, S. E. and Self, P. G., "Morphology, crystallography, and origin of needle-fibre calcite in Quaternary pedogenic calcretes of South Australia," *Australian Journal of Soil Research*, **25**:429–444, (1987), NNA.921019.0176.

Quade, J. and Cerling, T. E., "Stable isotopic evidence for a pedogenic origin of carbonates in Trench 14 near Yucca Mountain, Nevada," *Science*, **250**:1549–1552, (1990), NNA.910326.0100.

Quade, J., Cerling, T. E., and Bowman, J. R., "Systematic variations in the carbon and oxygen isotopic composition of pedogenic carbonate along elevation transects in the Southern Great Basin, United States," *Geol. Soc. Amer. Bull*, **101**:464–475, (1989), NNA.910617.0011.

Reheis, M. C., Sowers, J. M., Taylor, E. M., McFadden, L. D., and Harden, J. W., "Morphology and genesis of carbonate soils on the Kyle Canyon fan, Nevada, U.S.A.," *Geoderma*, **52**:303–342, (1992), NNA.921019.0174.

Roedder, E., Whelan, J. F., and Vaniman, D. T., "Fluid inclusion studies of calcite veins from Yucca Mountain, Nevada, tuffs: Environment of formation," In *High Level Radioactive Waste Management*, Amer. Soc. Civil Eng. and Amer. Nuc. Soc., Proc. 5th Internat. Conf., Las Vegas, Nevada, 1854–1860 (1994), NNA.940607.0172.

Simkiss, K. and Wilbur, K. W., "Biomineralization," Academic Press, San Diego, 111–113, (1989), NNA.940523.0003.

Soil Survey Staff, "Soil Taxonomy," *U.S. Department of Agriculture Handbook 436*, 155–177, (1975), NNA.940523.0004.

Spaulding, W. G., "Vegetation and climates of the last 45,000 years in the vicinity of the Nevada Test Site, south-central Nevada," U.S. Geological Survey Open-File Report 83–535, (1983), NNA.890523.0110.

Spaulding, W. G., Robison, S. W., and Paillet, F. L., "Preliminary assessment of climatic change during Late Wisconsin time, southern Great Basin and vicinity, Arizona, California, and Nevada," U.S. Geological Survey Water-Resources Investigation Report 84-4328, (1984), NNA.870519.0110.

Stuckless, J. S., Peterman, Z. E., and Muhs, D. R., "U and Sr isotopes in ground water and calcite, Yucca Mountain, Nevada: Evidence against upwelling water," *Science*, **254**:551–554, (1991), NNA.920318.0087.

Szabo, B. J. and Kyser, T. K., "Ages and stable-isotope compositions of secondary calcite and opal in drill cores from Tertiary volcanic rocks of the Yucca Mountain area, Nevada," *Geol . Soc. Amer. Bull.*, **102**:1714–1719, (1990), NNA.910225.0068.

Taylor, E. M., and Huckins, H. E., "Carbonate and opaline silica fault-filling on the Bow Ridge Fault, Yucca Mountain, Nevada - deposition from pedogenic processes or upwelling groundwater?," *Geological Society of America Abstracts with Programs*, Flagstaff, Arizona, **18**:418, (1986), NNA.921019.0178.

Taylor, E. M. and Huckins, H. E., "Logs and Interpretations of Trench 14 on the Bow Ridge Fault at Exile Hill, Nye County, Nevada," *U. S. Geol. Survey Open-File Rept. 93-477*, (1995).

Vaniman, D. T., "Calcite deposits in fractures at Yucca Mountain, Nevada," In *High Level Radioactive Waste Management*, Amer. Soc. Civil Eng. and Amer. Nuc. Soc., Proc. 4th Internat. Conf., Las Vegas, Nevada, 1935–1939, (1993), NNA.931028.0001.

Vaniman, D. T., "Calcite deposits in drill cores USW G-2 and USW GU-3/G-3 at Yucca Mountain, Nevada: Preliminary report," Los Alamos National Laboratory report LA-12720-MS, (1994), NNA.930422.0058.

Vaniman, D. T. and Whelan, J. F., "Inferences of paleoenvironment from petrographic, chemical and stable-isotope studies of calcretes and fracture calcites," In *High Level Radioactive Waste Management*, Amer. Soc. Civil Eng. and Amer. Nuc. Soc., Proc. 5th Internat. Conf., Las Vegas, Nevada, 2730–2737, (1994), NNA.940607.0171.

Vaniman, D., Downey, J., Bish, D., O'Neil, J., and Levy, S., "Impact of fault-related mineral deposits on site characterization at Yucca Mountain: Studies as of July, 1985," Los Alamos National Laboratory Letter report TWS-ESS-1-7/85-20, (1985), NNA.870407.0275.

Vaniman, D. T., Bish, D. L., and Chipera, S., "A preliminary comparison of mineral deposits in faults near Yucca Mountain, Nevada, with possible analogs," Los Alamos National Laboratory report LA-11289-MS, (1988), NNA.880519.0017.

Vaniman, D. T., Ebinger, M. H., Bish, D. L., and Chipera, S. J., "Precipitation of calcite, dolomite, sepiolite, and silica from evaporated carbonate and tuffaceous waters of southern Nevada, USA," In *Proc. 7th Int. Symposium on Water-Rock Interaction, Park City, Utah, 13–18 July, 1992*, 687–691, (1992), NNA.930105.0015.

Vaniman, D. T., Chipera, S. J., and Bish, D. L., "Pedogenesis of siliceous calcretes at Yucca Mountain, Nevada," *Geoderma*, **63**:1–17, (1994).

Viles, H. A. and Goudie, A. S., "Reconnaissance studies of the tufa deposits of the Napier Range, N.W. Australia," *Earth Surface Processes and Landforms*, **15**:425–443, (1990), NNA.921019.0169.

Warren, R. G., Byers, F. M., Jr., Broxton, D. E., Freeman, S. H., and Hagan, R. C., "Phenocryst abundances and glass and phenocryst compositions as indicators of magmatic environments of large-volume ash flow sheets in southwestern Nevada," *Journal of Geophysical Research*, **94**:5987–6020, (1989).

Watts, N. L., "Quaternary pedogenic calcretes from the Kalahari (southern Africa): Mineralogy, genesis and diagenesis," *Sedimentology*, **27**:661–686, (1980), NNA.921019.0175.

Weiss, S. I., Noble, D. C., and Larson, L. T., "Task 3: Evaluation of mineral resource potential, caldera geology, and volcano-tectonic framework at and near Yucca Mountain," Report for October, 1990 - September, 1991. Dept. of Geological Sci., Mackay School of Mines, University of Nevada, Reno, (1991), NNA.940523.0008.

Whelan, J. F. and Stuckless, J. S., "Paleohydrologic implications of the stable isotopic composition of secondary calcite within the Tertiary volcanic rocks of Yucca Mountain, Nevada," In *High Level Radioactive Waste Management*, Amer. Soc. Civil Eng. and Amer. Nuc. Soc., Proc. 3rd Internat. Conf., Las Vegas, Nevada, 1572–1581, (1992), NNA.930121.0109.

White, D. E., Brannock, W. W., and Murata, K. J., "Silica in hot-spring waters," *Geochimica et Cosmochimica Acta*, **10**:27–59, (1956), NNA.921019.0168.

Wright, V. P., "The role of fungal biomineralization in the formation of Early Carboniferous soil fabrics," *Sedimentology*, **33**:831–838, (1986), NNA.921019.0173.

Wright, V. P., "Terrestrial stromatolites and laminar calcretes: A review," *Sedimentary Geology*, **65**:1–13, (1989), NNA.921019.0172.

Data Sources:

Notebook TWS-EES-1-8/87-1, p. 120–152
Notebook TWS-EES-1-12-89-3, p. 28–57
Notebook TWS-EES-1-12-90-4, p. 13–152
Notebook TWS-EES-1-3-92-1, p. 1–142
Notebook TWS-EES-1-5-92-3, p. 59–67

Explanatory Notes to Appendix Tables

The Appendix tables 1 through 7 compile the available chemical and quantitative mineralogic data for 65 samples. Chemical data for all samples were collected by INAA. For selected samples, additional data were collected by XRF, AA, LOI (for volatiles), and/or ion chromatography (IC). Total iron is reported as FeO for all analyses. All Appendix tables except 6 include quantitative XRD analyses of mineralogy; in Appendix 5 some mineral abundances are calculated based on combined XRD and chemical constraints (XRD/chem) and in Appendix 6 the XRD mineralogic data are semi-quantitative. For all chemical data, the uncertainties in analytical precision are listed in parentheses after each entry; these uncertainties are ± one-standard-deviation values in the corresponding decimal placeholders of the last significant figures. For quantitative mineralogic data, the same listing of uncertainties is used, but here the uncertainties are ± two standard deviations.

Where quantitative numbers with uncertainties are not listed, the entries may indicate semiquantitaive mineral abundances (major, minor, and trace, with question marks indicating probable but not definite identification, in Appendix 6), a maximum possible concentration (<n), or no detection (-). In addition, an entry indicating *not applicable* (n/a) is used if an analysis was not made for that chemical constituent by that particular method, or if data were obtained but the sample collection and preparation methods used provide a possibility of chemical contamination for that constituent.

Several INAA analyses were obtained in duplicate, and the INAA entries for these samples represent the averages of the two analyses:

Appendix 1:	880,p1; 883,p1; 879,p1; 882,p1; 901,p1
Appendix 3:	429,p3; 430,p3
Appendix 4:	920,p1
Appendix 5:	1,p25; 7,p1; 47,p1; 773,p1; 922,p1
Appendix 6:	all samples
Appendix 7:	601,p1; 753,p1; 755,p1; 760,p1

Appendix 8 lists the duplicate analyses from which these averages were obtained.

Appendix 1: Quantitative Chemical (INAA) and Mineralogic (XRD) Data for Wall-Rock Tuffs and Calcretes from Trench 14A, Exile Hill

sample:	431,p1	880,p1	883,p1	879,p1	882,p1*	901,p1
tuff or calcrete type:	*vitric Rainier Mesa*	*vitric nonwelded tuff*	*bulk slope calcrete*	*bulk vein calcrete*	*bulk vein calcrete*	*thin vein calcrete*
*Chemistry (SiO_2-P_2O_5 by XRF; **K_2O by AA; volatiles by LOI; listings below volatiles by INAA*						
SiO_2 %	74.2(7)	n/a	n/a	n/a	n/a	n/a
TiO_2 %	0.107(3)	n/a	n/a	n/a	n/a	n/a
Al_2O_3 %	12.3(3)	n/a	n/a	n/a	n/a	n/a
FeO %	0.62(2)	n/a	n/a	n/a	n/a	n/a
MnO %	0.057(1)	n/a	n/a	n/a	n/a	n/a
MgO %	0.38(1)	n/a	n/a	n/a	n/a	n/a
P_2O_5	0.009(1)	n/a	n/a	n/a	n/a	n/a
**K_2O %	5.01(13)	n/a	n/a	n/a	n/a	n/a
volatiles %	3.4(3)	n/a	n/a	n/a	n/a	n/a
Na_2O %	3.10(4)	2.69(3)	0.723(7)	0.948(10)	1.509(17)	0.929(9)
K_2O %	n/a	4.2(7)	1.3(2)	1.1(2)	2.1(3)	<0.4
CaO %	0.5(2)	1.8(2)	25.4(4)	23.5(5)	17.3(4)	27.7(5)
FeO %	0.581(8)	0.937(10)	0.671(7)	0.779(8)	0.405(5)	0.0310(5)
Sc µg/g	3.40(5)	1.928(19)	1.594(17)	1.87(2)	1.884(20)	0.1200(12)
Cr µg/g	n/a	1.1(2)	5.0(2)	2.8(4)	1.30(19)	0.47(8)
Co µg/g	0.216(9)	0.454(15)	1.659(19)	2.03(3)	1.025(18)	0.551(7)
Ni µg/g	<25	<11	<20	<20	<20	8.7(1.6)
Zn µg/g	44(9)	-	-	-	-	2.6(2)
As µg/g	5.4(2)	4.2(3)	6.9(2)	8.65(19)	7.5(2)	12.7(2)
Se µg/g	<0.4	<0.3	<0.4	<0.3	<0.3	0.25(6)
Br µg/g	0.96(10)	1.27(17)	13.6(1.1)	7.8(7)	7.7(6)	32(3)
Rb µg/g	230(5)	147(2)	45.7(1.1)	33.9(1.1)	91.6(1.6)	4.8(3)
Sr µg/g	20(9)	267(14)	577(14)	791(17)	625(16)	1045(12)
Zr µg/g	90(10)	189(13)	57(8)	91(9)	41(9)	<6
Ag µg/g	n/a	-	-	-	-	-
Sb µg/g	0.512(15)	0.40(2)	0.689(16)	0.281(15)	0.449(16)	0.157(7)
Cs µg/g	6.02(9)	4.06(5)	1.81(2)	2.04(3)	2.96(4)	0.296(6)
Ba µg/g	26(8)	153(10)	172(7)	209(9)	70(7)	25(3)
La µg/g	20.3(3)	34.3(4)	11.56(12)	19.20(20)	10.68(12)	1.122(18)
Ce µg/g	48.3(7)	80.7(8)	22.1(2)	39.0(4)	23.6(3)	2.15(6)
Nd µg/g	15.2(1.3)	36(3)	8.5(1.1)	15.3(1.9)	9.2(1.5)	1.2(5)
Sm µg/g	4.24(6)	8.92(9)	1.689(20)	3.02(4)	2.25(2)	0.203(8)
Eu µg/g	0.108(4)	0.569(14)	0.208(7)	0.345(9)	0.126(6)	0.0150(13)
Tb µg/g	0.724(17)	1.26(3)	0.217(10)	0.391(13)	0.389(13)	0.033(3)
Yb µg/g	3.05(4)	3.54(4)	0.786(15)	1.30(2)	1.64(2)	0.158(8)
Lu µg/g	0.438(7)	0.480(9)	0.120(3)	0.187(5)	0.241(5)	0.0261(16)
Hf µg/g	3.40(5)	6.90(11)	1.94(3)	3.05(5)	1.79(4)	0.118(9)
Ta µg/g	2.20(5)	1.63(5)	0.392(16)	0.67(3)	1.06(4)	0.056(3)
W µg/g	1.9(2)	1.1(5)	1.6(3)	0.9(2)	1.4(3)	1.49(19)
Au ng/g	<1.5	3.5(2.6)	5.2(1.4)	7.5(1.8)	8.7(2.0)	7.4(1.2)
Th µg/g	20.7(3)	21.0(2)	5.68(6)	10.26(10)	9.52(10)	0.590(9)
U µg/g	6.86(15)	5.55(15)	7.00(12)	2.48(7)	6.23(13)	2.24(5)
XRD						
`	7(1)	1(1)	1(1)	tr	4(1)	tr
cristobalite	-	tr	-	-	-	-
feldspar	9(1)	13(2)	6(1)	10(1)	10(1)	-
biotite	-	-	tr	tr	tr	-
amphibole	-	tr	tr	-	-	-
glass	82(2)	74(3)	-	-	30(4)*	-
clinoptilolite	-	5(1)	1(1)	9(1)	-	-
calcite	-	3(1)	50(3)	48(2)	37(2)	52(3)
opal-A	-	-	41(1)	3(9)	10(4)*	14(10)
illite	2(1)	-	-	-	-	-
smectite	tr	4(1)	1(1)	30(9)	9(3)	34(10)

*In sample 882,p1, total of 40% amorphous material is apportioned among glass and opal-A using the calcite/opal-A ratio as measured in nearby vein 901,p1.

Appendix 2: Quantitative Chemical (XRF, AA, LOI, INAA) and Mineralogic (XRD) Data for Wall-Rock Tuffs Exposed in Trench 14, Exile Hill

sample:	428,p1	428,p2	3,p1	4,p1	6,p1	921,p1	427,p1
tuff type:	*Tiva*	*Tiva vapor-phase*	*slightly altered Tiva*	*hematite altered Tiva*	*hematite altered Tiva*	*opal altered Tiva*	*vitric tuff*
Chemistry (SiO_2 - P_2O_5 by XRF; *K_2O by AA; volatiles by LOI; others by INAA)							
SiO_2 %	75.3(8)	74.9(7)	75.9(8)	74.15(7)	78.14(8)	n/a	72.2(7)
TiO_2 %	0.147(4)	0.151(4)	0.207(5)	0.267(7)	0.227(6)	n/a	0.184(5)
Al_2O_3 %	12.7(3)	12.8(3)	12.2(3)	11.1(3)	10.4(3)	n/a	12.9(3)
FeO %	0.92(3)	0.616(17)	0.87(2)	1.14(3)	1.08(3)	n/a	1.03(3)
MnO %	0.099(3)	0.094(3)	0.105(3)	0.092(2)	0.083(2)	n/a	0.097(3)
MgO %	0.23(1)	0.33(1)	0.28(1)	0.40(1)	0.46(1)	n/a	0.34(1)
P_2O_5	0.007(1)	0.003(1)	0.022(2)	0.021(2)	0.016(2)	n/a	0.026(3)
*K_2O %	4.9(1)	4.92(12)	4.6(1)	4.1(1)	4.0(1)	n/a	5.08(13)
volatiles %	1.19(12)	1.75(17)	1.38(14)	3.9(4)	1.72(17)	n/a	4.3(4)
Na_2O %	3.87(5)	3.61(5)	3.75(5)	3.49(5)	3.26(5)	3.62(4)	2.92(4)
K_2O %	n/a	n/a	n/a	n/a	n/a	4.2(6)	n/a
CaO %	-	<0.5	<0.8	0.9(3)	0.6(2)	0.24(11)	<0.5
FeO %	0.871(12)	0.812(11)	0.976(14)	1.177(17)	1.020(14)	0.797(8)	0.883(12)
Sc µg/g	1.45(2)	1.65(2)	1.94(3)	2.83(4)	2.34(3)	1.408(14)	1.94(3)
Cr µg/g	n/a	n/a	n/a	n/a	n/a	<3	n/a
Co µg/g	0.173(9)	0.178(4)	0.373(9)	0.635(11)	0.492(9)	0.221(9)	1.89(3)
Ni µg/g	-	<20	<25	<15	<20	<20	<20
Zn µg/g	73(15)	74(15)	86(18)	68(14)	61(12)	63.7(1.0)	74(15)
As µg/g	11.4(3)	7.7(3)	8.1(3)	3.7(3)	3.3(3)	8.8(3)	4.9(3)
Se µg/g	<0.4	<0.3	<0.5	<0.3	<0.3	<0.4	<0.2
Br µg/g	0.37(10)	0.24(10)	0.25(11)	0.30(12)	<0.3	0.398(14)	0.92(12)
Rb µg/g	188(6)	189(4)	149(5)	106(4)	103(3)	185(2)	183(5)
Sr µg/g	37(8)	31(5)	39(9)	52(9)	43(9)	29(7)	134(12)
Zr µg/g	208(10)	256(7)	266(13)	336(12)	298(10)	178(9)	208(8)
Ag µg/g	n/a	n/a	n/a	n/a	n/a	-	n/a
Sb µg/g	0.28(2)	0.291(12)	0.203(15)	0.217(14)	0.213(13)	0.398(14)	0.491(16)
Cs µg/g	3.30(5)	3.33(5)	2.68(4)	2.03(3)	2.00(3)	3.18(4)	4.87(7)
Ba µg/g	64(8)	38(6)	134(8)	329(11)	250(9)	42(4)	166(8)
La µg/g	29.5(4)	23.3(3)	39.7(6)	73.5(1.0)	67.6(1.0)	29.2(3)	38.2(5)
Ce µg/g	54.2(8)	71.2(1)	95.2(1.3)	150(2)	135(2)	61.2(6)	88.1(1.2)
Nd µg/g	25(2)	24.7(1.6)	34(3)	52(4)	50(3)	23.0(1.7)	34(2)
Sm µg/g	6.00(9)	7.26(10)	7.91(11)	8.29(12)	8.35(12)	6.00(6)	8.28(12)
Eu µg/g	0.272(7)	0.323(6)	0.555(12)	1.15(2)	1.010(17)	0.265(7)	0.480(9)
Tb µg/g	0.95(2)	1.21(2)	1.11(2)	0.829(14)	0.889(15)	0.88(2)	1.14(2)
Yb µg/g	3.27(5)	3.63(5)	3.11(5)	2.37(4)	2.41(4)	2.95(3)	3.66(5)
Lu µg/g	0.471(10)	0.515(11)	0.444(10)	0.361(9)	0.350(8)	0.420(6)	0.513(11)
Hf µg/g	7.56(13)	8.77(12)	7.93(13)	8.07(13)	7.46(12)	7.18(10)	6.87(11)
Ta µg/g	1.64(5)	1.73(3)	1.34(3)	0.948(16)	0.923(16)	1.53(4)	1.74(5)
W µg/g	2.1(3)	<2	1.7(8)	<2	<2	1.6(4)	1.7(3)
Au ng/g	<2	<2	<2	<2	<5	12.6(1.8)	<3
Th µg/g	24.3(3)	24.5(3)	20.2(3)	15.4(2)	15.0(2)	23.8(2)	24.3(3)
U µg/g	4.57(14)	3.95(12)	5.00(14)	5.97(17)	5.36(15)	4.91(11)	5.12(14)
XRD							
quartz	3(1)	13(1)	11(1)	tr	2(1)	3(1)	2(1)
tridymite	7(1)	13(1)	18(2)	31(3)	41(4)	10(1)	-
cristobalite	22(2)	9(4)	10(1)	8(4)	7(4)	18(2)	2(1)
feldspar	63(10)	59(11)	54(11)	59(16)	50(16)	51(7)	9(1)
amphibole	-	-	-	tr	tr	-	-
biotite	-	-	-	-	-	tr	-
hematite	-	tr	1(1)	1(1)	1(1)	tr	-
glass	-	-	-	-	-	-	85(2)
opal-A	-	-	-	-	-	11(8)	-
opal-CT	-	-	tr	tr	tr	-	-
illite	-	-	1(1)	-	-	-	-
smectite	4(1)	4(1)	1(1)	1(1)	-	7(2)	-
sepiolite	-	-	-	<<5	<5	-	-
clinoptilolite	-	-	-	-	-	-	2(1)

Appendix 3: Quantitative Chemical (INAA) and Mineralogic (XRD) Data for B-Horizon Soil Samples from Trench 14, Exile Hill

sample:	429,p1	429,p2	429,p3	430,p1	430,p2	430,p3
soil constituent and size:	*Btk horizon, <425 µm*	*Btk horizon, <45 µm*	*Btk horizon, clay*	*2Btj horizon, <425 µm*	*2Btj horizon, <45 µm*	*2Btj horizon, clay*
*Chemistry (SiO_2 - P_2O_5 by XRF; *K_2O by AA; volatiles by LOI; others by INAA)*						
SiO_2 %	66.1(7)	n/a	n/a	66.4(7)	n/a	n/a
TiO_2 %	0.525(13)	n/a	n/a	0.479(12)	n/a	n/a
Al_2O_3 %	14.6(4)	n/a	n/a	15.0(4)	n/a	n/a
FeO %	2.80(8)	n/a	n/a	3.02(8)	n/a	n/a
MnO %	0.088(2)	n/a	n/a	0.065(2)	n/a	n/a
MgO %	1.33(3)	n/a	n/a	1.21(3)	n/a	n/a
P_2O_5	0.052(5)	n/a	n/a	0.045(5)	n/a	n/a
*K_2O %	3.90(10)	n/a	n/a	3.48(9)	n/a	n/a
volatiles %	4.9(5)	n/a	n/a	5.8(6)	n/a	n/a
Na_2O %	2.92(4)	2.23(3)	0.169(3)	2.36(3)	1.45(2)	0.077(2)
K_2O %	n/a	n/a	3.9(5)	n/a	n/a	2.3(3)
CaO %	2.0(2)	2.4(3)	2.2(2)	1.75(19)	1.6(2)	2.7(2)
FeO %	2.67(4)	4.82(7)	5.14(5)	2.87(4)	4.47(6)	5.10(5)
Sc µg/g	6.26(9)	11.63(16)	13.66(14)	7.02(10)	11.47(16)	13.93(14)
Cr µg/g	23.5(4)	58.3(9)	47.6(7)	26.1(4)	48.4(8)	45.1(7)
Co µg/g	5.72(8)	10.04(14)	n/a	6.49(9)	9.28(13)	n/a
Ni µg/g	21(9)	<50	<80	12(6)	40(13)	<100
Zn µg/g	68.2(1.4)	100(10)	-	74(8)	105(10)	-
As µg/g	5.3(3)	9.1(6)	10.3(4)	5.2(3)	8.0(3)	8.4(4)
Se µg/g	<0.3	<0.9	<1.2	<0.4	<0.5	<0.7
Br µg/g	2.4(3)	3.6(4)	14.4(1.2)	0.90(15)	2.3(3)	3.8(4)
Rb µg/g	126(2)	136(3)	188(3)	122.4(1.8)	148(3)	128(3)
Sr µg/g	304(13)	342(20)	145(30)	268(8)	252(17)	165(30)
Zr µg/g	380(14)	820(20)	155(30)	295(9)	347(18)	150(30)
Ag µg/g	-	<0.5	0.7(2)	<1.0	-	-
Sb µg/g	0.82(3)	1.48(4)	1.70(4)	0.98(2)	1.45(4)	1.47(4)
Cs µg/g	4.58(7)	6.89(11)	13.44(15)	5.71(8)	9.31(14)	10.09(12)
Ba µg/g	799(19)	650(20)	317(14)	672(14)	531(17)	245(14)
La µg/g	60.8(9)	70.3(1.0)	49.0(5)	47.3(7)	46.5(7)	49.6(5)
Ce µg/g	111.9(1.6)	144(2)	100.5(1.0)	85.8(1.2)	88.8(1.3)	105.4(1.1)
Nd µg/g	44(3)	53(5)	38(4)	36(2)	35(3)	38(4)
Sm µg/g	7.37(10)	9.38(14)	7.83(8)	6.19(9)	6.61(9)	8.08(8)
Eu µg/g	1.19(2)	1.43(3)	1.08(3)	1.076(15)	1.04(2)	1.12(3)
Tb µg/g	0.811(19)	1.08(3)	0.96(3)	0.703(13)	0.83(2)	1.09(4)
Yb µg/g	2.64(4)	4.18(7)	3.26(4)	2.47(4)	3.34(5)	3.65(5)
Lu µg/g	0.405(10)	0.673(16)	0.486(9)	0.384(9)	0.525(12)	0.535(10)
Hf µg/g	9.33(16)	21.4(4)	4.97(10)	7.98(12)	9.79(20)	5.07(10)
Ta µg/g	1.35(4)	1.81(5)	n/a	1.23(2)	1.55(5)	n/a
W µg/g	2.1(4)	2.8(8)	n/a	1.7(4)	2.5(3)	n/a
Au ng/g	<4	<5	5.3(3)	<3	4.8(2.4)	11.5(3.6)
Th µg/g	15.7(2)	25.0(4)	24.1(2)	15.5(2)	19.8(3)	26.2(3)
U µg/g	3.10(11)	5.42(20)	2.53(10)	4.24(12)	5.19(15)	3.93(13)
XRD						
quartz	21(1)	16(1)	2(1)	18(1)	11(1)	-
tridymite	5(1)	1(1)	-	2(1)	1(1)	-
cristobalite	2(1)	-	-	3(1)	tr	-
feldspar	39(6)	26(3)	6(2)	35(5)	19(2)	-
amphibole	1(1)	3(1)	-	1(1)	1(1)	-
biotite	-	2(1)	-	-	2(1)	-
chlorite	-	1(1)	-	-	-	-
hematite	tr	-	-	tr	1(1)	-
opal-A	15(8)	32(6)	-	27(7)	41(8)	-
illite	6(2)	-	29(15)	tr	-	32(17)
smectite	9(2)	17(5)	59(30)	12(4)	22(7)	65(35)
kaolinite	-	-	2(1)			-
calcite	-	tr	1(1)	-	-	-
zeolite	2(1)	2(1)	-	2(1)	2(1)	3(2)

Appendix 4: Quantitative Chemical (INAA) and Mineralogic (XRD) Data for Slope-Parallel Calcretes from Trench 14, Exile Hill

sample:	243,p1	245,p2	245,p3	245,p4	246,p1	246,p2
calcrete type:	*bulk*	*opal-CT*	*dense*	*ooidal*	*ooidal*	*root-fossil rich*
Chemistry (INAA)						
Na_2O %	0.612(9)	0.0138(3)	0.0343(6)	0.756(11)	0.293(4)	0.302(4)
CaO %	27.9(5)	0.34(2)	24.3(5)	29.5(6)	30.8(6)	37.1(7)
FeO %	0.569(8)	0.0196(4)	0.0173(3)	0.696(10)	0.1407(20)	0.1256(18)
Sc µg/g	1.42(2)	0.0312(4)	0.0203(3)	1.59(2)	0.358(5)	0.299(4)
Cr µg/g	n/a	n/a	n/a	n/a	n/a	n/a
Co µg/g	2.23(3)	0.506(8)	0.472(7)	2.47(3)	0.702(10)	1.306(18)
Ni µg/g	<7	<2	3.7(1.2)	9(4)	<6	10.0(1.6)
Zn µg/g	18.3(4)	1.29(13)	1.29(13)	23.8(7)	4.4(4)	3.9(3)
As µg/g	5.64(17)	0.062(17)	3.68(8)	5.61(15)	10.05(20)	12.21(19)
Se µg/g	0.11(4)	<0.1	0.10(3)	<0.2	0.20(5)	0.21(3)
Br µg/g	9.1(6)	0.46(3)	10.0(7)	9.4(7)	16.7(1.6)	12.9(8)
Rb µg/g	29.4(6)	0.18(7)	<0.4	39.2(9)	6.1(4)	7.2(3)
Sr µg/g	392(7)	7.1(1.6)	517(9)	641(12)	879(16)	946(15)
Zr µg/g	63(4)	<5	<8	74(5)	17(4)	10.8(1.8)
Ag µg/g	0.74(4)	0.029(10)	0.159(13)	0.91(3)	0.46(3)	1.41(3)
Sb µg/g	1.010(18)	1.93(3)	1.052(17)	0.536(13)	0.725(15)	0.291(7)
Cs µg/g	1.327(19)	0.017(2)	0.016(3)	1.68(3)	0.325(8)	0.337(6)
Ba µg/g	228(6)	<6	60(3)	260(7)	160(5)	140(4)
La µg/g	13.17(19)	0.44(10)	0.18(4)	19.4(3)	9.24(13)	2.57(4)
Ce µg/g	23.6(3)	0.52(9)	0.45(10)	28.9(4)	17.0(2)	5.09(8)
Nd µg/g	9.4(8)	<1.5	<2	13.4(1.1)	6.0(7)	2.0(4)
Sm µg/g	1.76(3)	0.09(3)	-	2.45(4)	0.766(17)	0.389(9)
Eu µg/g	0.270(5)	0.0078(11)	0.0044(11)	0.327(7)	0.053(3)	0.0503(17)
Tb µg/g	0.207(5)	0.0084(11)	0.0067(18)	0.260(8)	0.059(3)	0.047(2)
Yb µg/g	0.731(12)	0.028(3)	0.034(3)	0.887(16)	0.160(7)	0.153(5)
Lu µg/g	0.110(3)	-	-	0.135(5)	0.025(2)	0.0253(16)
Hf µg/g	1.72(3)	0.040(4)	0.027(4)	2.06(4)	0.515(13)	0.323(9)
Ta µg/g	0.298(8)	<0.01	0.0048(20)	0.412(11)	0.077(5)	0.071(3)
W µg/g	1.05(17)	0.09(2)	0.97(7)	1.57(14)	1.98(4)	3.18(11)
Au ng/g	5.2(1.0)	2.4(3)	2.4(4)	3.3(1.0)	6.3(8)	6.0(8)
Th µg/g	4.06(6)	0.125(4)	0.062(4)	5.28(7)	1.336(19)	0.938(13)
U µg/g	7.53(16)	18.3(4)	15.2(3)	3.64(9)	8.51(17)	4.21(10)
XRD						
quartz	3(1)	-	-	2(1)	tr	tr
tridymite	-	-	-	tr	-	-
cristobalite	1(1)	-	-	tr	-	-
feldspar	6(1)	-	-	9(1)	2(1)	3(1)
amphibole	-	-	-	tr	-	-
biotite	tr	-	-	tr	tr	-
clay	tr	-	-	1(1)	5(2)	5(2)
zeolite	1(1)	-	-	1(1)	-	-
gypsum	-	-	-	-	1(1)	-
sepiolite	-	-	4(1)	-	-	-
opal-A	42(3)	-	-	31(4)	35(4)	29(4)
opal-CT	-	99(2)	50(5)	-	-	-
calcite	47(2)	1(1)	45(2)	56(3)	57(3)	63(3)

Appendix 4: Quantitative Chemical (INAA) and Mineralogic (XRD) Data for Slope-Parallel Calcretes from Trench 14, Exile Hill (continued)

sample:	246,p3	248,p1	248,p2	250,p1	250,p2	920,p1
calcrete type:	*dense*	*dense*	*ooidal*	*ooidal*	*dense*	*root-fossil rich*
Chemistry (INAA)						
Na_2O %	0.1290(19)	0.0683(13)	0.218(3)	0.667(9)	0.192(3)	0.428(5)
K_2O %	n/a	n/a	n/a	n/a	n/a	0.39(10)
CaO %	22.8(5)	35.6(8)	37.5(7)	33.9(8)	27.7(5)	26.6(4)
FeO %	0.0149(3)	0.0414(6)	0.1351(19)	0.402(6)	0.168(2)	0.1438(16)
Sc µg/g	0.0284(4)	0.0942(13)	0.317(4)	1.002(14)	0.339(5)	0.348(4)
Cr µg/g	n/a	n/a	n/a	n/a	n/a	0.68(9)
Co µg/g	0.428(6)	0.452(6)	1.001(14)	1.78(3)	0.540(8)	0.895(10)
Ni µg/g	7.4(1.1)	<5	5(2)	<10	<8	4(2)
Zn µg/g	1.08(15)	1.91(17)	4.3(2)	12.4(5)	5.7(2)	6.4(3)
As µg/g	8.64(16)	10.4(2)	8.62(14)	10.9(2)	7.94(19)	9.59(14)
Se µg/g	0.14(4)	0.17(3)	<0.19	0.15(6)	<0.14	0.25(6)
Br µg/g	11.4(8)	13.4 (1.0)	11.7(1.0)	11.2(9)	11.3(1.0)	13.5(8)
Rb µg/g	0.63(13)	1.38(17)	7.2(3)	28.3(6)	7.1(3)	9.7(3)
Sr µg/g	543(10)	532(10)	593(11)	565(10)	423(9)	707(8)
Zr µg/g	<5	<7	19(3)	78(4)	15(3)	20(3)
Ag µg/g	0.87(2)	0.186(15)	0.26(2)	0.23(3)	0.166(20)	-
Sb µg/g	1.025(17)	0.969(16)	0.475(10)	0.535(12)	0.732(14)	0.777(13)
Cs µg/g	0.029(2)	0.093(4)	0.321(7)	1.107(17)	0.325(7)	0.296(6)
Ba µg/g	57(3)	116(3)	105(3)	241(6)	197(5)	139(5)
La µg/g	0.20(5)	0.74(2)	2.64(4)	11.46(16)	7.09(10)	6.00(8)
Ce µg/g	0.40(10)	1.34(4)	5.00(8)	22.8(3)	12.53(18)	11.68(15)
Nd µg/g	<0.7	1.1(3)	3.0(4)	8.1(8)	4.7(5)	4.2(7)
Sm µg/g	-	0.110(19)	0.465(8)	1.43(2)	0.607(19)	0.645(13)
Eu µg/g	0.0052(13)	0.0135(13)	0.068(3)	0.203(4)	0.064(3)	0.111(3)
Tb µg/g	0.0035(11)	0.0092(16)	0.055(3)	0.151(5)	0.048(3)	0.061(3)
Yb µg/g	0.018(2)	0.047(4)	0.204(5)	0.548(11)	0.162(5)	0.212(7)
Lu µg/g	-	-	0.0297(12)	0.090(3)	0.0237(13)	0.033(3)
Hf µg/g	0.032(4)	0.073(5)	0.578(12)	1.82(3)	0.547(12)	0.685(14)
Ta µg/g	0.006(3)	0.014(2)	0.079(4)	0.266(4)	0.070(4)	0.082(4)
W µg/g	1.40(12)	1.75(13)	2.01(9)	1.96(12)	1.19(16)	1.62(14)
Au ng/g	6.6(6)	1.9(6)	5.3(6)	4.7(8)	4.0(6)	7.7(1.2)
Th µg/g	0.071(3)	0.204(5)	0.978(14)	3.57(5)	1.24 1(18)	1.286(15)
U µg/g	11.4(2)	8.58(17)	3.46(7)	3.36(8)	9.18(19)	7.21(10)
XRD						
quartz	-	-	1(1)	1(1)	tr	tr
tridymite	-	-	-	1(1)	-	-
cristobalite	-	-	-	-	-	-
feldspar	-	-	2(1)	7(1)	2(1)	6(1)
amphibole	-	-	-	-	-	-
biotite	-	-	-	-	-	-
clay	-	1(1)	tr	1(1)	tr	5(2)
zeolite	-	-	-	tr	-	-
gypsum	-	-	-	-	-	tr
sepiolite	5(2)	-	-	-	-	-
opal-A	57(3)	37(3)	35(3)	33(4)	49(2)	41(3)
opal-CT	-	-	-	-	-	-
calcite	38(2)	62(3)	62(3)	57(3)	49(2)	48(2)

Appendix 5: Quantitative Chemical (XRF, AA, LOI, INAA) and Mineralogic (XRD) Data for Vein-Filling Calcretes from Trench 14, Exile Hill

sample:	1,p25	7,p1	47,p1	773,p1	48,p2	48,p2
calcrete type:	*channel sample*	*channel sample*	*channel sample*	*channel sample*	*bulk ash-bearing lamina*	*<45 mm ash-bearing lamina*
*Chemistry (SiO_2 - P_2O_5 by XRF; *K_2O by AA; volatiles by LOI; others by INAA)*						
SiO_2 %	38.7(4)	41.2(4)	n/a	n/a	55.0(6)	n/a
TiO_2 %	0.084(2)	0.057(1)	n/a	n/a	0.259(7)	n/a
Al_2O_3 %	2.81(7)	1.66(4)	n/a	n/a	9.7(2)	n/a
FeO %	0.55(2)	0.31(1)	n/a	n/a	1.41(4)	n/a
MnO %	0.010(1)	0.002(1)	n/a	n/a	0.033(1)	n/a
MgO %	1.28(3)	1.08(3)	n/a	n/a	0.88(2)	n/a
P_2O_5	0.027(3)	0.028(3)	n/a	n/a	0.068(7)	n/a
*K_2O %	0.76(2)	0.42(1)	n/a	n/a	2.62(7)	n/a
volatiles %	27.6(2.8)	26.8(2.7)	n/a	n/a	13.4(1.3)	n/a
Na_2O %	0.577(8)	0.379(6)	0.653(10)	0.335(5)	2.14(3)	0.305(4)
CaO %	27.8(6)	27.9(5)	28.4(6)	31.6(6)	16.2(5)	41.8(8)
FeO %	0.575(8)	0.311(5)	0.440(7)	0.240(3)	1.316(19)	0.652(9)
Sc µg/g	1.21(2)	0.771(11)	1.072(16)	0.625(9)	2.97(4)	1.50(2)
Cr µg/g	n/a	n/a	n/a	n/a	12.65(19)	7.46(19)
Co µg/g	3.55(5)	1.85(3)	1.86(3)	1.46(2)	3.10(4)	2.75(4)
Ni µg/g	n/a	<6	10(3)	7(2)	<20	<20
Zn µg/g	21(4)	9(2)	12.0(5)	8.0(4)	33.9(8)	15.4(6)
As µg/g	6.9(2)	7.40(14)	6.82(19)	7.54(17)	5.4(3)	10.4(2)
Se µg/g	<0.3	0.14(5)	<0.3	<0.2	<0.2	0.24(10)
Br µg/g	6.5(5)	9.8(6)	11.7(9)	10.5(1.1)	7.8(5)	18.6(1.6)
Rb µg/g	27.0(1.2)	16.6(5)	23.4(5)	13.9(4)	73.6(1.4)	15.0(6)
Sr µg/g	880(50)	850(40)	738(13)	719(13)	510(11)	744(15)
Zr µg/g	69(7)	44(4)	57(5)	28(4)	150(7)	126(6)
Ag µg/g	n/a	n/a	n/a	n/a	<0.2	-
Sb µg/g	0.80(2)	0.897(14)	0.809(17)	0.942(17)	0.598(17)	0.630(16)
Cs µg/g	1.24(2)	0.803(13)	0.801(14)	0.610(10)	2.04(4)	0.844(17)
Ba µg/g	172(7)	141(4)	229(6)	115(4)	620(12)	206(6)
La µg/g	9.93(15)	7.19(13)	12.6(2)	6.90(10)	33.9(5)	13.63(19)
Ce µg/g	19.5(3)	14.0(2)	22.9(4)	13.0(2)	60.1(8)	25.6(4)
Nd µg/g	7.3(1.0)	5.6(6)	8.9(8)	5.2(6)	23.5(1.5)	11.3(1.0)
Sm µg/g	1.35(2)	0.95(2)	1.55(3)	0.831(19)	4.16(6)	2.03(3)
Eu µg/g	0.211(6)	0.135(4)	0.244(5)	0.109(3)	0.740(13)	0.296(7)
Tb µg/g	0.159(5)	0.103(4)	0.165(5)	0.087(4)	0.455(11)	0.215(8)
Yb µg/g	0.586(15)	0.445(9)	0.544(11)	0.337(8)	1.357(19)	0.752(15)
Lu µg/g	0.090(3)	0.076(2)	0.086(3)	0.055(2)	0.205(5)	0.122(3)
Hf µg/g	1.65(3)	0.93(2)	1.41(2)	0.796(17)	3.76(6)	3.28(5)
Ta µg/g	0.294(11)	0.170(5)	0.249(7)	0.156(5)	0.76(2)	0.224(9)
W µg/g	1.27(15)	1.09(12)	1.36(17)	n/a	0.9(4)	1.96(19)
Au ng/g	7.1(2.6)	10.6(2.8)	8.6(6)	9.1(1.0)	5.1(1.6)	14.0(1.4)
Th µg/g	3.32(5)	2.21(3)	3.96(6)	2.15(3)	9.51(13)	3.53(5)
U µg/g	7.5(2)	8.51(15)	5.92(13)	8.04(17)	3.96(10)	3.73(9)
XRD						
quartz	3(1)	1(1)	4(1)	1(1)	10(1)	2(1)
tridymite	-	-	1(1)	-	-	-
cristobalite	-	-	-	-	-	-
feldspar	8(1)	4(1)	8(1)	5(1)	35(4)	4(1)
amphibole	-	-	-	-	1(1)	tr
biotite	-	-	-	-	-	tr
clay	1(1)	-	1(1)	tr	3(1)	tr
zeolite	1(1)	-	1(1)	-	5(1)	tr
gypsum	-	-	-	-	-	-
sepiolite	-	-	-	-	-	-
opal-A	31(4)	41(3)	36(3)	35(3)	29(5)	19(4)
opal-CT	-	-	-	-	-	-
calcite	56(3)	54(3)	49(2)	59(3)	17(1)	75(4)

Appendix 5: Quantitative Chemical (XRF, AA, LOI, INAA) and Mineralogic (XRD) Data for Vein-Filling Calcretes from Trench 14, Exile Hill (continued)

sample:	1,p13	1,p15	1,p16	1,p18	1,p19	1,p20	1,p23
calcrete lamina type:	*sepiolite + calcite*	*ooidal*	*dense*	*root-fossil rich*	*ooidal*	*root-fossil rich*	*dense*
Chemistry (INAA)							
Na_2O %	0.150(2)	1.181(17)	0.523(7)	0.313(4)	0.628(9)	0.411(6)	0.0984(14)
CaO %	33.6(5)	21.1(4)	28.8(6)	39.1(7)	32.4(6)	33.9(7)	34.9(6)
FeO %	0.136(2)	1.133(16)	0.540(8)	0.298(4)	0.455(6)	0.316(4)	0.0658(9)
Sc µg/g	0.319(5)	2.71(4)	1.340(19)	0.734(10)	1.098(16)	0.812(11)	0.1224(17)
Cr µg/g	n/a	n/a	n/a	n/a	n/a	n/a	n/a
Co µg/g	1.29(2)	4.64(7)	1.60(2)	2.53(4)	2.71(4)	2.85(4)	0.702(10)
Ni µg/g	n/a	30(5)	8(3)	<12	7(3)	5(2)	5.4(1.9)
Zn µg/g	12(3)	41(2)	15.1(4)	8.1(5)	17.3(5)	11.9(3)	2.8(2)
As µg/g	10.8(2)	5.74(12)	7.65(19)	6.94(15)	6.69(14)	7.76(15)	13.07(19)
Se µg/g	0.14(6)	<0.3	<0.2	<0.15	<0.2	0.11(5)	0.20(4)
Br µg/g	26.1(1.2)	4.5(3)	8.2(6)	8.0(7)	6.3(6)	8.8(8)	11.1(6)
Rb µg/g	6.3(4)	57.5(1.0)	25.4(6)	13.4(4)	25.4(6)	15.0(4)	2.3(2)
Sr µg/g	1020(40)	556(12)	698(13)	895(16)	946(16)	927(15)	1234(20)
Zr µg/g	11(3)	125(7)	61(5)	30(4)	84(4)	59(3)	8(3)
Ag µg/g	n/a	3.34(5)	0.61(4)	0.26(3)	2.34(3)	1.74(5)	0.353(11)
Sb µg/g	0.339(8)	0.889(16)	0.772(16)	0.516(11)	0.440(11)	0.485(11)	0.942(14)
Cs µg/g	0.472(9)	2.86(4)	1.307(19)	0.687(12)	1.019(16)	0.679(11)	0.121(5)
Ba µg/g	126(4)	293(6)	154(5)	132(4)	178(5)	141(4)	72(3)
La µg/g	2.70(4)	19.8(3)	10.98(16)	6.23(9)	14.6(2)	8.75(12)	0.976(15)
Ce µg/g	4.89(9)	37.6(5)	21.5(3)	12.19(17)	26.7(4)	16.4(2)	2.01(6)
Nd µg/g	2.3(5)	14.6(9)	8.0(8)	4.6(5)	10.5(9)	6.5(6)	<2
Sm µg/g	0.414(8)	2.52(4)	1.44(3)	0.831(16)	1.48(2)	0.972(15)	0.160(19)
Eu µg/g	0.063(2)	0.413(8)	0.205(5)	0.130(4)	0.245(5)	0.154(3)	0.0211(19)
Tb µg/g	0.052(2)	0.293(8)	0.159(5)	0.091(4)	0.152(5)	0.102(4)	0.018(2)
Yb µg/g	0.182(8)	1.099(16)	0.598(12)	0.368(8)	0.598(12)	0.425(9)	0.080(4)
Lu µg/g	0.026(2)	0.175(4)	0.095(3)	0.0585(18)	0.097(3)	0.070(2)	-
Hf µg/g	0.305(11)	3.35(5)	1.56(3)	0.798(16)	2.13(4)	1.30(2)	0.169(8)
Ta µg/g	0.067(4)	0.618(16)	0.302(9)	0.154(6)	0.243(8)	0.173(5)	0.027(3)
W µg/g	20.2(3)	2.05(12)	1.16(16)	1.44(15)	1.90(14)	3.12(13)	1.40(6)
Au ng/g	15.0(2.8)	2.6(8)	3.1(1.0)	8.2(8)	11.5(1.0)	9.4(1.0)	6.4(6)
Th µg/g	0.888(15)	7.14(10)	3.58(5)	2.00(3)	3.37(5)	2.33(3)	0.331(7)
U µg/g	3.46(7)	7.27(12)	9.34(19)	5.26(11)	4.44(10)	4.54(10)	12.6(2)
	XRD/chem	*XRD*	*XRD*	*XRD*	*XRD*	*XRD*	*XRD*
quartz	-	5(1)	3(1)	1(1)	3(1)	2(1)	1(1)
tridymite	-	1(1)	-	-	-	-	-
cristobalite	-	-	tr	-	-	-	-
feldspar	-	15(2)	5(1)	3(1)	5(1)	8(1)	-
amphibole	-	tr	tr	tr	tr	-	-
biotite	-	tr	tr	tr	tr	tr	-
clay	-	2(1)	tr	2(1)	2(1)	3(1)	2(1)
zeolite	-	2(1)	1(1)	tr	tr	tr	tr
gypsum	-	-	-	-	-	-	-
sepiolite	39(2)	-	-	-	-	-	-
opal-A	-	41(3)	41(3)	24(4)	26(3)	24(3)	38(3)
opal-CT	-	-	-	-	-	-	-
calcite	61(1)	34(2)	50(3)	70(4)	64(3)	63(3)	59(3)

Appendix 5: Quantitative Chemical (INAA) and Mineralogic (XRD or XRD/chem) Data for Vein-Filling Calcretes from Trench 14, Exile Hill (continued)

sample:	7,p2	7,p3	7,p4	7,p5	49,p1	349,p1	922,p1
calcrete lamina type:	*root-fossil rich*	*root-fossil rich*	*dense*	*ooidal*	*opal-CT + calcite*	*opal-A*	*root-fossil rich*
Chemistry (INAA)							
Na_2O %	0.0711(11)	0.0667(9)	0.155(2)	0.352(5)	0.0318(5)	0.0237(5)	0.885(10)
K_2O %	n/a	n/a	n/a	n/a	n/a	n/a	1.2(2)
CaO %	28.2(5)	29.9(6)	31.8(6)	30.4(6)	22,5(4)	0.34(5)	18.2(4)
FeO %	0.0598(8)	0.0611(9)	0.180(3)	0.340(5)	0.0170(4)	0.0237(4)	0.623(7)
Sc µg/g	0.1394(20)	0.143(2)	0.444(6)	0.772(11)	0.0133(4)	0.0181(3)	1.362(14)
Cr µg/g	n/a	n/a	n/a	n/a	n/a	n/a	1.63(18)
Co µg/g	0.760(11)	1.90(3)	1.255(18)	1.80(3)	0.249(6)	0.073(2)	2.86(3)
Ni µg/g	<5	<7	<8	<9	<4	<5	13(5)
Zn µg/g	2.04(20)	3.7(3)	5.3(3)	10(2)	130(30)	210(40)	29.5(7)
As µg/g	6.07(12)	6.73(19)	9.42(15)	8.22(15)	5.05(11)	0.34(7)	7.8(2)
Se µg/g	<0.15	<0.15	0.19(4)	0.13(5)	-	-	<0.2
Br µg/g	9.1(6)	10.2(9)	13.1(1.3)	11.2(1.1)	8.0(4)	1.02(7)	7.5(7)
Rb µg/g	1.77(18)	2.1(2)	9.0(3)	16.3(4)	<0.5	-	34.6(9)
Sr µg/g	504(10)	568(10)	804(13)	858(14)	690(30)	39(5)	791(12)
Zr µg/g	<11	<7	10(3)	37(4)	<8	<15	120(7)
Ag µg/g	0.308(18)	0.47(2)	0.38(2)	0.23(3)	n/a	n/a	-
Sb µg/g	0.629(11)	1.19(2)	0.543(11)	0.421(9)	1.152(16)	1.27(2)	0.437(15)
Cs µg/g	0.150(5)	0.164(5)	0.598(10)	0.840(13)	0.028(5)	0.033(5)	1.45(2)
Ba µg/g	57(2)	56(3)	78(3)	140(4)	38(7)	<40	426(11)
La µg/g	1.10(2)	0.98(2)	2.22(3)	6.01(8)	8.65(12)	11.29(16)	20.3(2)
Ce µg/g	2.24(5)	2.42(6)	4.72(8)	11.99(18)	0.18(6)	0.27(8)	38.5(4)
Nd µg/g	0.9(3)	1.3(3)	2.3(4)	4.8(6)	1.2(5)	<2	15.7(1.8)
Sm µg/g	0.198(12)	0.219(10)	0.445(14)	0.841(16)	0.035(16)	<0.16	3.13(3)
Eu µg/g	0.0252(16)	0.0247(19)	0.054(2)	0.125(3)	0.0032(15)	<0.004	0.385(9)
Tb µg/g	0.027(2)	0.028(2)	0.063(3)	0.100(4)	<0.01	<0.007	0.387(11)
Yb µg/g	0.131(4)	0.173(6)	0.273(6)	0.448(8)	0.021(5)	<0.020	1.31(2)
Lu µg/g	0.0202(11)	0.0279(15)	0.0420(17)	0.072(2)	-	<0.019	0.193(5)
Hf µg/g	0.094(6)	0.100(6)	0.374(9)	0.923(17)	<0.02	0.023(11)	3.48(5)
Ta µg/g	0.020(2)	0.018(3)	0.100(4)	0.176(6)	<0.01	<0.01	0.57(2)
W µg/g	0.89(8)	1.02(12)	1.12(6)	1.28(11)	0.67(5)	0.63(13)	0.7(2)
Au ng/g	9.5(8)	4.8(8)	9.0(6)	11.4(1.0)	5.5(1.2)	9.8(2.0)	29.3(3.0)
Th µg/g	0.423(7)	0.436(8)	1.162(16)	2.29(3)	0.053(6)	0.080(7)	8.38(8)
U µg/g	4.88(10)	6.24(13)	7.44(15)	6.01(12)	11.1(2)	22.9(4)	4.65(10)
	XRD	*XRD*	*XRD*	*XRD*	*XRD/chem*	*XRD/chem*	*XRD*
quartz	-	-	tr	2(1)	-	-	1(1)
tridymite	-	-	-	-	-	-	-
cristobalite	-	-	-	-	-	-	-
feldspar	-	-	2(1)	8(1)	-	-	11(2)
amphibole	-	-	-	1(1)	-	-	-
biotite	-	-	-	-	-	-	tr
clay	tr	-	-	1(1)	-	-	10(3)
zeolite	-	-	-	-	-	-	9(1)
gypsum	-	-	-	-	-	-	-
sepiolite	-	-	-	-	-	-	-
opal-A	49(3)	42(3)	42(3)	26(4)	-	100(1)	37(5)
opal-CT	-	-	-	-	56(2)	-	6(2)
calcite	51(3)	58(3)	56(3)	62(3)	44(1)	-	26(2)

Appendix 6: Quanmtitative Chemical (IC, INAA) and Semi-Quantitative Mineralogic (XRD) Data for Ashed Root Samples from the Vicinity of Trench 14, Exile Hill (samples 350, 351, 352) and from Higher Elevation at Rainier Mesa (719, 720)

sample:	350,p1	351,p1	351,p2	352,p1	719,p1	720,p1
plant type:	*boxthorn*	*creosote (sheath)*	*creosote (inner)*	*Mormon tea*	*piñon*	*juniper*
Chemistry (Cl, N, C_2O_4, P_2O_5, and S by IC; others by INAA)						
Cl %	3.16(1)	0.466(5)	0.597(2)	0.256(1)	1.97(2)	0.197(1)
N %	1.48(4)	1.40(4)	0.56(1)	2.79(4)	2.28(1)	2.12(3)
C_2O_4 %	47.7(1.3)	52.2(1.3)	42.9(6)	24.3(2)	8.07(20)	19.4(3)
P_2O_5 %	2.75(28)	0.66(6)	11.4(6)	0.49(2)	2.97(23)	0.86(12)
S %	1.00(3)	3.20(2)	2.37(16)	0.707(1)	0.86(12)	0.422(28)
Na_2O %	0.919(9)	0.560(6)	1.258(13)	0.551(6)	0.841(9)	0.318(3)
K_2O %	5.0(6)	4.4(5)	3.4(5)	1.4(2)	16.5(1.8)	2.3(3)
CaO %	28.8(6)	29.3(5)	27.4(5)	30.0(5)	13.7(3)	29.0(5)
FeO %	0.1719(19)	0.291(3)	0.322(5)	0.538(5)	0.860(9)	0.489(5)
Sc µg/g	0.270(3)	0.524(5)	0.153(4)	1.165(12)	1.663(17)	1.132(12)
Cr µg/g	6.3(3)	7.0(2)	45.0(9)	10.70(18)	18.6(4)	8.2(4)
Co µg/g	1.655(20)	1.876(19)	12.75(14)	1.635(16)	1.85(2)	1.77(2)
Ni µg/g	25(7)	53(5)	219(20)	15(5)	34(8)	18(8)
Zn µg/g	47.3(9)	81.0(1.1)	205(5)	36.0(6)	221(2)	153.8(1.8)
As µg/g	2.4(3)	0.81(14)	4.4(4)	1.29(13)	2.5(3)	1.57(19)
Se µg/g	2.9(3)	3.2(2)	8.3(1.0)	0.75(11)	0.8(2)	1.3(3)
Br µg/g	234(18)	82(8)	83(7)	48(3)	56(5)	26.7(1.6)
Rb µg/g	7.7(6)	16.6(6)	13.6(1.5)	19.3(6)	103(2)	23.9(1.0)
Sr µg/g	3820(40)	3000(30)	2840(50)	1311(14)	615(16)	1299(20)
Zr µg/g	<12	17(4)	8(4)	75(5)	115(11)	42(9)
Ag µg/g	0.39(5)	0.15(5)	0.71(4)	0.24(6)	0.31(11)	3.36(9)
Sb µg/g	0.088(12)	0.237(10)	0.94(3)	0.241(10)	0.285(17)	0.381(18)
Cs µg/g	0.227(13)	0.466(12)	0.15(3)	0.746(13)	1.66(3)	1.09(2)
Ba µg/g	161(10)	389(10)	394(15)	291(7)	270(10)	623(15)
La µg/g	1.63(3)	3.90(4)	4.14(7)	10.30(11)	25.0(3)	30.1(3)
Ce µg/g	3.47(17)	8.14(13)	9.3(5)	18.93(20)	46.4(5)	22.2(3)
Nd µg/g	<5	3.1(1.0)	2.1(1.7)	6.5(9)	18.7(1.9)	19(2)
Sm µg/g	0.238(8)	0.578(8)	0.399(14)	1.245(13)	3.40(4)	3.49(4)
Eu µg/g	0.038(3)	0.092(4)	0.086(19)	0.200(5)	0.369(9)	0.434(11)
Tb µg/g	0.030(5)	0.071(6)	0.04(2)	0.143(5)	0.379(13)	0.461(14)
Yb µg/g	0.10(2)	0.248(14)	0.08(2)	0.504(14)	1.08(2)	1.20(3)
Lu µg/g	0.016(4)	0.043(3)	0.013(4)	0.079(3)	0.162(6)	0.179(6)
Hf µg/g	0.26(3)	0.41(2)	0.21(2)	1.92(3)	2.95(6)	1.23(4)
Ta µg/g	0.061(6)	0.096(6)	0.056(6)	0.207(8)	0.401(17)	0.221(13)
W µg/g	74.9(1.0)	2.0(3)	12.0(6)	1.8(2)	3.0(4)	3.9(4)
Au ng/g	55(4)	25.0(2.0)	123(8)	60.8(3.4)	49.9(3.6)	9.2(2.4)
Th µg/g	0.48(2)	1.061(17)	0.21(4)	3.08(4)	6.78(8)	3.26(4)
U µg/g	0.24(7)	0.83(5)	<0.4	0.71(5)	2.61(10)	1.09(7)
XRD						
whewellite	**MAJOR**	**MAJOR**	**MAJOR**	**MAJOR**	**MAJOR**	**MAJOR**
amorphous	**minor?**	**minor?**	**minor?**	**MAJOR**	**MAJOR**	**MAJOR**
zeolite	-	-	-	trace?	-	-
quartz	-	-	trace	-	trace	trace
biotite	trace	trace	trace?	trace	trace	trace
amphibole	-	trace	-	trace	-	-
feldspar	-	-	-	**minor**	**minor**	trace
chlorite/kaol	-	-	-	trace	-	-
Ash/Root weight fraction	0.0832	0.1452	0.0371	0.1161	0.0402	0.0834

Appendix 7: Quantitative Chemical (INAA) and Mineralogic (XRD) Data for Local Springs, Seeps, and a Paleozoic Carbonate

sample:	251,p1	751,p1	753,p1	601,p1
locality:	*South Crater Flat*	*GMC Spring*	*IMV pit*	*UE-25 P#1*
sample type:	*calcite root cast, seep deposit*	*opal-A*	*opal-CT*	*Roberts Mt. Fm. dolomite*
Chemistry (INAA)				
Na_2O %	0.0599(8)	0.0618(10)	0.1556(16)	0.0405(10)
K_2O %	n/a	0.12(4)	0.09(4)	0.13(5)
CaO %	49.9(8)	0.12(5)	0.20(3)	27.7(4)
FeO %	0.0267(4)	0.0912(9)	0.0416(6)	0.1413(14)
Sc µg/g	0.0516(7)	0.200(2)	0.1112(12)	0.570(6)
Cr µg/g	n/a	n/a	n/a	20.4(2)
Co µg/g	0.182(4)	0.203(6)	0.072(4)	3.35(3)
Ni µg/g	<1.5	<4	<3	54(4)
Zn µg/g	-	2.7(2)	0.96(15)	12.2(5)
As µg/g	12.2(2)	0.87(7)	0.14(5)	2.74(12)
Se µg/g	0.71(7)	0.22(6)	-	<0.4
Br µg/g	23.7(1.1)	1.38(8)	0.27(4)	1.48(11)
Rb µg/g	1.3(2)	4.9(2)	2.7(2)	3.2(4)
Sr µg/g	960(40)	46(4)	16(4)	72(7)
Zr µg/g	<5	<15	<10	19(4)
Ag µg/g	n/a	-	-	5.35(8)
Sb µg/g	0.113(5)	0.553(8)	0.795(12)	0.350(9)
Cs µg/g	0.315(6)	0.464(6)	0.382(7)	0.243(8)
Ba µg/g	332(6)	<20	12(3)	14(4)
La µg/g	0.407(6)	17.05(17)	0.201(11)	6.36(6)
Ce µg/g	0.64(5)	59.7(6)	0.46(7)	9.23(11)
Nd µg/g	1.1(5)	14.4(1.0)	<1.2	5.3(8)
Sm µg/g	0.075(6)	3.08(4)	0.08(3)	0.987(11)
Eu µg/g	0.0074(10)	0.437(6)	0.0072(16)	0.194(5)
Tb µg/g	0.0122(14)	0.359(6)	0.0050(17)	0.144(5)
Yb µg/g	0.065(5)	1.511(15)	0.019(5)	0.431(12)
Lu µg/g	0.0112(16)	0.239(3)	<0.006	0.0641(20)
Hf µg/g	0.032(7)	0.107(7)	0.072(9)	0.598(18)
Ta µg/g	0.010(2)	0.019(30	0.013(3)	0.164(7)
W µg/g	0.54(6)	<0.8	<0.15	n/a
Au ng/g	1.0(4)	<1.3	0.7(6)	6.7(1.4)
Th µg/g	0.135(6)	3.36(3)	0.224(9)	0.670(12)
U µg/g	2.85(5)	27.0(3)	19.2(3)	2.51(6)
XRD				
quartz	tr	-	tr	2(1)
feldspar	tr	-	-	-
opal-A	-	100(1)	-	-
opal-CT	-	-	100(2)	-
calcite	100(2)	-	-	4(1)
dolomite	-	-	-	94(14)

Appendix 7: Quantitative Chemical (INAA) and Mineralogic (XRD) Data for Local Springs, Seeps, and a Paleozoic Carbonate (continued)

sample:	754,p1	755,p1	766,p1	760,p1
locality:	*Travertine Point*	*Travertine Point*	*Grapevine Spring*	*Nevares Spring*
sample type:	*black calcite vein*	*white calcite vein*	*black calcite vein*	*surface of spring mound*
Chemistry (INAA)				
Na_2O %	0.0951(10)	0.0449(5)	0.0753(8)	0.0452(5)
K_2O %	-	<0.03	<0.04	<0.06
CaO %	52.7(8)	52.9(8)	52.7(7)	53.1(6)
FeO %	0.00630(18)	0.00301(17)	0.00352(15)	0.0443(7)
Sc µg/g	0.00281(11)	0.00482(16)	0.00147(11)	0.0882(10)
Cr µg/g	n/a	n/a	n/a	n/a
Co µg/g	0.172(2)	0.0074(10)	1.562(16)	0.177(5)
Ni µg/g	<2	1.3(6)	4.9(6)	<3
Zn µg/g	2.40(9)	12.37(18)	0.62(8)	3.5(3)
As µg/g	38.5(4)	29.0(3)	14.42(15)	2.21(6)
Se µg/g	-	-	<0.1	-
Br µg/g	0.36(4)	0.046(19)	9.8(6)	6.3(4)
Rb µg/g	<0.4	<0.16	<0.4	1.7(3)
Sr µg/g	1187(12)	1264(13)	1694(17)	1306(13)
Zr µg/g	3.2(5)	2.7(9)	<2.0	<5
Ag µg/g	-	-	-	-
Sb µg/g	0.0164(19)	0.0026(7)	0.160(3)	0.027(4)
Cs µg/g	0.0076(11)	0.0025(12)	0.0186(11)	0.414(8)
Ba µg/g	14.7(1.1)	10.2(1.0)	128(2)	91(4)
La µg/g	0.012(6)	0.013(4)	0.017(4)	0.236(6)
Ce µg/g	<0.07	0.024(12)	0.441(17)	0.49(5)
Nd µg/g	<0.6	<0.5	<0.6	<1.2
Sm µg/g	<0.005	<0.009	<0.006	0.039(3)
Eu µg/g	<0.0012	0.0006(4)	<0.0013	0.0058(11)
Tb µg/g	<0.004	<0.004	<0.003	0.005(2)
Yb µg/g	<0.009	<0.011	<0.010	0.019(5)
Lu µg/g	<0.0015	<0.002	<0.003	0.0027(11)
Hf µg/g	0.028(3)	0.022(3)	<0.006	0.037(9)
Ta µg/g	<0.003	<0.002	<0.003	0.008(2)
W µg/g	0.93(9)	0.16(5)	1.09(9)	<0.2
Au ng/g	2.2(6)	<0.6	<0.8	<0.7
Th µg/g	0.005(2)	0.005(2)	0.0035(17)	0.102(8)
U µg/g	0.254(16)	0.358(17)	0.71(2)	0.325(19)
XRD				
quartz	-	-	-	tr
feldspar	-	-	-	-
opal-A	-	-	-	-
opal-CT	-	-	-	-
calcite	100(2)	100(2)	100(2)	100(2)
dolomite	tr	-	-	-

Appendix 8: Compilation of Replicate Analyses by INAA

sample:	1,p25a	1,p25b	7,p1a	7,p1b	47,p1a	47,p1b
Na_2O %	0.587(8)	0.567(8)	0.390(6)	0.368(5)	0.698(10)	0.607(9)
CaO %	27.8(6)	27.7(5)	27.7(5)	28.0(5)	28.3(5)	28.4(6)
FeO %	0.580(8)	0.569(8)	0.322(5)	0.299(4)	0.472(7)	0.408(6)
Sc µg/g	1.21(2)	1.21(2)	0.809(11)	0.732(10)	1.126(16)	1.018(14)
Cr µg/g	n/a	n/a	n/a	n/a	n/a	n/a
Co µg/g	3.69(5)	3.40(5)	1.85(3)	1.85(3)	2.02(3)	1.70(2)
Ni µg/g	n/a	n/a	n/a	n/a	7(3)	13(3)
Zn µg/g	22(4)	20(4)	9(2)	9(2)	13.0(4)	10.9(5)
As µg/g	6.9(2)	6.91(14)	7.16(14)	7.63(14)	6.87(13)	6.77(19)
Se µg/g	<0.2	<0.3	<0.2	0.14(5)	<0.20	<0.3
Br µg/g	6.4(5)	6.5(3)	9.9(4)	9.7(6)	11.2(7)	12.1(9)
Rb µg/g	27.6(1.2)	26.3(9)	16.7(5)	16.5(5)	25.5(5)	22.4(5)
Sr µg/g	880(50)	880(50)	840(40)	860(30)	731(12)	744(13)
Zr µg/g	76(7)	62(6)	48(4)	39(2)	58(4)	56(5)
Ag µg/g	n/a	n/a	n/a	n/a	0.318(15)	0.32(3)
Sb µg/g	0.84(2)	0.759(14)	0.918(14)	0.875(14)	0.786(13)	0.831(17)
Cs µg/g	1.24(2)	1.24(2)	0.815(13)	0.790(11)	0.856(14)	0.746(12)
Ba µg/g	178(7)	165(5)	140(4)	141(4)	231(5)	227(6)
La µg/g	10.43(15)	9.43(13)	8.98(13)	5.40(8)	9.94(14)	15.3(2)
Ce µg/g	20.5(3)	18.5(3)	17.1(2)	10.90(15)	17.9(3)	27.8(4)
Nd µg/g	7.7(1.0)	6.8(7)	6.7(5)	4.5(6)	7.7(6)	10.1(8)
Sm µg/g	1.37(2)	1.33(2)	1.07(2)	0.829(16)	1.43(2)	1.67(3)
Eu µg/g	0.209(6)	0.212(5)	0.145(4)	0.125(2)	0.247(5)	0.240(5)
Tb µg/g	0.162(5)	0.155(5)	0.108(4)	0.0982(17)	0.165(5)	0.165(5)
Yb µg/g	0.602(15)	0.569(11)	0.471(9)	0.419(9)	0.557(9)	0.531(11)
Lu µg/g	0.093(3)	0.086(2)	0.0755(14)	0.066(2)	0.0850(19)	0.086(3)
Hf µg/g	1.72(3)	1.57(3)	1.04(2)	0.824(15)	1.42(2)	1.40(2)
Ta µg/g	0.302(11)	0.285(10)	0.173(5)	0.166(3)	0.251(7)	0.247(7)
W µg/g	1.22(15)	1.32(8)	1.12(12)	1.05(9)	1.52(9)	1.19(17)
Au ng/g	8.1(2.6)	6.0(1.6)	9.1(1.8)	12.1(2.8)	9.1(8)	8.1(1.2)
Th µg/g	3.43(5)	3.20(5)	2.28(3)	2.14(3)	4.28(6)	3.64(5)
U µg/g	7.4(2)	7.51(14)	8.79(14)	8.22(15)	5.63(10)	6.21(13)

sample:	350,p1a	350,p1b	351,p1a	351,p1b	351,p2a	351,p2b
Na_2O %	0.910(9)	0.928(9)	0.566(6)	0.554(6)	1.248(12)	1.268(13)
K_2O %	5.1(6)	4.9(6)	4.4(5)	4.4(5)	3.8(5)	3.0(4)
CaO %	28.2(6)	29.4(4)	29.4(4)	29.2(5)	27.5(5)	27.3(4)
FeO %	0.1680(19)	0.1758(18)	0.296(3)	0.285(3)	0.328(5)	0.316(3)
Sc µg/g	0.275(3)	0.264(3)	0.521(5)	0.527(5)	0.176(4)	0.1303(13)
Cr µg/g	5.9(3)	6.6(3)	6.6(2)	7.4(2)	46.0(9)	43.9(4)
Co µg/g	1.645(20)	1.664(18)	1.929(19)	1.822(18)	11.93(12)	13.57(14)
Ni µg/g	21(5)	24(4)	56(5)	50(5)	320(20)	118(6)
Zn µg/g	46.6(9)	47.9(9)	81.5(1.1)	80.4(1.1)	203(5)	206(2)
As µg/g	2.5(3)	2.38(19)	0.97(12)	0.66(14)	3.3(4)	5.5(2)
Se µg/g	2.9(3)	2.8(2)	3.2(2)	3.1(2)	8.5(1.0)	8.1(4)
Br µg/g	234(18)	234(17)	78(5)	96(8)	88(7)	77(5)
Rb µg/g	7.8(6)	7.5(5)	16.4(6)	16.8(6)	13.6(1.5)	13.6(7)
Sr µg/g	3800(40)	3840(40)	3010(30)	2990(30)	2830(50)	2850(30)
Zr µg/g	<18	<12	20(4)	13(4)	-	8(4)
Ag µg/g	0.45(5)	0.33(5)	0.17(5)	0.12(4)	-	0.71(4)
Sb µg/g	0.087(12)	0.088(8)	0.229(10)	0.244(11)	1.08(3)	0.803(19)
Cs µg/g	0.226(13)	0.228(10)	0.474(12)	0.457(11)	0.15(3)	0.147(9)
Ba µg/g	159(10)	163(7)	386(9)	391(10)	413(15)	375(9)
La µg/g	1.56(3)	1.696(18)	3.78(4)	4.02(4)	7.04(7)	1.24(3)
Ce µg/g	3.33(17)	3.60(16)	7.90(13)	8.37(12)	15.5(5)	3.12(16)
Nd µg/g	<6	<5	2.9(9)	3.3(1.0)	3.5(1.7)	<6
Sm µg/g	0.228(8)	0.248(6)	0.579(7)	0.576(8)	0.653(14)	0.144(7)
Eu µg/g	0.037(3)	0.039(3)	0.089(4)	0.095(4)	0.146(19)	0.026(3)
Tb µg/g	0.031(5)	0.029(5)	0.070(6)	0.071(5)	0.06(2)	0.020(5)
Yb µg/g	0.11(2)	0.099(13)	0.250(14)	0.246(14)	0.10(2)	0.05(2)
Lu µg/g	0.014(4)	0.018(3)	0.043(2)	0.042(3)	0.014(4)	0.011(3)
Hf µg/g	0.34(3)	0.189(20)	0.49(2)	0.322(17)	<0.2	0.212(15)
Ta µg/g	0.062(6)	0.060(5)	0.097(6)	0.094(6)	-	0.056(6)
W µg/g	75.4(1.0)	74.4(7)	2.1(2)	1.9(3)	12.1(6)	11.8(4)
Au ng/g	54(4)	56.9(3.6)	25.1(2.0)	24.8(2.0)	112(6)	133(8)
Th µg/g	0.45(2)	0.510(18)	1.036(17)	1.085(17)	0.20(4)	0.213(14)
U µg/g	0.20(7)	0.27(4)	0.85(4)	0.80(5)	<0.8	<0.4

Appendix 8: Compilation of Replicate Analyses by INAA (continued)

sample:	352,p1a	352,p1b	429,p3a	429,p3b	430,p3a	430,p3b
Na_2O %	0.557(6)	0.544(5)	0.171(3)	0.167(3)	0.077(2)	0.076(3)
K_2O %	1.4(2)	1.35(14)	3.9(5)	3.8(5)	2.3(3)	2.3(3)
CaO %	30.0(5)	30.0(4)	2.2(2)	2.11(19)	2.4(2)	2.9(2)
FeO %	0.543(5)	0.533(5)	5.15(5)	5.13(5)	5.09(5)	5.10(5)
Sc µg/g	1.189(12)	1.141(11)	13.68(14)	13.64(14)	13.92(14)	13.94(14)
Cr µg/g	10.75(17)	10.65(18)	47.3(7)	47.8(6)	45.4(7)	44.7(6)
Co µg/g	1.633(16)	1.637(16)	n/a	n/a	n/a	n/a
Ni µg/g	15(4)	15(5)	<80	<80	<100	-
Zn µg/g	36.5(6)	35.4(6)	-	-	-	-
As µg/g	1.14(13)	1.44(7)	10.1(4)	10.5(4)	8.3(4)	8.5(4)
Se µg/g	0.69(9)	0.80(11)	<1.2	<1.2	<0.9	<0.7
Br µg/g	48(3)	48(3)	14.6(1.2)	14.1(1.0)	3.9(4)	3.6(4)
Rb µg/g	19.6(6)	19.0(6)	188(3)	188(3)	127(3)	129(3)
Sr µg/g	1314(13)	1308(14)	130(30)	160(30)	160(30)	170(30)
Zr µg/g	91(5)	59(5)	140(30)	170(20)	150(30)	150(20)
Ag µg/g	0.28(6)	0.19(5)	0.7(2)	<1.5	-	-
Sb µg/g	0.234(10)	0.247(8)	1.67(4)	1.72(4)	1.50(4)	1.44(4)
Cs µg/g	0.746(11)	0.746(13)	13.49(15)	13.39(13)	10.11(12)	10.06(11)
Ba µg/g	289(7)	293(7)	325(14)	308(12)	248(14)	241(12)
La µg/g	10.55(11)	10.04(10)	48.9(5)	49.1(5)	49.3(5)	49.8(5)
Ce µg/g	19.96(20)	17.90(18)	99.9(1.0)	101.1(1.0)	105.3(1.1)	105.5(1.1)
Nd µg/g	6.8(9)	6.2(9)	38(4)	38(3)	36(4)	40(4)
Sm µg/g	1.334(13)	1.156(12)	7.81(8)	7.84(8)	8.05(8)	8.10(8)
Eu µg/g	0.204(4)	0.196(5)	1.08(3)	1.08(2)	1.11(3)	1.13(2)
Tb µg/g	0.158(5)	0.128(5)	0.94(3)	0.98(3)	1.10(4)	1.08(3)
Yb µg/g	0.569(14)	0.438(10)	3.26(4)	3.26(4)	3.63(5)	3.66(4)
Lu µg/g	0.088(3)	0.069(2)	0.486(9)	0.486(9)	0.536(10)	0.533(9)
Hf µg/g	2.30(3)	1.54(3)	5.02(10)	4.91(8)	5.05(10)	5.09(9)
Ta µg/g	0.216(7)	0.197(8)	n/a	n/a	n/a	n/a
W µg/g	1.7(2)	1.81(8)	n/a	n/a	n/a	n/a
Au ng/g	64.1(3.4)	57.5(3.0)	4.0(2.8)	6.6(3.0)	11.0(3.2)	12.0(3.6)
Th µg/g	3.72(4)	2.43(2)	24.0(4)	24.1(2)	26.0(3)	26.3(3)
U µg/g	0.79(5)	0.62(3)	2.60(10)	2.46(10)	3.93(12)	3.93(13)

sample:	601,p1a	601,p1b	719,p1a	719,p1b	720,p1a	720,p1b
Na_2O %	0.0396(8)	0.0413(9)	0.801(8)	0.880(9)	0.310(3)	0.325(3)
K_2O %	0.13(4)	0.13(5)	16.6(1.6)	16.4(1.8)	2.3(3)	2.3(3)
CaO %	27.9(4)	27.4(4)	14.0(3)	13.4(3)	29.0(5)	28.9(5)
FeO %	0.1428(14)	0.1397(14)	0.804(8)	0.916(9)	0.484(5)	0.494(5)
Sc µg/g	0.573(6)	0.566(6)	1.684(17)	1.642(16)	1.096(11)	1.168(12)
Cr µg/g	20.4(2)	20.3(2)	18.0(4)	19.2(3)	8.4(4)	8.0(3)
Co µg/g	3.43(3)	3.27(3)	1.72(2)	1.98(2)	1.76(2)	1.77(2)
Ni µg/g	52(4)	56(4)	35(8)	33(8)	18(8)	<30
Zn µg/g	12.6(5)	11.7(5)	224(2)	218(2)	156.0(1.8)	151.6(1.6)
As µg/g	2.67(10)	2.80(12)	2.3(2)	2.7(3)	1.55(19)	1.58(10)
Se µg/g	<0.3	<0.4	0.9(2)	0.64(18)	1.5(3)	1.17(18)
Br µg/g	1.50(11)	1.46(11)	49(3)	62(5)	26.3(1.6)	27.0(1.6)
Rb µg/g	3.2(3)	3.2(4)	101.7(1.6)	104.0(1.6)	23.5(1.0)	24.3(9)
Sr µg/g	72(6)	71(7)	632(16)	598(14)	1320(20)	1278(18)
Zr µg/g	17(4)	20(4)	144(11)	86(9)	43(9)	41(9)
Ag µg/g	4.99(7)	5.71(8)	0.32(10)	0.30(11)	-	3.36(9)
Sb µg/g	0.351(9)	0.349(9)	0.283(17)	0.287(16)	0.378(18)	0.384(14)
Cs µg/g	0.245(8)	0.241(8)	1.56(3)	1.75(3)	1.10(2)	1.08(2)
Ba µg/g	15(3)	13(4)	261(10)	279(10)	624(15)	622(13)
La µg/g	6.41(6)	6.31(6)	28.5(3)	21.5(2)	29.3(3)	30.9(3)
Ce µg/g	9.31(11)	9.14(11)	51.7(5)	41.1(4)	20.6(3)	23.8(2)
Nd µg/g	5.5(7)	5.1(8)	19.2(1.9)	18.1(1.9)	18(2)	20(2)
Sm µg/g	0.996(10)	0.977(11)	3.18(3)	3.62(4)	3.44(3)	3.53(4)
Eu µg/g	0.196(4)	0.191(5)	0.345(9)	0.393(9)	0.432(11)	0.435(10)
Tb µg/g	0.143(5)	0.144(5)	0.324(13)	0.433(12)	0.467(14)	0.454(12)
Yb µg/g	0.426(11)	0.436(12)	1.03(2)	1.13(2)	1.21(3)	1.19(2)
Lu µg/g	0.0654(18)	0.0627(20)	0.160(6)	0.164(5)	0.182(6)	0.176(5)
Hf µg/g	0.587(15)	0.608(18)	3.28(6)	2.61(4)	1.33(4)	1.13(3)
Ta µg/g	0.164(7)	0.164(7)	0.353(16)	0.448(17)	0.215(13)	0.226(12)
W µg/g	26.4(3)	25.0(3)	2.9(4)	3.0(4)	4.1(4)	3.7(2)
Au ng/g	5.4(1.0)	8.0(1.4)	53.1(3.6)	46.7(3.4)	7.7(1.2)	10.6(1.6)
Th µg/g	0.678(12)	0.662(12)	7.74(8)	5.82(6)	3.01(4)	3.50(3)
U µg/g	2.48(5)	2.53(6)	2.89(10)	2.32(9)	1.06(7)	1.12(5)

Appendix 8: Compilation of Replicate Analyses by INAA (continued)

sample:	753.p1a	753.p1b	755.p1a	755.p1b	760.p1a	760.p1b
Na_2O %	0.1576(16)	0.1535(15)	0.0471(5)	0.0426(5)	0.0433(4)	0.0471(5)
K_2O %	0.08(4)	0.10(4)	<0.03	<0.03	<0.06	<0.07
CaO %	0.20(3)	0.19(3)	53.5(6)	53.1(8)	52.4(6)	53.7(6)
FeO %	0.0427(5)	0.0404(6)	0.00205(9)	0.00397(17)	0.0395(6)	0.0491(7)
Sc µg/g	0.1152(12)	0.1072(11)	0.00392(8)	0.00571(16)	0.0764(8)	0.1000(10)
Cr µg/g	n/a	n/a	n/a	n/a	n/a	n/a
Co µg/g	0.074(4)	0.069(4)	0.0064(5)	0.0083(10)	0.152(4)	0.202(5)
Ni µg/g	<3	<4	<2	1.3(6)	<3	<3
Zn µg/g	1.09(12)	0.82(15)	12.04(12)	12.69(18)	3.3(2)	3.6(3)
As µg/g	0.13(5)	0.14(3)	30.4(3)	27.6(3)	2.17(6)	2.25(5)
Se µg/g	-	-	-	-	-	-
Br µg/g	0.25(4)	0.29(3)	0.038(15)	0.053(19)	6.3(4)	6.3(4)
Rb µg/g	2.78(16)	2.7(2)	<0.2	<0.16	1.5(2)	1.9(3)
Sr µg/g	16(3)	16(4)	1348(13)	1180(12)	1308(13)	1304(13)
Zr µg/g	<10	<11	2.5(3)	2.8(9)	<5	<7
Ag µg/g	-	-	-	-	-	-
Sb µg/g	0.794(11)	0.795(12)	0.0026(7)	<0.006	0.022(3)	0.031(4)
Cs µg/g	0.377(6)	0.387(7)	0.0022(6)	0.0028(12)	0.385(7)	0.443(8)
Ba µg/g	12(3)	<10	10.6(9)	9.7(1.0)	90(3)	92(4)
La µg/g	0.223(11)	0.178(9)	0.008(3)	0.017(4)	0.189(5)	0.282(6)
Ce µg/g	0.54(6)	0.38(7)	0.024(12)	<0.07	0.42(4)	0.56(5)
Nd µg/g	<1.2	<2.0	<0.5	<0.6	<1.2	<1.5
Sm µg/g	0.08(3)	0.07(3)	<0.009	-	0.033(3)	0.045(3)
Eu µg/g	0.0082(14)	0.0062(16)	0.00042(17)	0.0008(4)	0.0050(9)	0.0065(11)
Tb µg/g	0.0050(17)	<0.015	<0.004	<0.004	0.005(2)	<0.015
Yb µg/g	0.019(5)	<0.02	<0.011	<0.011	0.018(6)	0.020(5)
Lu µg/g	<0.006	<0.01	<0.003	<0.0020	0.0027(11)	<0.006
Hf µg/g	0.084(8)	0.059(9)	0.021(2)	0.022(3)	0.032(7)	0.041(9)
Ta µg/g	0.013(2)	0.012(3)	<0.002	<0.002	0.0064(19)	0.009(2)
W µg/g	<0.5	<0.15	0.12(5)	0.19(5)	<0.3	<0.2
Au ng/g	0.7(6)	<0.8	<0.7	<0.6	<0.7	<1.0
Th µg/g	0.227(7)	0.221(9)	<0.007	0.005(2)	0.086(6)	0.117(8)
U µg/g	18.6(2)	19.8(3)	0.368(15)	0.347(17)	0.301(18)	0.348(19)

sample:	773.p1a	773.p1b	879.p1a	879.p1b	880.p1a	880.p1b
Na_2O %	0.332(5)	0.337(5)	0.871(9)	1.024(10)	2.79(3)	2.59(3)
K_2O %	n/a	n/a	1.09(19)	1.2(2)	4.4(7)	4.0(6)
CaO %	31.4(6)	31.8(6)	23.1(5)	23.8(5)	1.4(2)	2.1(2)
FeO %	0.239(3)	0.241(3)	0.714(7)	0.844(8)	0.998(10)	0.876(9)
Sc µg/g	0.608(9)	0.641(9)	1.708(17)	2.04(2)	1.906(19)	1.950(19)
Cr µg/g	n/a	n/a	2.5(2)	3.1(4)	1.1(2)	<3
Co µg/g	1.390(20)	1.52(2)	1.428(19)	2.64(3)	0.430(15)	0.477(8)
Ni µg/g	7(2)	<6	<20	<20	<20	<11
Zn µg/g	8.6(4)	7.3(3)	-	-	-	-
As µg/g	7.54(15)	7.53(17)	8.50(15)	8.80(19)	3.9(3)	4.4(3)
Se µg/g	<0.2	<0.11	<0.4	<0.3	<0.4	<0.3
Br µg/g	9.6(6)	11.4(1.1)	8.4(7)	7.1(6)	1.13(16)	1.41(17)
Rb µg/g	14.0(4)	13.8(3)	28.3(1.1)	39.4(1.1)	146(2)	147.2(1.8)
Sr µg/g	712(13)	725(12)	820(17)	762(13)	259(14)	274(8)
Zr µg/g	29(4)	27(3)	79(9)	102(8)	190(13)	188(7)
Ag µg/g	0.74(3)	0.55(3)	-	-	-	-
Sb µg/g	0.954(16)	0.930(17)	0.255(13)	0.307(15)	0.39(2)	0.410(16)
Cs µg/g	0.610(10)	0.609(9)	1.80(3)	2.28 (3)	3.99(5)	4.12(5)
Ba µg/g	119(4)	111(4)	175(8)	243(9)	156(10)	150(8)
La µg/g	6.39(9)	7.41(10)	18.49(18)	19.90(20)	32.6(3)	35.9(4)
Ce µg/g	12.03(18)	14.0(2)	34.2(3)	43.7(4)	78.6(8)	82.8(8)
Nd µg/g	5.1(6)	5.3(6)	12.4(1.6)	18.2(1.9)	39(3)	32(3)
Sm µg/g	0.752(19)	0.909(19)	2.49(2)	3.55(4)	9.43(9)	8.40(8)
Eu µg/g	0.104(3)	0.113(3)	0.284(9)	0.406(9)	0.629(14)	0.508(9)
Tb µg/g	0.085(4)	0.089(3)	0.319(12)	0.462(13)	1.33(3)	1.19(3)
Yb µg/g	0.346(8)	0.327(7)	1.168(20)	1.44(2)	3.66(4)	3.42(4)
Lu µg/g	0.057(2)	0.052(2)	0.175(4)	0.198(5)	0.492(9)	0.468(8)
Hf µg/g	0.879(17)	0.713(14)	2.80(5)	3.30(5)	6.92(10)	6.88(11)
Ta µg/g	0.155(5)	0.156(5)	0.64(3)	0.69(3)	1.61(5)	1.64(5)
W µg/g	n/a	n/a	0.75(16)	1.0(2)	1.2(5)	1.0(4)
Au ng/g	9.3(8)	8.8(1.0)	7.6(1.6)	7.3(1.8)	2.7(2.6)	4.2(2.2)
Th µg/g	1.93(3)	2.37(3)	10.25(10)	10.26(10)	20.7(2)	21.2(2)
U µg/g	8.03(15)	8.04(17)	2.65(7)	2.30(7)	5.45(15)	5.65(15)

Appendix 8: Compilation of Replicate Analyses by INAA (continued)

sample:	882,p1a	882,p1b	883,p1a	883,p1b	901,p1a	901,p1b
Na_2O %	1.326(13)	1.692(17)	0.722(7)	0.723(7)	0.931(9)	0.927(9)
K_2O %	2.0(3)	2.1(3)	1.21(19)	1.3(2)	<0.4	<0.5
CaO %	15.9(3)	18.6(4)	26.0(4)	24.8(4)	27.5(4)	27.8(5)
FeO %	0.315(3)	0.494(5)	0.620(6)	0.722(7)	0.0308(5)	0.0311(5)
Sc µg/g	1.810(18)	1.958(20)	1.515(15)	1.672(17)	0.1163(12)	0.1236(12)
Cr µg/g	1.20(19)	1.40(15)	4.5(2)	5.47(16)	0.29(6)	0.64(8)
Co µg/g	1.108(18)	0.941(12)	1.560(19)	1.757(18)	0.563(6)	0.539(7)
Ni µg/g	<20	<20	<30	<20	10.0(1.6)	7.4(1.6)
Zn µg/g	-	-	-	-	2.50(19)	2.7(2)
As µg/g	7.37(14)	7.7(2)	6.83(20)	7.0(2)	12.61(19)	12.7(2)
Se µg/g	<0.5	<0.3	<0.4	<0.4	0.29(5)	0.20(6)
Br µg/g	8.0(6)	7.4(6)	12.7(8)	14.4(1.1)	28.4(1.7)	35(3)
Rb µg/g	93.2(1.6)	90.0(1.5)	45.8(1.1)	45.5(9)	4.7(3)	4.8(3)
Sr µg/g	573(16)	677(11)	581(14)	572(11)	1042(12)	1047(11)
Zr µg/g	34(9)	47(6)	46(8)	67(7)	<7	<6
Ag µg/g	-	-	-	-	-	-
Sb µg/g	0.490(15)	0.408(16)	0.686(16)	0.692(16)	0.169(5)	0.144(7)
Cs µg/g	3.01(4)	2.91(3)	1.78(2)	1.84(2)	0.283(5)	0.308(6)
Ba µg/g	51(6)	89(7)	154(7)	189(6)	26(2)	23(3)
La µg/g	9.18(9)	12.18(12)	11.63(12)	11.49(11)	1.060(13)	1.184(18)
Ce µg/g	21.1(2)	26.1(3)	22.9(2)	21.3(2)	2.05(5)	2.25(6)
Nd µg/g	7.8(1.3)	10.6(1.5)	8.5(1.1)	8.4(1.1)	1.0(4)	1.4(5)
Sm µg/g	2.11(2)	2.39(2)	1.717(20)	1.660(19)	0.200(8)	0.206(6)
Eu µg/g	0.092(6)	0.160(5)	0.192(7)	0.224(6)	0.0147(13)	0.0153(13)
Tb µg/g	0.387(13)	0.391(11)	0.226(10)	0.207(7)	0.031(3)	0.034(2)
Yb µg/g	1.63(2)	1.64(2)	0.789(15)	0.782(13)	0.153(6)	0.162(8)
Lu µg/g	0.243(5)	0.239(5)	0.121(3)	0.119(3)	0.0255(12)	0.0267(16)
Hf µg/g	1.67(3)	1.91(4)	1.67(3)	2.21(3)	0.119(8)	0.117(9)
Ta µg/g	1.07(4)	1.04(4)	0.397(16)	0.386(14)	0.055(3)	0.056(3)
W µg/g	1.42(19)	1.3(3)	1.6(2)	1.6(3)	1.33(19)	1.64(19)
Au ng/g	8.1(1.4)	9.3(2.0)	5.6(1.4)	4.7(1.4)	7.2(8)	7.5(6)
Th µg/g	8.83(9)	10.21(10)	5.86(6)	5.50(6)	0.599(8)	0.580(9)
U µg/g	6.79(12)	5.67(13)	6.92(10)	7.08(12)	2.44(4)	2.04(5)

sample:	920,p1a	920,p2b	922,p1a	922,p1b
Na_2O %	0.464(5)	0.392(4)	0.961(10)	0.808(8)
K_2O %	0.49(10)	0.29(7)	1.4(2)	1.06(19)
CaO %	26.0(4)	27.2(4)	16.9(4)	19.4(4)
FeO %	0.1228(12)	0.1647(16)	0.555(6)	0.691(7)
Sc µg/g	0.368(4)	0.327(3)	1.320(13)	1.403(14)
Cr µg/g	0.51(9)	0.84(8)	1.45(14)	1.81(18)
Co µg/g	0.733(7)	1.036(10)	3.03(3)	2.69(3)
Ni µg/g	<7	4(2)	10(5)	15(5)
Zn µg/g	5.7(3)	7.1(3)	29.5(7)	-
As µg/g	9.65(13)	9.53(14)	7.5(2)	8.0(2)
Se µg/g	0.27(6)	0.23(6)	<0.2	<0.3
Br µg/g	13.4(8)	13.5(8)	7.2(6)	7.7(7)
Rb µg/g	11.1(3)	8.3(3)	37.3(9)	31.8(9)
Sr µg/g	692(7)	721(8)	746(11)	836(12)
Zr µg/g	20(3)	20(3)	122(7)	117(7)
Ag µg/g	-	-	-	-
Sb µg/g	0.768(13)	0.786(12)	0.440(14)	0.433(15)
Cs µg/g	0.302(6)	0.290(6)	1.471(19)	1.42(2)
Ba µg/g	139(5)	138(4)	401(10)	451(11)
La µg/g	7.76(8)	4.24(4)	20.00(20)	20.6(2)
Ce µg/g	15.38(15)	7.97(8)	39.4(4)	37.6(4)
Nd µg/g	5.0(7)	3.3(6)	15.0(1.4)	16.3(1.8)
Sm µg/g	0.809(13)	0.481(11)	3.10(3)	3.16(3)
Eu µg/g	0.133(3)	0.088(3)	0.372(8)	0.397(9)
Tb µg/g	0.076(3)	0.046(3)	0.382(10)	0.391(11)
Yb µg/g	0.245(10)	0.178(7)	1.321(19)	1.30(2)
Lu µg/g	0.040(3)	0.0262(16)	0.188(4)	0.197(5)
Hf µg/g	0.726(14)	0.643(13)	3.51(5)	3.45(5)
Ta µg/g	0.096(4)	0.067(4)	0.59(2)	0.55(2)
W µg/g	1.48(14)	1.75(14)	<1.2	0.7(2)
Au ng/g	8.0(1.2)	7.3(1.0)	27.0(1.2)	31.6(3.0)
Th µg/g	1.478(15)	1.093(11)	8.47(8)	8.29(8)
U µg/g	7.19(10)	7.22(9)	5.16(10)	4.13(10)

Los Alamos
NATIONAL LABORATORY
Los Alamos, New Mexico 87545